arXiv:1403.5610v1 [astro-ph.HE] 22 Mar 2014

March 2014

Bayesian Reconstruction of the Velocity Distribution of Weakly Interacting Massive Particles from Direct Dark Matter Detection Data

Chung-Lin Shan

Physics Division, National Center for Theoretical Sciences
No. 101, Sec. 2, Kuang-Fu Road, Hsinchu City 30013, Taiwan, R.O.C.

Department of Physics, Hangzhou Normal University
No. 16, Xuelin Street, Xiasha Higher Education Zone, Hangzhou 310036, Zhejiang, China

Kavli Institute for Theoretical Physics China, Chinese Academy of Sciences
No. 55, Zhong Guan Cun East Street, Beijing 100190, China

E-mail: clshan@phys.nthu.edu.tw

Abstract

In this paper, we extended our earlier work on the reconstruction of the (time–averaged) one–dimensional velocity distribution of Galactic Weakly Interacting Massive Particles (WIMPs) and introduce the Bayesian fitting procedure to the theoretically predicted velocity distribution functions. In this reconstruction process, the (rough) velocity distribution reconstructed by using raw data from direct Dark Matter detection experiments directly, i.e. measured recoil energies, with one or more different target materials, has been used as "reconstructed–input" information. By assuming a fitting velocity distribution function and scanning the parameter space based on the Bayesian analysis, the astronomical characteristic parameters, e.g. the Solar and Earth's orbital velocities, will be pinned down as the output results.

Our Monte–Carlo simulations show that this Bayesian scanning procedure could reconstruct the true (input) WIMP velocity distribution function pretty precisely with negligible systematic deviations of the reconstructed characteristic Solar and Earth's velocities and 1σ statistical uncertainties of $\lesssim$ 20 km/s. Moreover, for the use of an improper fitting velocity distribution function, our reconstruction process could still offer useful information about the shape of the velocity distribution. In addition, by comparing these estimates to theoretical predictions, one could distinguish different (basic) functional forms of the theoretically predicted one–dimensional WIMP velocity distribution function with 2σ to 4σ confidence levels.

1 Introduction

Currently, direct Dark Matter detection experiments searching for Weakly Interacting Massive Particles (WIMPs) are one of the promising methods for understanding the nature of Dark Matter (DM) and identifying them among new particles produced at colliders as well as studying the (sub)structure of our Galactic halo [1, 2, 3, 4].

In our earlier work [5], we developed methods for reconstructing the (moments of the) time–averaged one–dimensional velocity distribution of halo WIMPs by using the measured recoil energies directly. This analysis requires no prior knowledge about the WIMP density near the Earth nor about their scattering cross section on nucleus, the unique required information is the mass of incident WIMPs. We therefore turned to develop the method for determining the WIMP mass model–independently by combining two experimental data sets with two different target nuclei [6]. By combining these methods and using two or three experimental data sets with different detector materials, one could reconstruct the one–dimensional velocity distribution of Galactic WIMPs directly. However, as presented in Ref. [5], with a few hundreds or even thousands recorded WIMP events, only estimates of the reconstructed velocity distribution with pretty large statistical uncertainties at a few (< 10) points could be obtained.

Therefore, in order to offer more detailed information about the Galactic WIMP velocity distribution, we introduce in this paper the Bayesian analysis into our model–independent reconstruction procedure developed in Ref. [5] to be able to determine, e.g. the position of the peak of the one–dimensional velocity distribution function and the concrete values of the characteristic Solar and Earth's orbital velocities.

The remainder of this paper is organized as follows. In Sec. 2, we first review the model–independent method for reconstructing the time–averaged one–dimensional velocity distribution of halo WIMPs by using data from direct DM detection experiments directly. Then we introduce the Bayesian analysis and give the basic formulae needed in the extended reconstruction process. In Sec. 3, we present numerical results of the reconstructed WIMP velocity distribution functions based on Monte–Carlo simulations for different generating and fitting velocity distributions. Different input WIMP masses as well as impure (pseudo–)data sets mixed with (artificially added) unrejected background events will also be considered. We conclude in Sec. 4. Some technical details for our analysis will be given in Appendix.

2 Formalism

In this section, we develop the formulae needed for our Bayesian reconstruction of the one–dimensional velocity distribution function of halo WIMPs by using direct Dark Matter detection data directly.

We first review the model–independent method for reconstructing the time–averaged WIMP velocity distribution by using experimental data, i.e. measured recoil energies, from direct detection experiments. This "reconstructed data" (with estimated statistical uncertainties) will be used as input information for the further Bayesian analysis. Then, in the second part of this section, we review the basic concept of the Bayesian analysis and give the formulae needed in our extended reconstruction procedure.

2.1 Model–independent reconstruction of one–dimensional WIMP velocity distribution

In this subsection, we review briefly the method for reconstructing the one–dimensional WIMP velocity distribution from experimental data directly. Detailed derivations and discussions can be found in Ref. [5].

2.1.1 From the recoil spectrum

The basic expression for the differential event rate for elastic WIMP–nucleus scattering is given by [1]:

$$\frac{dR}{dQ} = \mathcal{A} F^2(Q) \int_{v_{\rm min}}^{v_{\rm max}} \left[\frac{f_1(v)}{v}\right] dv \,. \tag{1}$$

Here R is the direct detection event rate, i.e. the number of events per unit time and unit mass of detector material, Q is the energy deposited in the detector, $F(Q)$ is the elastic nuclear form factor, $f_1(v)$ is the one–dimensional velocity distribution function of the WIMPs impinging on the detector, v is the absolute value of the WIMP velocity in the laboratory frame. The constant coefficient $\mathcal{A}$ is defined as

$$\mathcal{A} \equiv \frac{\rho_0 \sigma_0}{2 m_\chi m_{\rm r,N}^2} \,, \tag{2}$$

where ρ_0 is the WIMP density near the Earth and σ_0 is the total cross section ignoring the form factor suppression. The reduced mass $m_{\rm r,N}$ is defined by

$$m_{\rm r,N} \equiv \frac{m_\chi m_{\rm N}}{m_\chi + m_{\rm N}} \,, \tag{3}$$

where m_χ is the WIMP mass and $m_{\rm N}$ that of the target nucleus. Finally, $v_{\rm min}$ is the minimal incoming velocity of incident WIMPs that can deposit the energy Q in the detector:

$$v_{\rm min} = \alpha \sqrt{Q} \tag{4}$$

with the transformation constant

$$\alpha \equiv \sqrt{\frac{m_{\rm N}}{2 m_{\rm r,N}^2}} \,, \tag{5}$$

and $v_{\rm max}$ is the maximal WIMP velocity in the Earth's reference frame, which is related to the escape velocity from our Galaxy at the position of the Solar system, $v_{\rm esc} \gtrsim 600$ km/s.

In our earlier work [5], it was found that, by using a time–averaged recoil spectrum dR/dQ and assuming that no directional information exists, the normalized one–dimensional velocity distribution function of incident WIMPs, $f_1(v)$, can be solved from Eq. (1) directly as

$$f_1(v) = \mathcal{N} \left\{ -2Q \cdot \frac{d}{dQ} \left[\frac{1}{F^2(Q)} \left(\frac{dR}{dQ} \right) \right] \right\}_{Q = v^2/\alpha^2} \,, \tag{6}$$

where the normalization constant $\mathcal{N}$ is given by

$$\mathcal{N} = \frac{2}{\alpha} \left\{ \int_0^\infty \frac{1}{\sqrt{Q}} \left[\frac{1}{F^2(Q)} \left(\frac{dR}{dQ} \right) \right] dQ \right\}^{-1} \,. \tag{7}$$

Here the integral goes over the entire physically allowed range of recoil energies: starting at $Q = 0$, and the upper limit of the integral has been written as ∞. Note that, because $f_1(v)$ in Eq. (6) is the normalized velocity distribution, the normalization constant $\mathcal{N}$ here is independent of the constant coefficient $\mathcal{A}$ defined in Eq. (2). Hence, as the most important consequence, the velocity distribution function of halo WIMPs reconstructed by Eq. (6) is independent of the local WIMP density ρ_0 as well as of the WIMP–nucleus cross section σ_0. However, not only the overall normalization constant $\mathcal{N}$ given in Eq. (7), but also the shape of the velocity distribution, through the transformation $Q = v^2/\alpha^2$ in Eq. (6), depends on the WIMP mass m_χ (involved in the coefficient α defined in Eq. (5)).

2.1.2 From experimental data directly

In order to use the expressions (6) and (7) for reconstructing $f_1(v)$, one needs a functional form for the recoil spectrum dR/dQ. In practice this requires usually a fit to experimental data. However, data fitting will re–introduce some model dependence and make the error analysis more complicated. Hence, expressions that allow to reconstruct $f_1(v)$ directly from data (i.e. measured recoil energies) have also been developed [5]. We started by considering experimental data described by

$$Q_n - \tfrac{b_n}{2} \leq Q_{n,i} \leq Q_n + \tfrac{b_n}{2}\,, \qquad\qquad i = 1,\ 2,\ \cdots,\ N_n,\ n = 1,\ 2,\ \cdots,\ B. \tag{8}$$

Here the entire experimental possible energy range between the minimal and maximal cut–offs $Q_{\rm min}$ and $Q_{\rm max}$ has been divided into B bins with central points Q_n and widths b_n. In each bin, N_n events will be recorded.

As argued in Ref. [5], the statistical uncertainty on the "slope of the recoil spectrum", $[d/dQ\,(dR/dQ)]_{Q=Q_n}$, appearing in the expression (6), scales like the bin width to the power -1.5. In addition, the wider the bin width, the more the recorded events in this bin, and thus the smaller the statistical uncertainty on the estimator of $[d/dQ\,(dR/dQ)]_{Q=Q_n}$. Hence, since the recoil spectrum dR/dQ is expected to be approximately exponential [5], in order to approximate the spectrum in a rather wider range, instead of the conventional standard linear approximation, the following exponential ansatz for the measured recoil spectrum (before normalized by the exposure $\mathcal{E}$) in the nth bin has been introduced [5]:

$$\left(\frac{dR}{dQ}\right)_{\text{expt},\ n} \equiv \left(\frac{dR}{dQ}\right)_{\text{expt},\ Q \simeq Q_n} \equiv r_n\, e^{k_n (Q - Q_{s,n})}\,. \tag{9}$$

Here r_n is the standard estimator for $(dR/dQ)_{\rm expt}$ at $Q = Q_n$:

$$r_n = \frac{N_n}{b_n}\,, \tag{10}$$

k_n is the logarithmic slope of the recoil spectrum in the nth $Q-$bin, which can be computed numerically from the average value of the measured recoil energies in this bin:

$$\overline{Q - Q_n}|_n = \left(\frac{b_n}{2}\right) \coth\left(\frac{k_n b_n}{2}\right) - \frac{1}{k_n}\,, \tag{11}$$

where

$$\overline{(Q - Q_n)^\lambda}|_n \equiv \frac{1}{N_n} \sum_{i=1}^{N_n} \left(Q_{n,i} - Q_n\right)^\lambda\,. \tag{12}$$

Then the shifted point $Q_{s,n}$ in the ansatz (9), at which the leading systematic error due to the ansatz is minimal [5], can be estimated by

$$Q_{s,n} = Q_n + \frac{1}{k_n} \ln \left[\frac{\sinh(k_n b_n/2)}{k_n b_n/2} \right] . \tag{13}$$

Note that $Q_{s,n}$ differs from the central point of the nth bin, Q_n.

Now, substituting the ansatz (9) into Eq. (6) and then letting $Q = Q_{s,n}$, we can obtain that

$$f_{1,\mathrm{rec}}(v_{s,n}) = \mathcal{N} \left[\frac{2 Q_{s,n} r_n}{F^2(Q_{s,n})} \right] \left[\frac{d}{dQ} \ln F^2(Q) \Big|_{Q=Q_{s,n}} - k_n \right] . \tag{14}$$

Here

$$v_{s,n} = \alpha \sqrt{Q_{s,n}} \, , \tag{15}$$

and the normalization constant $\mathcal{N}$ given in Eq. (7) can be estimated directly from the data by

$$\mathcal{N} = \frac{2}{\alpha} \left[\sum_a \frac{1}{\sqrt{Q_a} \, F^2(Q_a)} \right]^{-1} , \tag{16}$$

where the sum runs over all events in the sample.

2.1.3 Windowing the data set

As mentioned above, the statistical uncertainty on the slope of the recoil spectrum around the central point Q_n, $[d/dQ \, (dR/dQ)]_{Q \simeq Q_n}$, is approximately proportional to $b_n^{-1.5}$. Thus, in order to reduce the statistical uncertainty on the velocity distribution reconstructed by Eq. (14), it seems to be better to use large bin width. However, neither the conventional linear approximation:

$$\left(\frac{dR}{dQ} \right)_{\mathrm{expt},\ Q=Q_n} = \frac{N_n}{b_n} \tag{17}$$

nor the exponential ansatz given in Eq. (9) can describe the real (but as yet unknown) recoil spectrum exactly. The neglected terms of higher powers of $Q - Q_n$ could therefore induce some uncontrolled systematic errors which increase with increasing bin width. Moreover, since the number of bins scales inversely with their size, by using larger bins we would be able to estimate $f_1(v)$ only at a smaller number of velocities. Additionally, once a quite large bin width is used, it would correspondingly lead to a quite large value of the first reconstructible point of $f_1(v)$, i.e. $f_{1,\mathrm{rec}}(v_{s,1})$, since the central point Q_1 as well as the shifted point $Q_{s,1}$ of the first bin would be quite large. Finally, choosing a fixed bin size, as one conventionally does, would let errors on the estimated logarithmic slopes, and hence also on the estimates of $f_1(v)$, increase quickly with increasing Q or v. This is due to the essentially exponential form of the expected recoil spectrum, which would lead to a quickly falling number of events in equal–sized bins. By some trial–and–error analyses it was found that the errors are roughly equal in all bins if the bin widths increase linearly [5].

Therefore, it has been introduced in Ref. [5] that one can first collect experimental data in relatively small bins and then combining varying numbers of bins into overlapping "windows". In particular, the first window would be identical with the first bin. One starts by binning the data, as in Eq. (8), where the bin widths satisfy

$$b_n = b_1 + (n-1)\delta \, , \tag{18}$$

i.e.

$$Q_n = Q_{\min} + \left(n - \frac{1}{2}\right) b_1 + \left[\frac{(n-1)^2}{2}\right] \delta \,. \tag{19}$$

Here the increment δ satisfies

$$\delta = \frac{2}{B(B-1)} \Big(Q_{\max} - Q_{\min} - B b_1 \Big) \,, \tag{20}$$

B being the total number of bins, and $Q_{(\min,\max)}$ are the experimental minimal and maximal cut–off energies. Assume up to n_W bins are collected into a window, with smaller windows at the borders of the range of Q.

In order to distinguish the numbers of bins and windows, hereafter Latin indices $n,\ m,\ \cdots$ are used to label bins, and Greek indices $\mu,\ \nu,\ \cdots$ to label windows. For $1 \le \mu \le n_W$, the μth window simply consists of the first μ bins; for $n_W \le \mu \le B$, the μth window consists of bins $\mu - n_W + 1,\ \mu - n_W + 2,\ \cdots,\ \mu$; and for $B \le \mu \le B + n_W - 1$, the μth window consists of the last $n_W - (\mu - B)$ bins. This can also be described by introducing the indices $n_{\mu-}$ and $n_{\mu+}$ which label the first and last bins contributing to the μth window, with

$$n_{\mu-} = \begin{cases} 1, & \text{for } \mu \le n_W, \\ \mu - n_W + 1, & \text{for } \mu \ge n_W, \end{cases} \tag{21a}$$

and

$$n_{\mu+} = \begin{cases} \mu, & \text{for } \mu \le B, \\ B, & \text{for } \mu \ge B. \end{cases} \tag{21b}$$

The total number of windows defined through Eqs. (21a) and (21b) is evidently $W = B + n_W - 1$, i.e. $1 \le \mu \le B + n_W - 1$.

As shown above, the basic observables needed for the reconstruction of $f_1(v)$ by Eq. (14) are the number of events in the nth $Q-$bin, N_n, as well as the average value of the measured recoil energies in this bin, $\overline{Q - Q_n}|_n$. For a "windowed" data set, one can easily calculate the number of events per window as

$$N_\mu = \sum_{n=n_{\mu-}}^{n_{\mu+}} N_n \,, \tag{22}$$

as well as the average value of the measured recoil energies

$$\overline{Q - Q_\mu}|_\mu = \frac{1}{N_\mu} \left(\sum_{n=n_{\mu-}}^{n_{\mu+}} N_n \overline{Q}|_n \right) - Q_\mu \,, \tag{23}$$

where Q_μ is the central point of the μth window. The exponential ansatz in Eq. (9) is now assumed to hold over an entire window. We can then estimate the prefactor as

$$r_\mu = \frac{N_\mu}{w_\mu} \,, \tag{24}$$

w_μ being the width of the μth window. The logarithmic slope of the recoil spectrum in the μth window, k_μ, as well as the shifted point $Q_{s,\mu}$ (from the central point of each "window", Q_μ) can be calculated as in Eqs. (11) and (13) with "bin" quantities replaced by "window" quantities. Finally, note that, due to the combination of bins into overlapping windows, these quantities are

all correlated (for $n_W \neq 1$). The covariance matrix of the estimates of $f_1(v)$ at adjacent values of $v_{s,\mu} = \alpha\sqrt{Q_{s,\mu}}$ is given by[1]

$$\begin{aligned}
&\mathrm{cov}\Big(f_{1,\mathrm{rec}}(v_{s,\mu}), f_{1,\mathrm{rec}}(v_{s,\nu})\Big) \\
&= \left[\frac{f_{1,\mathrm{rec}}(v_{s,\mu}) f_{1,\mathrm{rec}}(v_{s,\nu})}{r_\mu r_\nu}\right] \mathrm{cov}\left(r_\mu, r_\nu\right) + (2\mathcal{N})^2 \left[\frac{Q_{s,\mu} Q_{s,\nu} r_\mu r_\nu}{F^2(Q_{s,\mu}) F^2(Q_{s,\nu})}\right] \mathrm{cov}\left(k_\mu, k_\nu\right) \\
&\qquad - \mathcal{N}\left\{\left[\frac{f_{1,\mathrm{rec}}(v_{s,\mu})}{r_\mu}\right]\left[\frac{2 Q_{s,\nu} r_\nu}{F^2(Q_{s,\nu})}\right] \mathrm{cov}\left(r_\mu, k_\nu\right) + \Big(\mu \longleftrightarrow \nu\Big)\right\} . \qquad (25)
\end{aligned}$$

2.2 Bayesian analysis

In this subsection, we review the basic concept of the Bayesian analysis [7] (for its applications in physics, see e.g. Ref. [8], and for its recent applications in direct DM detection phenomenology, see e.g. Refs. [9, 10, 11, 12, 13, 14]) and extend this method to the use of the "reconstructed data" offered by our model–independent reconstruction process described in the previous subsection.

2.2.1 Baye's theorem

We start with the *Baye's theorem*: the probability of A given that B is true multiplies the probability of that B is true is equal to the probability of that A and B happen simultaneously, which is also equal to the probability of B given that A is true multiplies the probability of that A is true. This can simply expressed as

$$\mathrm{p}(A|B)\,\mathrm{p}(B) = \mathrm{p}(A \cap B) = \mathrm{p}(B|A)\,\mathrm{p}(A)\,, \qquad (26)$$

where $\mathrm{p}(A|B)$ is called the "conditional probability" of A given that B is true. As long as $\mathrm{p}(B) \neq 0$, the above equation can be rewritten as

$$\begin{aligned}
\mathrm{p}(A|B) &= \frac{\mathrm{p}(B|A)\,\mathrm{p}(A)}{\mathrm{p}(B)} \\
&= \frac{\mathrm{p}(B|A)\,\mathrm{p}(A)}{\mathrm{p}(B|A)\,\mathrm{p}(A) + \mathrm{p}(B|\overline{A})\,\mathrm{p}(\overline{A})}\,, \qquad (27)
\end{aligned}$$

where $\mathrm{p}(\overline{A}) = 1 - \mathrm{p}(A)$ is the probability of the complement of A, i.e. the probability of that A is not happen.

2.2.2 Bayesian statistics

Applying the Baye's theorem described above, one can directly have that

$$\mathrm{p}(\mathrm{theory}|\mathrm{result}) = \frac{\mathrm{p}(\mathrm{result}|\mathrm{theory})}{\mathrm{p}(\mathrm{result})} \cdot \mathrm{p}(\mathrm{theory})\,. \qquad (28)$$

This means that, given the observed result, the probability of that a specified theory is true is proportional to the probability of the observed result in the specified theory multiplies the probability of the specified theory.

[1]Note that Eq. (25) should in principle also include contributions involving the statistical error on the estimator for $\mathcal{N}$ in Eq. (16). However, this error and its correlations with the errors on the r_μ and k_μ have been found to be negligible compared to the errors included in Eq. (25) [5].

This statement can be understood as follows. If the observed result is predicted by a specified theory to be highly unlikely or even impossible/forbidden, then this observation makes the "degree of belief" of this specified theory small or even disproves this theory. In contrast, the observation of a prediction by a specified theory with a high probability will strengthen one's belief in this theory.

2.2.3 Bayesian analysis

By extending Eq. (28), we can obtain that

$$\mathrm{p}(\Theta|\mathrm{data}) = \frac{\mathrm{p}(\mathrm{data}|\Theta)}{\mathrm{p}(\mathrm{data})} \cdot \mathrm{p}(\Theta)\,. \tag{29}$$

Here $\Theta = \{a_1, a_2, \cdots, a_{N_{\mathrm{Bayesian}}}\}$ denotes a specified (combination of the) value(s) of the fitting parameter(s); $\mathrm{p}(\Theta)$, called "prior probability", represents our degree of belief about Θ being the true value(s) of fitting parameter(s), which is often given in form of the (multiplication of the) probability distribution(s) of the fitting parameter(s). $\mathrm{p}(\mathrm{data})$, called "evidence", is the total probability of obtaining the particular set of data, which is in practice irrespective of the actual value(s) of the parameter(s) and can be treated as a normalization constant; it will not be of interest in our further discussion. $\mathrm{p}(\mathrm{data}|\Theta)$ denotes the probability of the observed result, once the specified (combination of the) value(s) of the fitting parameter(s) happens, which can usually be described by the *likelihood* function of Θ, $\mathcal{L}(\Theta)$. Finally, $\mathrm{p}(\Theta|\mathrm{data})$, called the "posterior probability density function" for Θ, representes the probability of that the specified (combination of the) value(s) of the fitting parameter(s) happens, given the observed result.

2.2.4 Bayesian reconstruction of $f_1(v)$

Now, we can describe the procedure of our Bayesian reconstruction of the one–dimensional WIMP velocity distribution function in detail.

First, by using Eqs. (14) to (16), one can obtain $W = B + n_W - 1$ reconstructed data points: $\Big(v_{s,\mu}, f_{1,\mathrm{rec}}(v_{s,\mu}) \pm \sigma_{f_1,s,\mu}\Big)$, for $\mu = 1,\ 2,\ \cdots,\ W$, where

$$\sigma_{f_1,s,\mu} \equiv \sqrt{\mathrm{cov}\Big(f_{1,\mathrm{rec}}(v_{s,\mu}), f_{1,\mathrm{rec}}(v_{s,\mu})\Big)} \tag{30}$$

denote the square roots of the diagonal entries of the covariance matrix given in Eq. (25). Choosing a theoretical prediction of the one–dimensional velocity distribution of halo WIMPs with one or more fitting parameters: $f_{1,\mathrm{th}}(v; a_1, a_2, \cdots, a_{N_{\mathrm{Bayesian}}})$ and assuming that the reconstructed data points is *Gaussian*–distributed around the theoretical predictions $f_{1,\mathrm{th}}(v_{s,\mu}; a_1, a_2, \cdots, a_{N_{\mathrm{Bayesian}}})$, the likelihood function for $\mathrm{p}(\mathrm{data}|\Theta)$ can then be defined by

$$\begin{aligned}
&\mathcal{L}\Big(f_{1,\mathrm{rec}}(v_{s,\mu}),\ \mu = 1,\ 2,\ \cdots,\ W;\ a_i,\ i = 1,\ 2,\ \cdots,\ N_{\mathrm{Bayesian}}\Big) \\
&\equiv \prod_{\mu=1}^{W} \mathrm{Gau}\Big(v_{s,\mu}, f_{1,\mathrm{rec}}(v_{s,\mu}), \sigma_{f_1,s,\mu}; a_1, a_2, \cdots, a_{N_{\mathrm{Bayesian}}}\Big)\,,
\end{aligned} \tag{31}$$

where

$$\begin{aligned}
&\mathrm{Gau}\Big(v_{s,\mu}, f_{1,\mathrm{rec}}(v_{s,\mu}), \sigma_{f_1,s,\mu}; a_1, a_2, \cdots, a_{N_{\mathrm{Bayesian}}}\Big) \\
&\equiv \frac{1}{\sqrt{2\pi}\,\sigma_{f_1,s,\mu}}\, e^{-\left[f_{1,\mathrm{rec}}(v_{s,\mu}) - f_{1,\mathrm{th}}(v_{s,\mu}; a_1, a_2, \cdots, a_{N_{\mathrm{Bayesian}}})\right]^2 \Big/ 2\sigma^2_{f_1,s,\mu}}\,.
\end{aligned} \tag{32}$$

Or, equivalently, we can use the *logarithmic* likelihood function given by

$$\begin{aligned}
&\ln\mathcal{L}\Big(f_{1,\rm rec}(v_{s,\mu}),\ \mu=1,\ 2,\ \cdots,\ W;\ a_i,\ i=1,\ 2,\ \cdots,\ N_{\rm Bayesian}\Big)\\
&=-\frac{1}{2}\sum_{\mu=1}^{W}\frac{\Big[f_{1,\rm rec}(v_{s,\mu})-f_{1,\rm th}(v_{s,\mu};a_1,a_2,\cdots,a_{N_{\rm Bayesian}})\Big]^2}{\sigma^2_{f_1,s,\mu}}-\sum_{\mu=1}^{W}\ln\Big(\sqrt{2\pi}\,\sigma_{f_1,s,\mu}\Big)\ . \qquad (33)
\end{aligned}$$

Note that in practical use the second term in Eq. (33) can be neglected, since it is just a constant for all scanned (combinations of) values of the fitting parameter(s) $(a_1, a_2, \cdots, a_{N_{\rm Bayesian}})$.

Finally, choosing the probability distribution function for each fitting parameter a_i, $\mathrm{p}_i(a_i)$, the posterior probability density on the left–hand side of Eq. (29) can then be given by

$$\begin{aligned}
&\mathrm{p}\Big(a_i,\ i=1,\ 2,\ \cdots,\ N_{\rm Bayesian}\ \Big|\ f_{1,\rm rec}(v_{s,\mu}),\ \mu=1,\ 2,\ \cdots,\ W\Big)\\
&\propto\mathcal{L}\Big(f_{1,\rm rec}(v_{s,\mu}),\ \mu=1,\ 2,\ \cdots,\ W;\ a_i,\ i=1,\ 2,\ \cdots,\ N_{\rm Bayesian}\Big)\prod_{i=1}^{N_{\rm Bayesian}}\mathrm{p}_i(a_i)\,. \qquad (34)
\end{aligned}$$

3 Numerical results

In this section, we present numerical results of our Bayesian reconstruction of the one–dimensional velocity distribution function of halo WIMPs based on Monte–Carlo simulations.

In order to test whether we can reconstruction $f_1(v)$ correctly with even an improper adopted model and/or incorrect expected value(s) of the fitting parameter(s), different choices of the WIMP velocity distribution function for generating signal events as well as different assumptions of $f_1(v)$ and/or (slightly) different value(s) of the fitting parameter(s) from the commonly adopted values for the Bayesian fitting process will be condisered in our simulations. In Tables 1, 3 and 8, we list the *input* setup for the chosen *input* velocity distribution functions used for *generating* WIMP signals as well as the scanning ranges, expected values and 1σ uncertainties of the fitting parameters used for different *fitting* velocity distributions. Additionally, a common maximal cut-off on the one-dimensional WIMP velocity distribution has been set as $v_{\rm max} = 700$ km/s.

The WIMP mass m_χ involved in the coefficient α in Eqs. (15) and (16) for estimating the reconstructed points $v_{s,\mu}$ as well as the normalization constant $\mathcal{N}$ has been assumed either to be known precisely with a negligible uncertainty from other (e.g. collider) experiments or be determined from direct detection experiments with *different* data sets. As in Ref. [5], a ^{76}Ge nucleus has been chosen as our detector material for reconstructing $f_1(v)$, whereas a ^{28}Si target and a *second* ^{76}Ge target have been used for determining m_χ [6].

As in Refs. [5, 15], the WIMP–nucleus cross section in Eq. (2) has been assumed to be only spin–independent (SI), $\sigma^{\rm SI}_{\chi\rm p} = 10^{-9}$ pb, and the commonly used analytic form for the elastic nuclear form factor:

$$F^2_{\rm SI}(Q)=\left[\frac{3j_1(qR_1)}{qR_1}\right]^2 e^{-(qs)^2} \qquad (35)$$

has been adopted. Here Q is the recoil energy transferred from the incident WIMP to the target nucleus, $j_1(x)$ is a spherical Bessel function, $q=\sqrt{2m_{\rm N}Q}$ is the transferred 3-momentum, for the effective nuclear radius we use $R_1=\sqrt{R_A^2-5s^2}$ with $R_A\simeq 1.2\,A^{1/3}$ fm and a nuclear skin thickness $s\simeq 1$ fm.

In our simulations, the experimental threshold energies have been assumed to be negligible ($Q_{\rm min} = 0$) and the maximal cut–off energies are set as $Q_{\rm max} = 100$ keV for all target nuclei[2]; the widths of the first energy bin in Eq. (18) have also been set commonly as $b_1 = 10$ keV. Additionally, we assumed that all experimental systematic uncertainties as well as the uncertainty on the measurement of the recoil energy could be ignored. The energy resolution of most existing and next–generation detectors should be good enough so that the very small measurement uncertainties can be neglected compared to the statistical uncertainties on our reconstructed results with only few events. Energy range between $Q_{\rm min}$ and $Q_{\rm max}$ have been divided into five bins and up to three bins have been combined to a window. ($3\times$) 5,000 experiments with 500 total events on average in one experiment have been simulated. In Secs. 3.1 to 3.3, the input WIMP mass has been fixed as $m_\chi = 100$ GeV. In Sec. 3.4, we consider the cases with a light WIMP mass of $m_\chi = 25$ GeV and a heavy one of $m_\chi = 250$ GeV. In addition, in Sec. 3.5, we consider also briefly the effects of unrejected background events for different input WIMP masses [16, 15].

Note that for our numerical simulations presented in this section, the actual numbers of generated signal and background events in each simulated experiment are Poisson–distributed around their expectation values *independently*. This means that, for example, for simulations shown in Figs. 30 we generate 400 (100) events *on average* for WIMP–signals (backgrounds) and the total event number recorded in one experiment is then the sum of these two numbers.

Regarding our degree of belief about the expected value of each fitting parameter a_i, i.e. $\mathrm{p}_i(a_i)$ in Eq. (34), two probability distribution functions have been considered. The simplest one is the flat–distribution:

$$\mathrm{p}_i(a_i) = 1\,, \qquad\qquad \text{for } a_{i,\rm min} \leq a_i \leq a_{i,\rm max}, \tag{37}$$

where $a_{i,(\rm min,max)}$ denote the minimal and maximal bounds of the scanning interval of the fitting parameter a_i. On the other hand, for the case that we have already prior knowledge about one fitting parameter, a Gaussian–distribution:

$$\mathrm{p}_i(a_i; \mu_{a,i}, \sigma_{a,i}) = \frac{1}{\sqrt{2\pi}\,\sigma_{a,i}}\, e^{-(a_i-\mu_{a,i})^2/2\sigma_{a,i}^2} \tag{38}$$

with the expected value $\mu_{a,i}$ of and the 1σ uncertainty $\sigma_{a,i}$ on the fitting parameter a_i is used.

Note that, in one simulated experiment, we scan the parameter space $(a_1, a_2, \cdots, a_{N_{\rm Bayesian}})$ in the volume $a_i \in [a_{i,\rm min}, a_{i,\rm max}]$, $i = 1, 2, \cdots, N_{\rm Bayesian}$ to find a particular point $(a_1^*, a_2^*, \cdots, a_{N_{\rm Bayesian}}^*)$, which maximizes the (numerator of the) posterior probability density $\mathrm{p}\Big(a_i,\ i=1,\ 2,\ \cdots,\ N_{\rm Bayesian}\ \Big|\ f_{1,\rm rec}(v_{s,\mu}),\ \mu=1,\ 2,\ \cdots,\ W\Big)$. After that all simulations have been done, we determine the median value of the (1σ lower and upper bounds of the) velocity distribution reconstructed by Eq. (14) from all experiments, denoted as $f_{1,\rm median}\left(\alpha_{(\rm median)}\sqrt{Q_{s,\mu,\rm Bayesian}}\right)$, for $\mu = 1,\ 2,\ \cdots,\ W$, and shown as solid black crosses in the (top–)left frame(s) of, e.g. Figs. 1. And we define further

$$\begin{aligned} &\mathrm{p}_{\rm median}\Big(a_i,\ i=1,\ 2,\ \cdots,\ N_{\rm Bayesian}\Big) \\ &\equiv \mathrm{p}\Big(a_i,\ i=1,\ 2,\ \cdots,\ N_{\rm Bayesian}\ \Big|\ f_{1,\rm median}\left(\alpha_{(\rm median)}\sqrt{Q_{s,\mu,\rm Bayesian}}\right),\ \mu=1,\ 2,\ \cdots,\ W\Big)\,. \end{aligned} \tag{39}$$

[2]Note that, due to the maximal cut-off on the one-dimensional WIMP velocity distribution, $v_{\rm max}$, a kinematic maximal cut–off energy

$$Q_{\rm max,kin} = \frac{v_{\rm max}^2}{\alpha^2} \tag{36}$$

has also been taken into account.

Input: simple Maxwellian velocity distribution $f_{1,\mathrm{Gau}}(v)$					
Fitting model	Parameter	Input/theoretical value	Scanning range	Expected value	1σ uncertainty
Simple	v_0 [km/s]	220	[160, 300]	230	20

Table 1: The input setup for the simple Maxwellian velocity distribution $f_{1,\mathrm{Gau}}(v)$ used for generating WIMP events as well as the scanning range, the expected value and the 1σ uncertainty on the unique fitting parameter v_0.

and check the points $(a_1^*, a_2^*, \cdots, a_{N_{\mathrm{Bayesian}}}^*)$ obtained from all simulated experiments to find the special ("best–fit") point $(a_{1,\mathrm{max}}, a_{2,\mathrm{max}}, \cdots, a_{N_{\mathrm{Bayesian}},\mathrm{max}})$, which maximizes $\mathrm{p}_{\mathrm{median}}(a_i,\ i = 1,\ 2,\ \cdots,\ N_{\mathrm{Bayesian}})$.

3.1 Simple Maxwellian velocity distribution

We consider first the simplest isothermal spherical Galactic halo model for generating WIMP events. The normalized one–dimensional simple Maxwellian velocity distribution function can be expressed as [1, 5]:

$$f_{1,\mathrm{Gau}}(v) = \frac{4}{\sqrt{\pi}} \left(\frac{v^2}{v_0^3}\right) e^{-v^2/v_0^2}\,, \tag{40}$$

where $v_0 \approx 220$ km/s is the Solar orbital velocity in the Galactic frame.

In Table 1, we list the input setup for the simple Maxwellian velocity distribution $f_{1,\mathrm{Gau}}(v)$ used for generating WIMP events as well as the scanning range, the expected value and the 1σ uncertainty on the unique fitting parameter v_0. Note that, for generating WIMP signals, $v_0 = 220$ km/s has been used, whereas for Bayesian fitting of this unique parameter we used a slightly different value of $v_0 = 230$ km/s and set a 1σ uncertainty of $\sigma(v_0) = 20$ km/s.

3.1.1 Simple Maxwellian velocity distribution

As the simplest Galactic halo model, we consider first the use of the simple Maxwellian velocity distribution $f_{1,\mathrm{Gau}}(v)$ given in Eq. (40) with an unique fitting parameter v_0 to fit the reconstructed–input data given by Eqs. (14) to (16) and (25).

In Fig. 1(a), we show the reconstructed simple Maxwellian velocity distribution function for an input WIMP mass of 100 GeV with a ^{76}Ge target. Here the flat distribution given by Eq. (37) for the fitting parameter v_0 has been used. The black crosses are the velocity distribution reconstructed by Eqs. (15) and (14): the vertical error bars show the square roots of the diagonal entries of the covariance matrix given in Eq. (25) (i.e. $\sigma_{f_{1,s,\mu}}$ given in Eq. (30)) and the horizontal bars indicate the sizes of the windows used for estimating $f_{1,\mathrm{rec}}(v_{s,\mu})$, respectively. The solid red curve is the *generating* simple Maxwellian velocity distribution with an input velue of $v_0 = 220$ km/s. While the dashed green curve indicates the *reconstructed* simple Maxwellian velocity distribution with the fitting parameter v_0 given by the *median* value of all simulated experiments, the dash–dotted blue curve indicates the *reconstructed* simple Maxwellian velocity distribution with v_0 which maximizes $\mathrm{p}_{\mathrm{median}}\,(a_i,\ i = 1,\ 2,\ \cdots,\ N_{\mathrm{Bayesian}})$ defined in Eq. (39).

Meanwhile, the light–green (light–blue) area shown here indicate the $1\,(2)\,\sigma$ statistical uncertainty bands of the Bayesian reconstructed velocity distribution function, which has been determined as follows. After scanning the reconstructed fitting parameter v_0 obtained from all

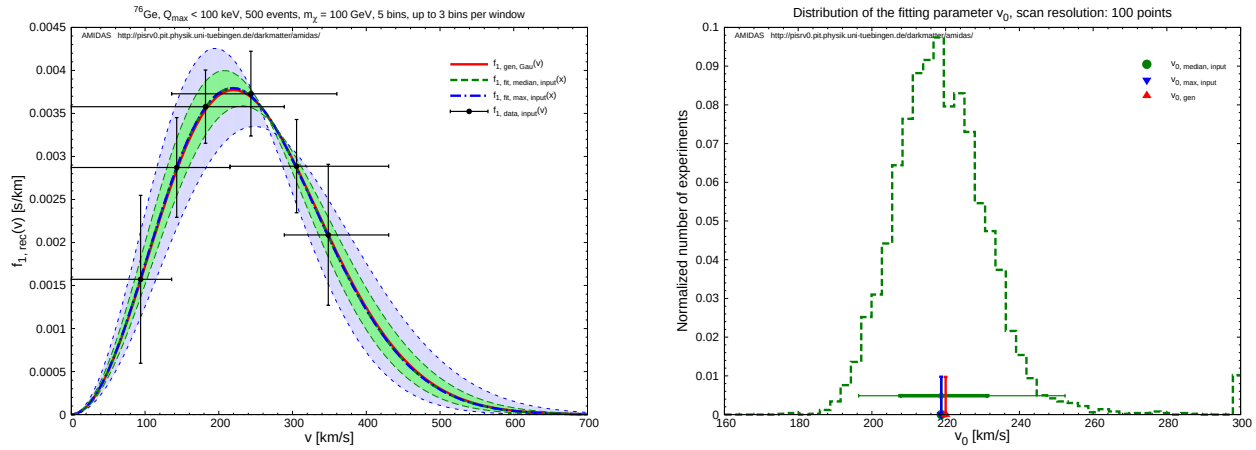

(a) (b)

Figure 1: (a) The reconstructed simple Maxwellian velocity distribution function for an input WIMP mass of 100 GeV with a ^{76}Ge target. The black crosses are the velocity distribution reconstructed by Eqs. (15) and (14): the vertical error bars show the square roots of the diagonal entries of the covariance matrix estimated by Eq. (25) (i.e., $\sigma_{f_1,s,\mu}$ given in Eq. (30)) and the horizontal bars indicate the sizes of the windows used for estimating $f_{1,\mathrm{rec}}(v_{s,\mu})$, respectively. The solid red curve is the *generating* simple Maxwellian velocity distribution with an input velue of $v_0 = 220$ km/s. While the dashed green curve indicates the *reconstructed* simple Maxwellian velocity distribution with the fitting parameter v_0 given by the *median* value of all simulated experiments, the dash–dotted blue curve indicates the *reconstructed* simple Maxwellian velocity distribution with v_0 which maximizes $\mathrm{p}_{\mathrm{median}}\,(a_i,\ i = 1,\ 2,\ \cdots,\ N_{\mathrm{Bayesian}})$ defined in Eq. (39). (b) The distribution of the Bayesian reconstructed fitting parameter v_0 in all simulated experiments. The red vertical line indicates the true (input) value of v_0, which has been labeled with the subscript "gen". The green vertical line indicates the median values of the simulated results, whereas and blue one indicates the value which maximizes $\mathrm{p}_{\mathrm{median}}$. In addition, the horizontal thick (thin) green bars show the 1 (2) σ ranges of the reconstructed results. See the text for further details.

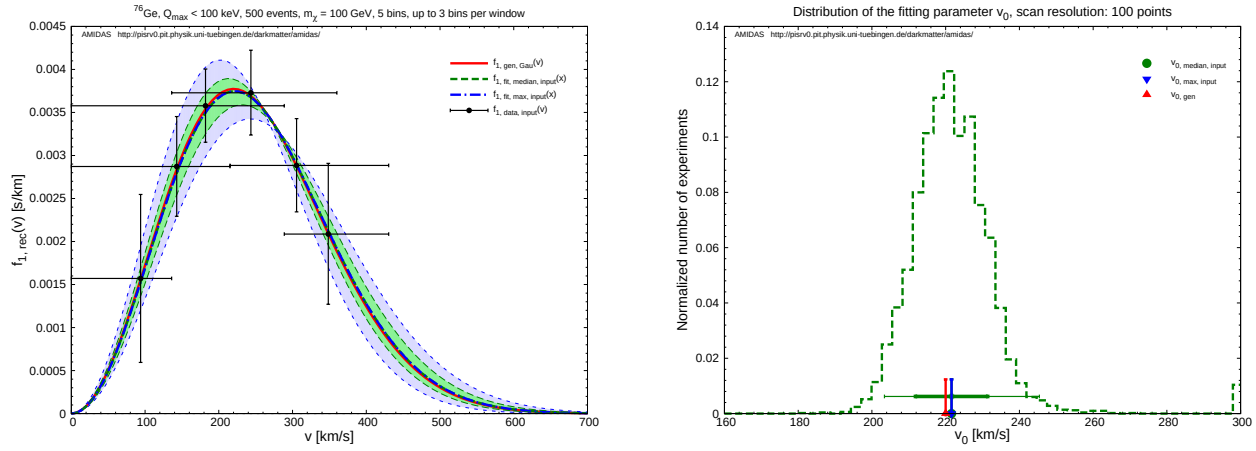

(a) (b)

Figure 2: As in Figs. 1, except that the Gaussian probability distribution given in Eq. (38) for v_0 with an expected value of $v_0 = 230$ km/s and a 1σ uncertainty of 20 km/s has been used.

Input: simple Maxwellian velocity distribution $f_{1,\mathrm{Gau}}(v)$						
Reconstruction: simple Maxwellian velocity distribution $f_{\mathbf{1,Gau}}(v)$						
Parameter	WIMP mass	Prob. dist.	Max. $\mathrm{p_{median}}$	Median	1σ range	2σ range
v_0 [km/s]	Input	Flat	218.8	$218.8\,^{+12.6}_{-11.2}\,(^{+33.6}_{-22.4})$	[207.6, 231.4]	[196.4, 252.4]
		Gaussian	221.6	$221.6 \pm 9.8\,(^{+23.8}_{-18.2})$	[211.8, 231.4]	[203.4, 245.4]
	Reconst.	Flat	220.2	$218.8\,^{+21.0}_{-16.8}\,(^{+49.0}_{-33.6})$	[202.0, 239.8]	[185.2, 267.8]
		Gaussian	220.2	$221.6\,^{+15.4}_{-12.6}\,(^{+33.6}_{-26.6})$	[209.0, 237.0]	[195.0, 255.2]

Table 2: The reconstructed results of v_0 for all four considered cases with the simple Maxwellian velocity distribution $f_{1,\mathrm{Gau}}(v)$ as well as the $1\,(2)\,\sigma$ uncertainty ranges of the median values.

simulated experiments and ordering according to their $\mathrm{p_{median}}$ values defined in Eq. (39) *descendingly*, we can not only determine the point which maximizes $\mathrm{p_{median}}$ (labeled with the subscript "max" in our plots[3]), but also the smallest and largest values of the first 68.27% (95.45%) of all these reconstructed v_0's. We then use the smallest (largest) value of the first 68.27% (95.45%) reconstructed v_0's to give the $1\,(2)\,\sigma$ lower (upper) boundaries of the Bayesian reconstructed velocity distribution function. This means that all of the velocity distributions with v_0's which give the largest 68.27% (95.45%) $\mathrm{p_{median}}$ values should be in the $1\,(2)\,\sigma$ light–green (light–blue) areas.

On the other hand, Fig. 1(b) shows the distribution of the Bayesian reconstructed fitting parameter v_0 in all simulated experiments. The red vertical line indicates the true (input) value of v_0, which has been labeled with the subscript "gen". The green vertical line indicates the median values of the simulated results, whereas and blue one indicates the value which maximizes $\mathrm{p_{median}}$. In addition, the horizontal thick (thin) green bars show the $1\,(2)\,\sigma$ ranges of the reconstructed results[4].

In Figs. 1, it can be seen clearly that, *without* a prior knowledge about the Solar orbital velocity, one could in principle pin down the parameter v_0 very precisely with $1\,(2)\,\sigma$ statistical uncertainties of only $^{+12.6}_{-11.2}\,(^{+33.6}_{-22.4})$ km/s (see Table 2). Moreover, by using the Bayesian reconstruction of the one–dimensional velocity distribution function, the large (1σ) statistical uncertainty given by Eqs. (14) to (16) can be reduced significantly: the band of the 2σ statistical uncertainty would be approximately equal to or even smaller than the (solid black) vertical 1σ uncertainty bars!

Furthermore, in Figs. 2 we consider the case with a rough prior knowledge about the Solar orbital velocity v_0. It has been found that, firstly, by using a Gaussian probability distribution for v_0 with a 1σ uncertainty of 20 km/s, one could reduce the $1\,(2)\,\sigma$ statistical uncertainties on the Bayesian reconstructed parameter v_0 to $\pm 9.8\,(^{+23.8}_{-18.2})$ km/s (see Table 2). Secondly and more importantly, although an expected value of $v_0 = 230$ km/s, which differs (slightly) from the true (input) one, is used, the value of the fitting parameter v_0 could still be pin down precisely with

[3]Note that the subscript "input" in Figs. 1 and 2 indicate that the WIMP mass needed in Eqs. (15) and (14) has been given as the input WIMP mass; whereas, the subscript "algo" in Figs. 3 and 4 indicate that the WIMP mass is reconstructed by the algorithmic procedure developed in Ref. [6].

[4]Note that the $1\,(2)\,\sigma$ ranges given here mean that, according to the order of the reconstructed values of v_0 *along* and centered at their *median* value $v_{0,\mathrm{median}}$, 68.27% (95.45%) of the reconstructed values in the simulated experiments are in this range.

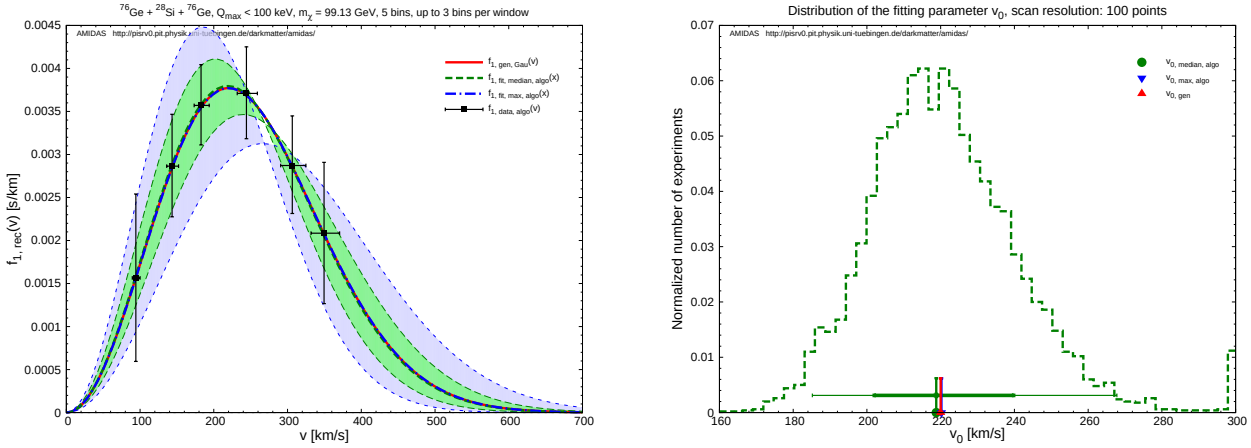

(a) (b)

Figure 3: As in Figs. 1, except that the WIMP mass m_χ needed in Eqs. (15) and (16) is reconstructed by the algorithmic procedure developed in Ref. [6] with a ^{28}Si target and a second ^{76}Ge target. While the vertical bars show the 1σ statistical uncertainties estimated by Eq. (25) taking into account the 1σ statistical uncertainty on the reconstructed WIMP mass, the horizontal bars shown here indicate the 1σ statistical uncertainties on the estimates of $v_{s,\mu}$ given in Eq. (15) due to the uncertainty on the reconstructed WIMP mass; the statistical and systematic uncertainties due to estimating of $Q_{s,\mu}$ have been neglected here.

a tiny systematic deviation (< 2 km/s).

In Figs. 3 and 4, we consider the case that the WIMP mass m_χ needed in Eqs. (15) and (16) is reconstructed by the algorithmic procedure developed in Ref. [6] with a ^{28}Si target and a second ^{76}Ge target. Note that, while the vertical bars show the 1σ statistical uncertainties estimated by Eq. (25) taking into account the 1σ statistical uncertainty on the reconstructed WIMP mass, the horizontal bars shown here indicate the 1σ statistical uncertainties on the estimates of $v_{s,\mu}$ given in Eq. (15) due to the uncertainty on the reconstructed WIMP mass; the statistical and systematic uncertainties due to estimating of $Q_{s,\mu}$ have been neglected here.

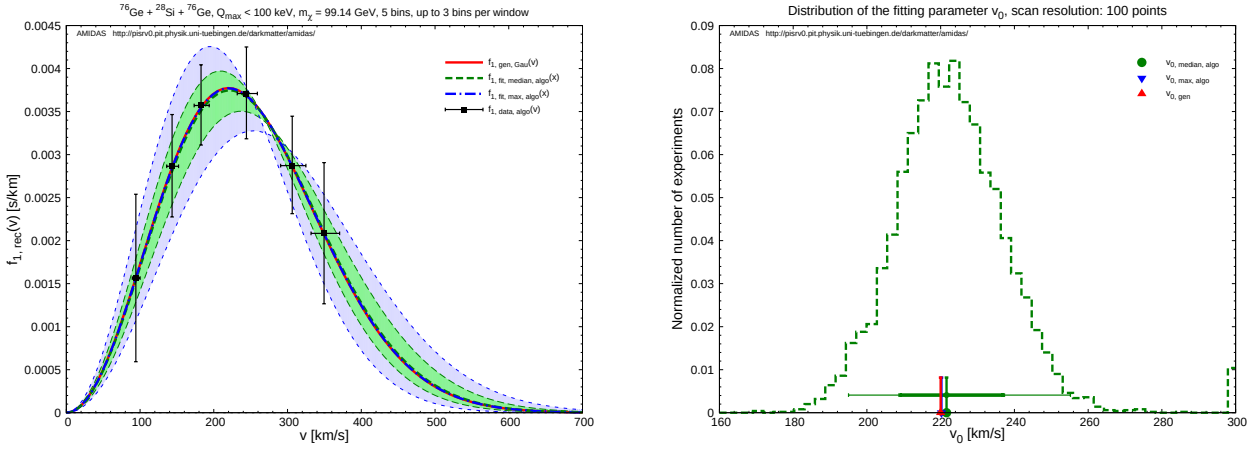

(a) (b)

Figure 4: As in Figs. 3, except that the Gaussian probability distribution for v_0 with an expected value of $v_0 = 230$ km/s and a 1σ uncertainty of 20 km/s has been used.

Input: shifted Maxwellian velocity distribution $f_{1,\mathrm{sh}}(v)$					
Fitting model	Parameter	Input/theoretical value	Scanning range	Expected value	1σ uncertainty
Simple	v_0 [km/s]	~ 295	[160, 400]	280	40
1–para. shifted	v_0 [km/s]	220	[160, 300]	230	20
Shifted	v_0 [km/s]	220	[160, 300]	230	20
	v_e [km/s]	231	[160, 300]	245	20
Variated shifted	v_0 [km/s]	220	[160, 300]	230	20
	Δv [km/s]	11	[−50, 80]	15	20

Table 3: The input setup for the shifted Maxwellian velocity distribution $f_{1,\mathrm{sh}}(v)$ used for generating WIMP signals as well as the theoretical estimated values, the scanning ranges, the expected values and the 1σ uncertainties on the fitting parameters used for different fitting velocity distribution functions.

It can be seen that, due to the extra *statistical fluctuation* on the reconstructed WIMP mass [6], the statistical uncertainties on the Bayesian reconstructed v_0 with both of the flat and the Gaussian probability distributions become $\sim 30\%$ to $\sim 60\%$ larger. However, same as the case with an input WIMP mass, the use of the Gaussian probability distribution can not only reduce the statistical uncertainty on v_0 significantly and therefore improve the Bayesian reconstructed velocity distribution, but also alleviate the "imprecisely" expected values of v_0.

In table 2, we list the reconstructed results of v_0 for all four considered cases in this subsection as well as the 1 (2) σ uncertainty ranges of the *median* values of v_0. It would be worth to emphasize that, the statistical uncertainties shown in Figs. 2 and 4 are (much) smaller than the *input* uncertainty on the expected value of v_0 of 20 km/s.

3.2 Shifted Maxwellian velocity distribution

By taking into account the orbital motion of the Solar system around our Galaxy as well as that of the Earth around the Sun, a more realistic shifted Maxwellian velocity distribution of halo WIMPs has been given by [1, 5]:

$$f_{1,\mathrm{sh}}(v) = \frac{1}{\sqrt{\pi}}\left(\frac{v}{v_0 v_\mathrm{e}}\right)\left[e^{-(v-v_\mathrm{e})^2/v_0^2} - e^{-(v+v_\mathrm{e})^2/v_0^2}\right]. \tag{41}$$

Here v_e is the time-dependent Earth's velocity in the Galactic frame [17, 1]:

$$v_\mathrm{e}(t) = v_0\left[1.05 + 0.07\cos\left(\frac{2\pi(t-t_\mathrm{p})}{1\ \mathrm{yr}}\right)\right], \tag{42}$$

with $t_\mathrm{p} \simeq$ June 2nd is the date on which the velocity of the Earth relative to the WIMP halo is maximal[5].

In Table 3, we list the input setup for the shifted Maxwellian velocity distribution $f_{1,\mathrm{sh}}(v)$ used for generating WIMP signals as well as the theoretical estimated values, the scanning

[5]In our simulations, the time dependence of the Earth's velocity in the Galactic frame, the second term of $v_\mathrm{e}(t)$, will be ignored, i.e. $v_\mathrm{e} = 1.05\, v_0$ is used.

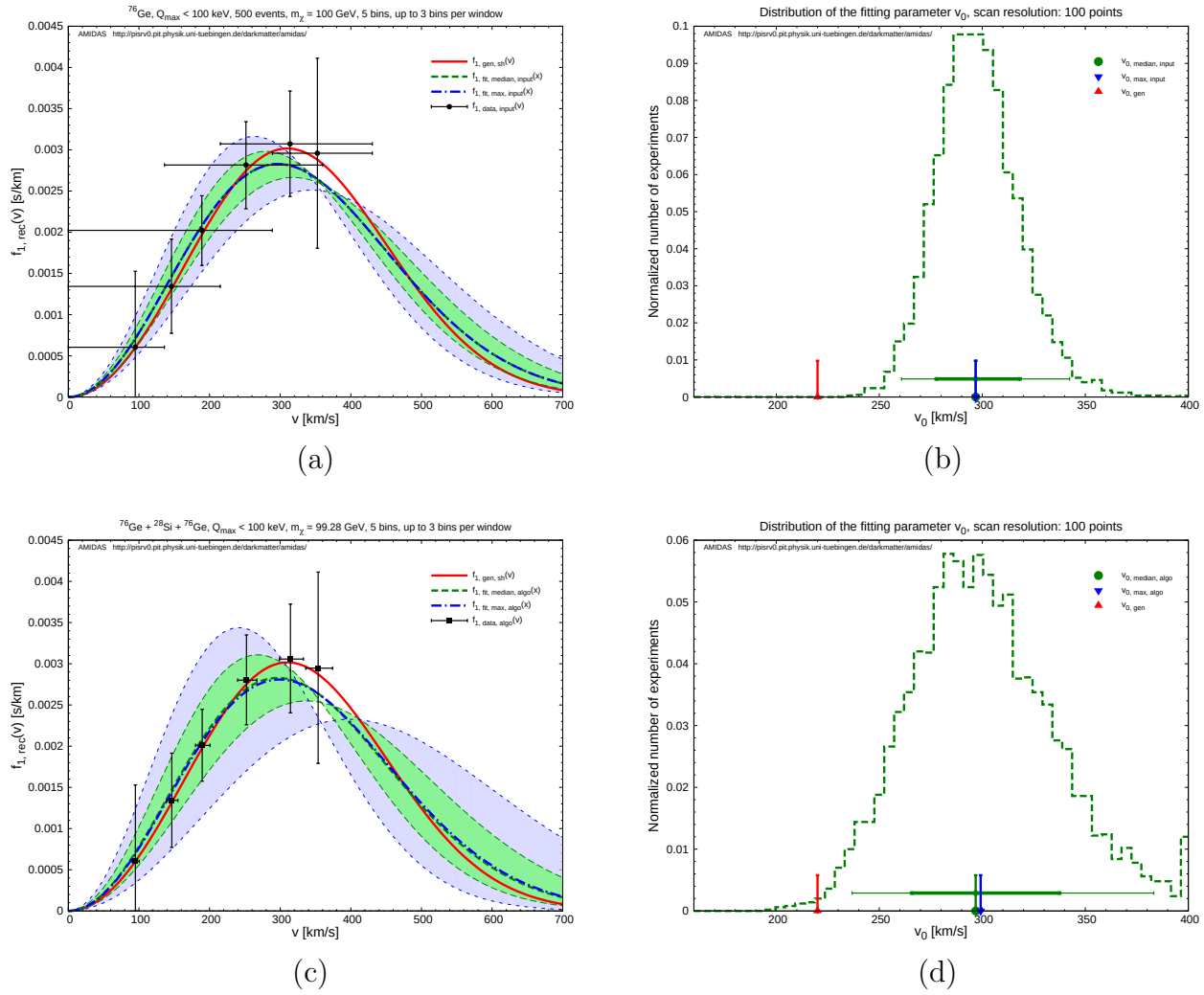

Figure 5: (a) (b) As in Figs. 1, except that the shifted Maxwellian velocity distribution function given in Eq. (41) has been used for generating WIMP signals. (c) (d) As in Figs. 3: the WIMP mass m_χ has been reconstructed with a ^{28}Si target and a second ^{76}Ge target.

ranges, the expected values and the 1σ uncertainties on the fitting parameters used for different fitting velocity distribution functions.

3.2.1 Simple Maxwellian velocity distribution

We consider first the simplest case of the simple Maxwellian velocity distribution function $f_{1,\mathrm{Gau}}(v)$ with the unique fitting parameter v_0 to fit the reconstructed–input data points given by Eqs. (14) and (25).

As in Sec. 3.1.1, in Figs. 5 we use first the flat probability distribution for the fitting parameter v_0 with either the precisely known (input) (upper) or the reconstructed (lower) WIMP mass, respectively. Figs. 5(a) and (c) show clearly that, although an "improper" choice for the fitting velocity distribution function and a simple flat probability distribution for v_0 (i.e. without any prior knowledge about v_0) have been used, the 1σ statistical uncertainty bands of the reconstructed WIMP velocity distribution function could in principle still cover the true (input) distribution. Quantitatively and more precisely, the deviations of the peaks of the reconstructed velocity distributions from that of the true (input) one are only ~ 10 km/s. Note that the 1σ statistical uncertainty on the fitting parameter v_0 is ~ 20 km/s to ~ 40 km/s (see Table 4).

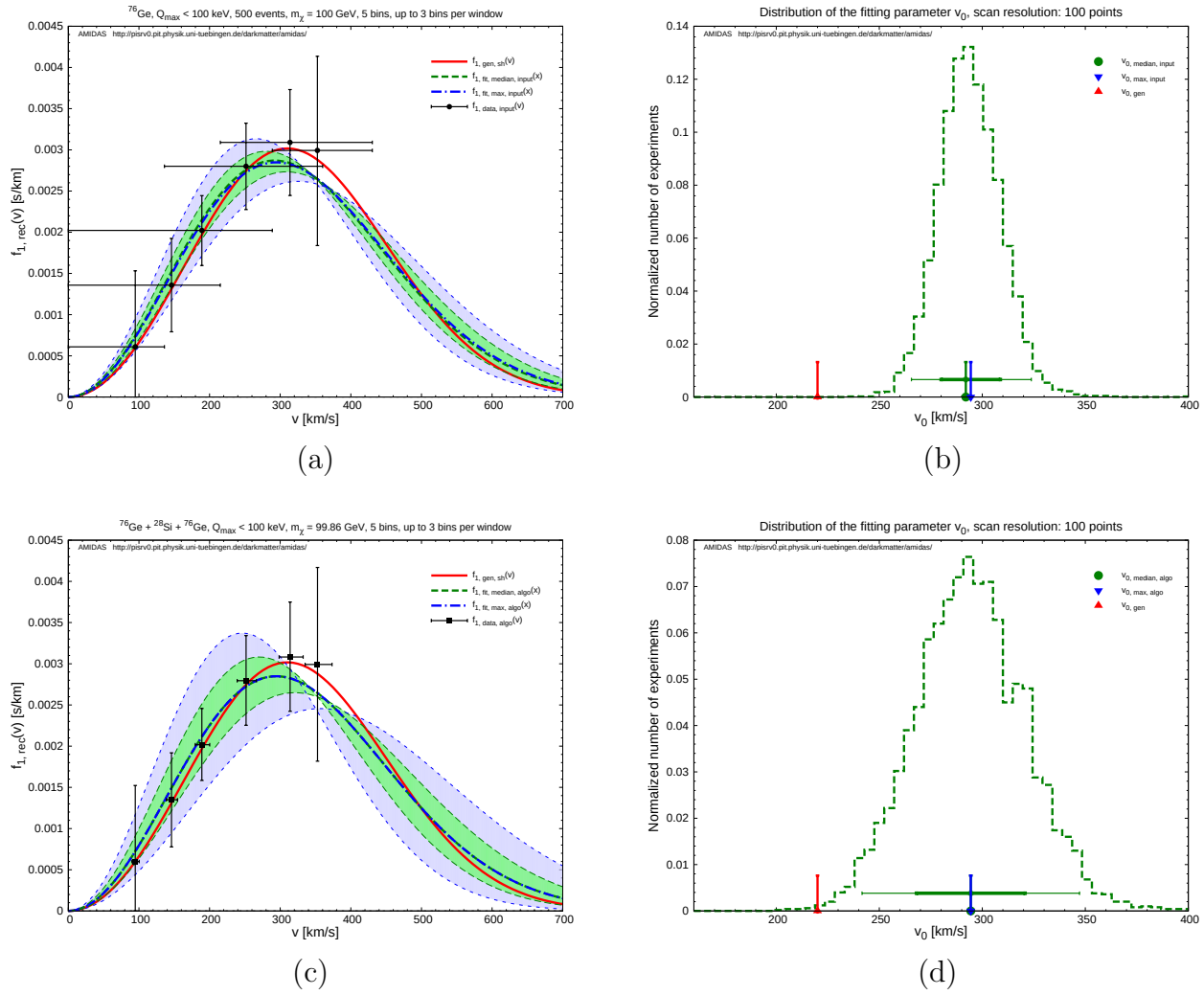

Figure 6: As in Figs. 5, except that the Gaussian probability distribution for v_0 with an expected value of $v_0 = 280$ km/s and a 1σ uncertainty of 40 km/s has been used.

However, our simulations show also that, with an "improper" assumption about the fitting velocity distribution function, one would obtain an "unexpected" result for the fitting parameter

Input: shifted Maxwellian velocity distribution $f_{1,\mathrm{sh}}(v)$						
Reconstruction: simple Maxwellian velocity distribution $f_{1,\mathrm{Gau}}(v)$						
Parameter	WIMP mass	Prob. dist.	Max. p_{median}	Median	1σ range	2σ range
v_0 [km/s]	Input	Flat	296.8	$296.8\,^{+21.6}_{-19.2}\,(^{+45.6}_{-36.0})$	[277.6, 318.4]	[260.8, 342.4]
		Gaussian	294.4	$292.0\,^{+16.8}_{-12.0}\,(^{+31.8}_{-26.4})$	[280.0, 308.8]	[265.6, 323.8]
	Reconst.	Flat	299.2	$296.8\,^{+40.8}_{-31.2}\,(^{+86.4}_{-60.0})$	[265.6, 337.6]	[236.8, 383.2]
		Gaussian	294.4	$294.4 \pm 26.4\,(\pm 52.8)$	[268.0, 320.8]	[241.6, 347.2]

Table 4: The reconstructed results of v_0 for all four considered cases with the simple Maxwellian velocity distribution $f_{1,\mathrm{Gau}}(v)$ as well as the $1\,(2)\,\sigma$ uncertainty ranges of the median values.

v_0: 2.5σ (with the reconstructed WIMP mass, Fig. 5(d)) to 4σ (with the input WIMP mass, Fig. 5(b)) deviations of the reconstructed Solar orbital velocity from the theoretical estimate of $v_0 \approx 220$ km/s would be obtained. Such observation would indicate clearly that our initial assumption about the fitting velocity distribution function would be incorrect or at least need to be modified.

Moreover, in Figs. 6 we assume that a rough prior knowledge about the Solar orbital velocity v_0 exists and use the Gaussian probability distribution for v_0 with an expected value of $v_0 = \textit{280}$ km/s and a 1σ uncertainty of *40* km/s. As observed earlier, with a prior knowledge about the fitting parameter v_0, one could reconstruct the velocity distribution function better: the $1\,(2)\,\sigma$ statistical uncertainties on v_0 could be reduced to $\sim 60\%$. Additionally, the reconstructed 1σ statistical uncertainties on v_0 with both of the input and the reconstructed WIMP masses are much smaller than the input 1σ value of 40 km/s.

In table 4, we list the reconstructed values of v_0 for all four considered cases with the simple Maxwellian velocity distribution $f_{1,\mathrm{Gau}}(v)$ as well as the $1\,(2)\,\sigma$ uncertainty ranges of the median values of v_0.

3.2.2 One–parameter shifted Maxwellian velocity distribution

In the previous Sec. 3.2.1., we have found that, by assuming (improperly) the simple Maxwellian velocity distribution $f_{1,\mathrm{Gau}}(v)$, in both cases with and without an expected value of the fitting parameter v_0, one would obtain a *much higher* reconstruction result: $v_{0,\mathrm{rec}} \simeq 295$ km/s, which is 2σ to 4σ apart from the theoretical estimate of $v_0 \approx 220$ km/s. This observation implies the need of a more suitable fitting velocity distribution function. Hence, as the second trial, we consider now the use of the *shifted* Maxwellian velocity distribution $f_{1,\mathrm{sh}}(v)$ given in Eq. (41) with *only one* fitting parameter, i.e. the Solar orbital velocity v_0. In this case, we fix simply that

$$v_{\mathrm{e}} = 1.05\, v_0\,. \tag{43}$$

and neglect the time–dependence of $v_{\mathrm{e}}(t)$.[6]

[6]Note that hereafter we use $f_{1,\mathrm{sh},v_0}(v)$ to denote the "one–parameter" shifted Maxwellian velocity distribution function, in order to distinguish this from the "original" one given in Eq. (41) with v_0 and v_{e} as two independent fitting parameters.

Input: shifted Maxwellian velocity distribution $f_{1,\mathrm{sh}}(v)$						
Reconstruction: one–parameter shifted Maxwellian velocity distribution $f_{1,\mathrm{sh},v_0}(v)$						
Parameter	WIMP mass	Prob. dist.	Max. $\mathrm{p}_{\mathrm{median}}$	Median	1σ range	2σ range
v_0 [km/s]	Input	Flat	217.4	$217.4\,^{+14.0}_{-11.2}\,(^{+29.4}_{-23.8})$	[206.2, 231.4]	[193.6, 246.8]
		Gaussian	221.6	$221.6\,^{+9.8}_{-8.4}\,(\pm 18.2)$	[213.2, 231.4]	[203.4, 239.8]
	Reconst.	Flat	218.8	$218.8\,^{+25.2}_{-22.4}\,(^{+56.0}_{-44.8})$	[196.4, 244.0]	[174.0, 274.8]
		Gaussian	221.6	$221.6\,^{+16.8}_{-15.4}\,(\pm 33.6)$	[206.2, 238.4]	[188.0, 255.2]

Table 5: The reconstructed results of v_0 for all four considered cases with the one–parameter shifted Maxwellian velocity distribution $f_{1,\mathrm{sh},v_0}(v)$ as well as the $1\,(2)\,\sigma$ uncertainty ranges of the median values.

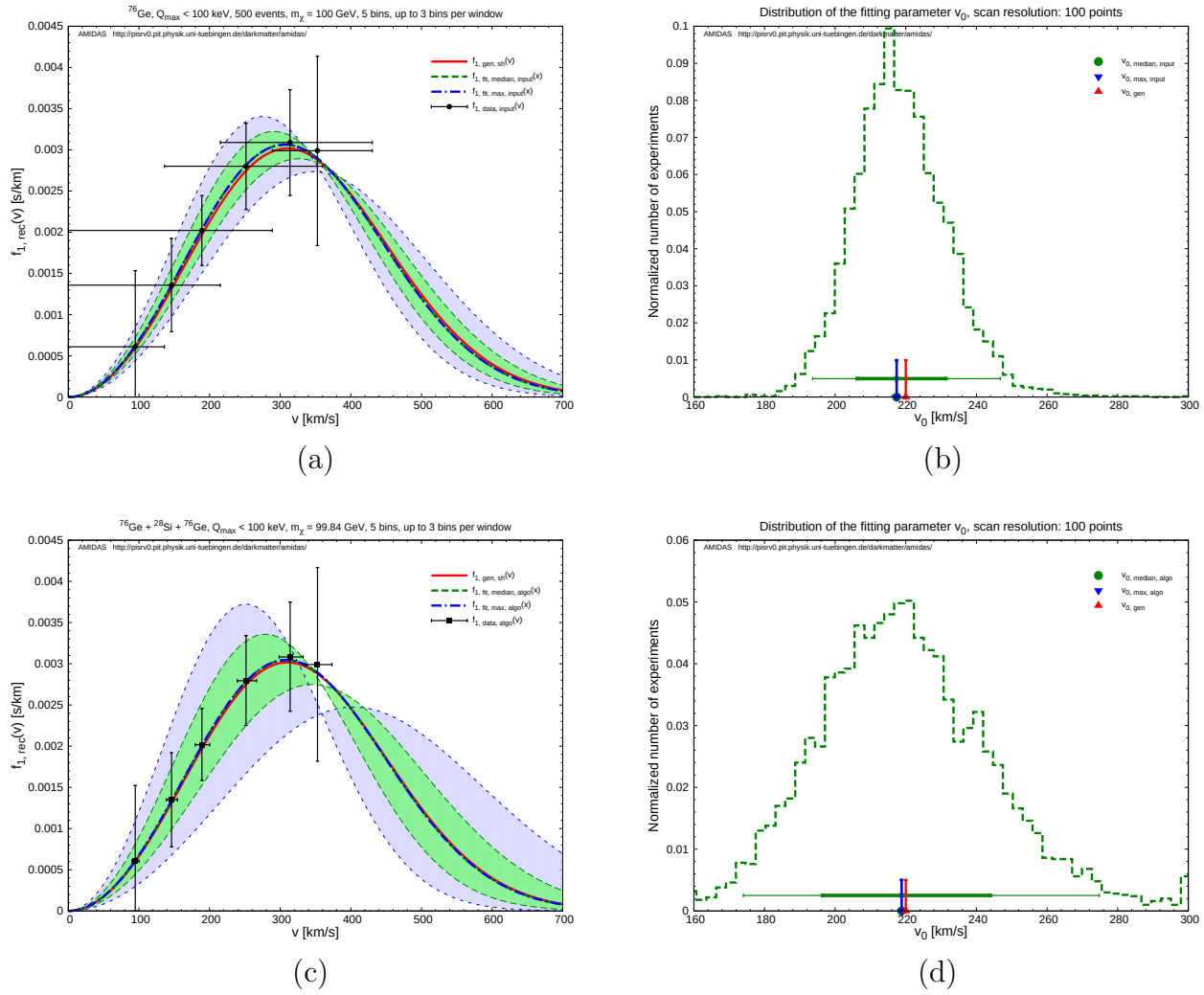

Figure 7: As in Figs. 5, except that the one–parameter shifted Maxwellian velocity distribution function $f_{1,\mathrm{sh},v_0}(v)$ with the unique fitting parameter v_0 has been used as the fitting velocity distribution.

In Figs. 7, we consider first the flat probability distribution for the fitting parameter v_0 with either the precisely known (input) (upper) or the reconstructed (lower) WIMP mass, respectively. It can be seen clearly that, with a more suitable assumption about the fitting function, one could indeed reconstruct the WIMP velocity distribution much closer to the true (input) one. Although no prior knowledge about v_0 is used, this most important characteristic parameter could in principle be pinned down very precisely: the difference between the *median* values of the reconstructed v_0 and the true (input) one would be $\lesssim 5$ km/s (see also Table 5).

In addition, with the input WIMP mass, the $1\,(2)\,\sigma$ statistical uncertainties on the reconstructed v_0 are only $^{+14.0}_{-11.2}\,(^{+29.4}_{-23.8})$ km/s. Even with the reconstructed WIMP mass, the $1\,(2)\,\sigma$ statistical uncertainties could still be limited as small as only $^{+25.2}_{-22.4}\,(^{+56.0}_{-44.8})$ km/s. It would be worth to emphasize that, compare to the uncertainty on the astronomical measurement of v_0 of ~ 20 km/s (or probably larger), the result offered by our Bayesian reconstruction method would be a pretty precise estimate and could help us to confirm the astronomical measurement of v_0.

Moreover, in Figs. 8 we give the reconstruction results with the Gaussian probability distribution for v_0 with an expected value of $v_0 = 230$ km/s and a 1σ uncertainty of 20 km/s. As summarized in Table 5, with a prior knowledge of the parameter v_0, the $1\,(2)\,\sigma$ statistical uncertainties could be reduced significantly to be $\lesssim 70\%$. Remind here that the expected value of the

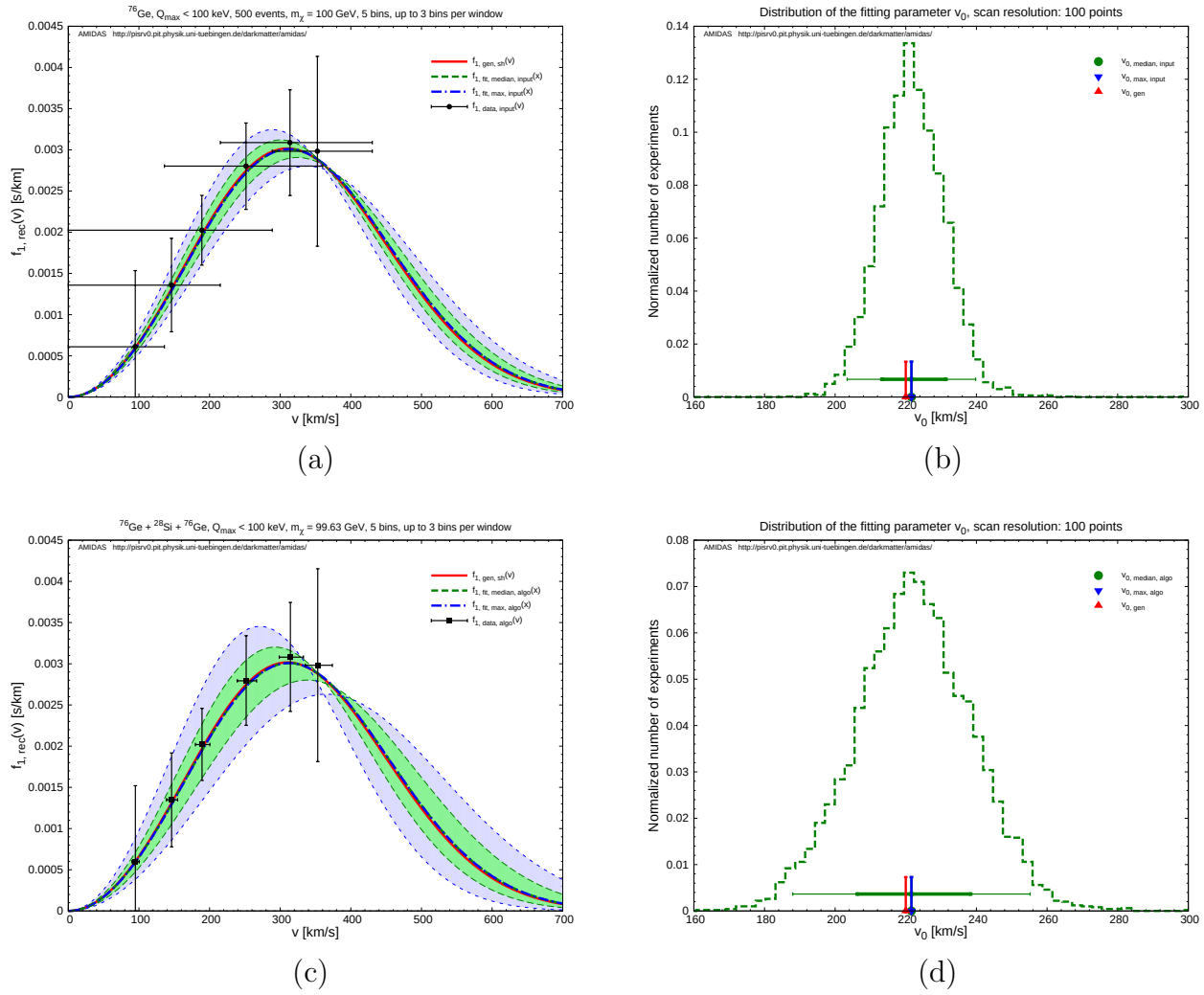

Figure 8: As in Figs. 7, except that the Gaussian probability distribution for v_0 with an expected value of $v_0 = 230$ km/s and a 1σ uncertainty of 20 km/s has been used.

Gaussian probability distribution of v_0 has been set as $v_0 = 230$ km/s, a bit different from the input value. Nevertheless, our simulations show that this "artificial" (systematic) error could be corrected in our reconstruction process for v_0.

In table 5, we list the reconstructed results of v_0 for all four considered cases with the one–parameter shifted Maxwellian velocity distribution $f_{1,\mathrm{sh},v_0}(v)$ as well as the $1\,(2)\,\sigma$ uncertainty ranges of the median values of v_0.

3.2.3 Shifted Maxwellian velocity distribution

Now we release the fixed relation between v_0 and v_e given in Eq. (43) and consider the reconstruction of these two parameters *simultaneously* and *independently*. In addition, we assume here that, from the (naive) trials with the simple and one–parameter shifted Maxwellian velocity distributions done previously, one could already obtain a rough idea about the shape of the velocity distribution of halo WIMPs. This information would in turn give us the prior knowledge about the expected values of the Solar and Earth's orbital velocities v_0 and v_e. Hence, we consider here only the Gaussian probability distribution for both of two fitting parameters with expected values of $v_0 = 230$ km/s and $v_e = 245$ km/s and a common 1σ uncertainty of 20 km/s (see Table

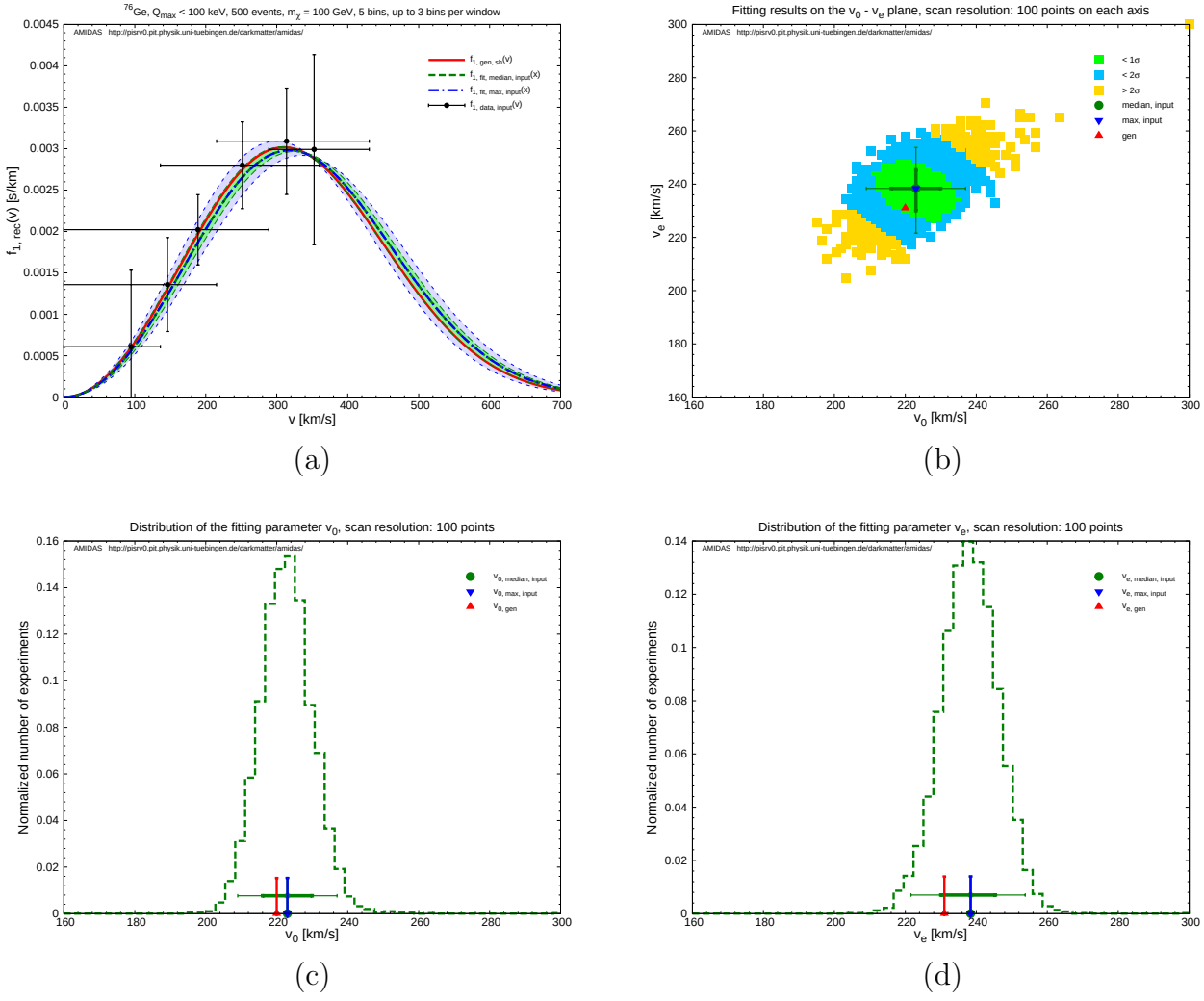

Figure 9: (a) As in Fig. 7(a), except that the shifted Maxwellian velocity distribution function given in Eq. (41) with two fitting parameters v_0 and v_e is used. The Gaussian probability distribution for both of two fitting parameters with expected values of $v_0 = 230$ km/s and $v_e = 245$ km/s and a common 1σ uncertainty of 20 km/s has been used. (b) The distribution of the Bayesian reconstructed fitting parameters v_0 and v_e in all simulated experiments on the $v_0 - v_e$ plane. The light–green (light–blue, gold) points indicate the $1\,(2)\,(>2)\,\sigma$ areas of the reconstructed combination of v_0 and v_e. The red upward–triangle indicates the input values of v_0 and v_e, which has been labeled with the subscript "gen". The green disk shows the median values of the simulated results, whereas and blue downward–triangle the point which maximizes p_{median}. The meaning of the horizontal thick (thin) green bars are the same as in Fig. 7(b). (c) As in Fig. 7(b). (d) Similar to (c): the distribution of the Bayesian reconstructed second fitting parameter v_e. See the text for further details.

3)[7].

In Fig. 9(a), we show the reconstructed shifted Maxwellian velocity distribution function as well as the $1\,(2)\sigma$ statistical uncertainty bands. Here the true (input) WIMP mass has been used. Comparing to Fig. 8(a), it can be seen clearly that, with a prior knowledge about the Solar and

[7]Remind that both of the expected values of the fitting parameters v_0 and v_e differ slightly from the true (input) values. Note also that the time–dependence of the Earth's orbital velocity is ignored here and v_e is thus treated as a *time–independent* fitting parameter.

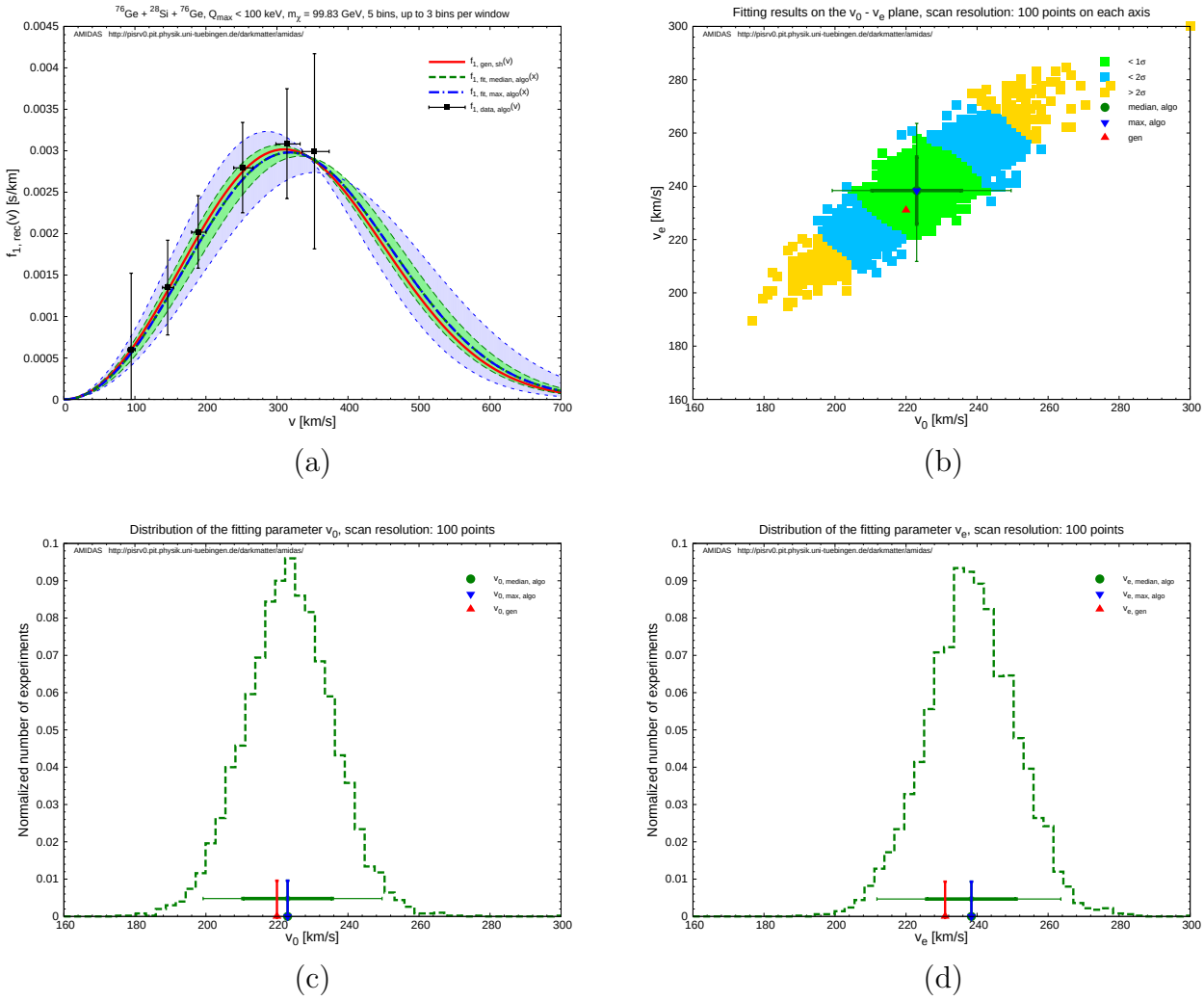

Figure 10: As in Figs. 9, except that the reconstructed WIMP mass has been used.

Earth's orbital velocities v_0 and v_e, one could in principle reconstruct the velocity distribution function with two fitting parameters more precisely: the $1\,(2)\,\sigma$ statistical uncertainty bands are much thiner and the deviations of v_0 and v_e are *only a few* km/s (see also Table 6)[8].

Fig. 9(b) shows the distribution of the Bayesian reconstructed fitting parameter v_0 and v_e in all simulated experiments on the $v_0 - v_e$ plane. The light–green (light–blue, gold) points indicate the $1\,(2)\,(>2)\,\sigma$ areas of the reconstructed combination of v_0 and v_e. Note here that these $1\,(2)\,(>2)\,\sigma$ areas are determined according to the *descending* order of the p_{median} values of the reconstructed combination of v_0 and v_e. This means that the light–green (light–blue, gold) areas are the reconstructed combinations of v_0 and v_e which give the largest 68.27% (95.45%) p_{median} values in all of the simulated experiments.

Moreover, the red upward–triangle indicates the input values of v_0 and v_e, which has been labeled with the subscript "gen". The green disk shows the median values of the simulated results, whereas and blue downward–triangle the point which maximizes p_{median}. In addition, the thick (thin) green crosses show the $1\,(2)\,\sigma$ (68.27% (95.45%)) ranges of the reconstructed results according to the order of the reconstructed values of v_0 or v_e *along* (centered at their

[8]Note however that, for using velocity distributions with two or more fitting parameters *without* constraints on these parameters (i.e. the use of the "flat" probability distribution), the distribution of the reconstructed results by our Bayesian analysis would be pretty wild, a part of them would even be on the boundary of the scanning ranges of these parameters.

Input: shifted Maxwellian velocity distribution $f_{1,\rm sh}(v)$						
Reconstruction: shifted Maxwellian velocity distribution $f_{1,\rm sh}(v)$						
Parameter	WIMP mass	Prob. dist.	Max. $\rm p_{median}$	Median	1σ range	2σ range
v_0 [km/s]	Input	Gaussian	223.0	$223.0 \pm 7.0\,(\pm 14.0)$	[216.0, 230.0]	[209.0, 237.0]
	Reconst.	Gaussian	223.0	$223.0 \pm 12.6\,(^{+26.6}_{-23.8})$	[210.4, 235.6]	[199.2, 249.6]
$v_{\rm e}$ [km/s]	Input	Gaussian	238.4	$238.4\,^{+7.0}_{-8.4}\,(^{+15.4}_{-16.9})$	[230.0, 245.4]	[221.6, 253.8]
	Reconst.	Gaussian	238.4	$238.4 \pm 12.6\,(^{+25.2}_{-26.6})$	[225.8, 251.0]	[211.8, 263.6]

Table 6: The reconstructed results of v_0 and $v_{\rm e}$ with the shifted Maxwellian velocity distribution $f_{1,\rm sh}(v)$ as well as the $1\,(2)\,\sigma$ uncertainty ranges of the median values.

median values $v_{0,\rm median}$ or $v_{\rm e,median}$).

Additionally, in Figs. 9(c) and (d), we give the distributions of the Bayesian reconstructed fitting parameter v_0 and $v_{\rm e}$ as well as the $1\,(2)\,\sigma$ statistical uncertainty ranges on the v_0 and $v_{\rm e}$ axes *separately*. Note here that we project all reconstructed combinations of $(v_0, v_{\rm e})$ on the v_0- or $v_{\rm e}-$axis. Comparing Fig. 9(c) to Fig. 8(b), it can be found that, while the deviations of v_0 are a little bit larger then the results with the "one–parameter" fitting velocity distribution, the $1\,(2)\,\sigma$ statistical uncertainties are reduced to $\sim 70\%$ (see Table 6 and Table 5).

As a comparison, in Figs. 10 we use the reconstructed WIMP mass. Fig. 10(b) shows that, as expected, the distribution of v_0 and $v_{\rm e}$ on the $v_0 - v_{\rm e}$ plane becomes wilder and extends toward the directions of higher (lower)–v_0 and higher (lower)–$v_{\rm e}$. Nevertheless, the "best–fit" combination of them which maximizes $\rm p_{median}$ as well as the median values of v_0 and $v_{\rm e}$ consistant very well with the true (input) values.

In table 5, we list the reconstructed results of v_0 and $v_{\rm e}$ with the shifted Maxwellian velocity distribution $f_{1,\rm sh}(v)$ as well as the $1\,(2)\,\sigma$ uncertainty ranges of the median values.

3.2.4 Variated shifted Maxwellian velocity distribution

In the previous Sec.3.2.3, it has been found that, by using the shifted Maxwellian velocity distribution given in Eq. (41) with two fitting parameters: v_0 and $v_{\rm e}$, one could reconstruct the ($1\,(2)\,\sigma$ statistical uncertainty bands of the) velocity distribution function as well as pin down the Solar orbital velocity v_0 pretty precisely. However, as shown in Figs. 9(d) and 10(d), the deviations of the reconstructed Earth's orbital velocity $v_{\rm e}$ from the true (input) value seem to be larger than the deviations of the reconstructed v_0. This might be caused by the strong (anti–)correlation between v_0 and $v_{\rm e}$. Hence, we consider now a variation of the shifted Maxwellian distribution function, in the hope that this pretty large systematic deviation of $v_{\rm e}$ could be reduced.

We rewrite the shifted Maxwellian velocity distribution given in Eq. (41) to the following "variated" form:

$$f_{1,{\rm sh},\Delta v}(v) = \frac{1}{\sqrt{\pi}} \left[\frac{v}{v_0\,(v_0+\Delta v)}\right] \left\{ e^{-[v-(v_0+\Delta v)]^2/v_0^2} - e^{-[v+(v_0+\Delta v)]^2/v_0^2} \right\}, \tag{44}$$

where

$$\Delta v \equiv v_{\rm e} - v_0 \tag{45}$$

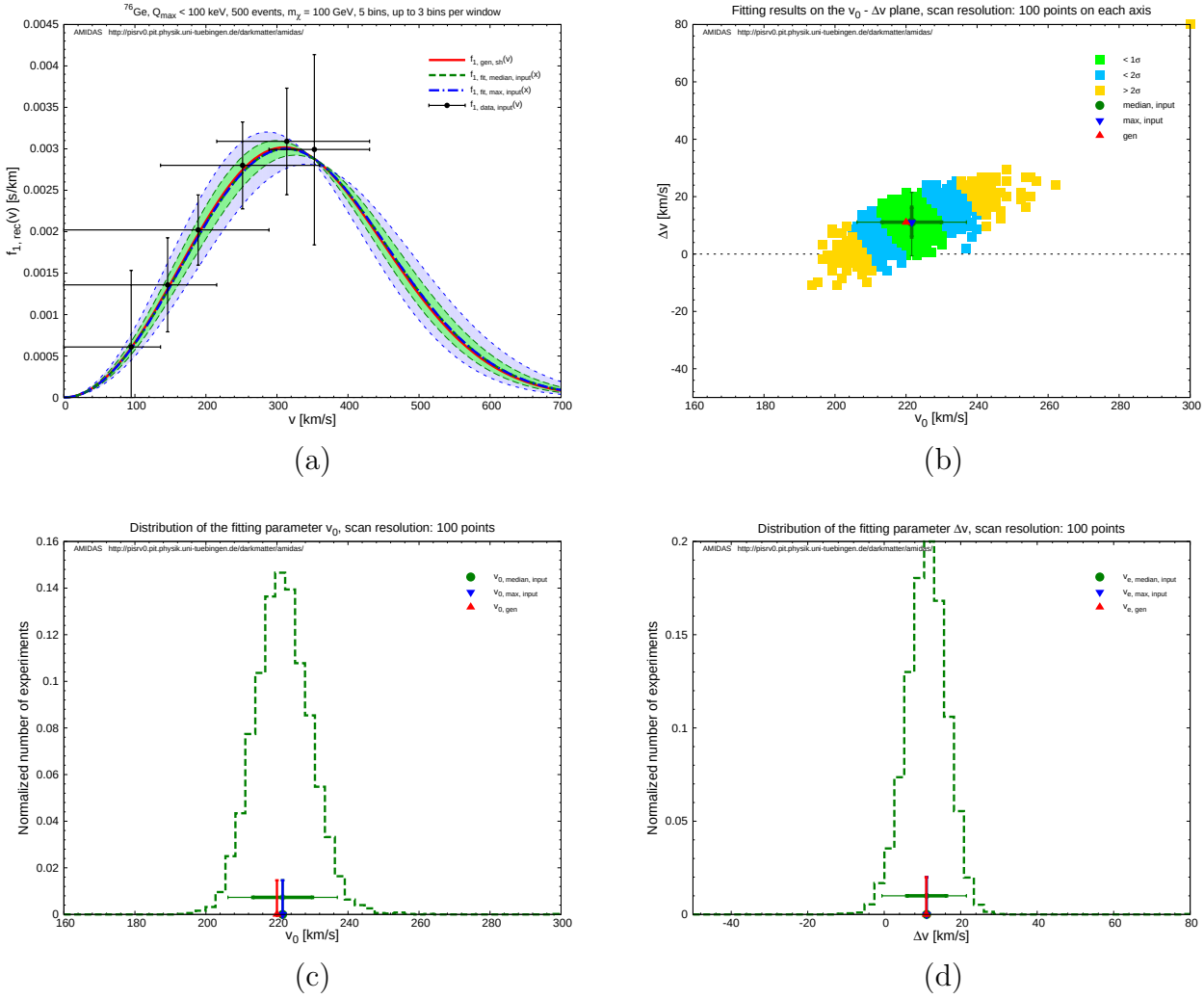

Figure 11: As in Figs. 9, except that the variated shifted Maxwellian velocity distribution function given in Eq. (44) with two fitting parameters v_0 and Δv is used. The Gaussian probability distribution for both of two fitting parameters with expected values of $v_0 = 230$ km/s and $\Delta v = 15$ km/s and a common 1σ uncertainty of 20 km/s has been used.

is the difference between v_0 and $v_e(t)$.[9]

As in the previous Sec.3.2.3, we assume here that, we have already a rough idea about the shape of the velocity distribution of halo WIMPs, and thus the prior knowledge about the expected values of the (difference between the) Solar and Earth's orbital velocities v_0 and Δv. Hence, we consider here only the Gaussian probability distribution for both of the fitting parameters with expected values of $v_0 = 230$ km/s and $\Delta v = 15$ km/s and a common 1σ uncertainty of 20 km/s (see Table 3). Two cases with both of the true (input) and the reconstructed WIMP masses have been considered.

By comparing Figs. 11 to Figs. 9 and Figs. 12 to Figs. 10, it can be seen obviously that the reconstructed velocity distribution function could indeed match the true (input) one much precisely, with however (slightly) larger 1 (2) σ statistical uncertainty bands. The systematic deviations of both of the two fitting parameters from the true (input) values would also be much smaller than given in the $v_0 - v_e$ case. This implies importantly that, the use of this variated

[9] As in the previous Sec.3.2.3, the time–dependence of the Earth's orbital velocity is ignored here and Δv is thus treated as a *time–independent* fitting parameter.

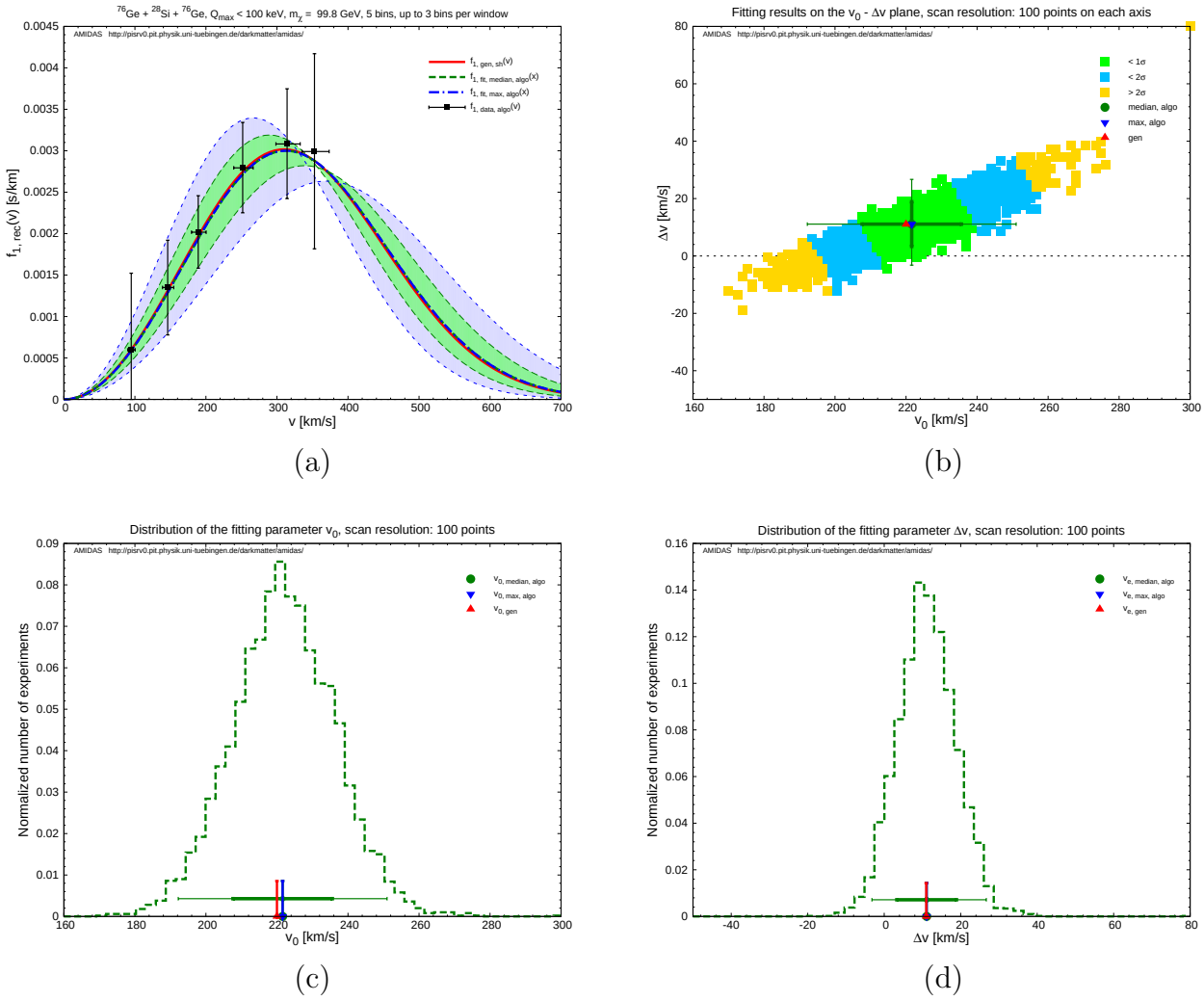

Figure 12: As in Figs. 11, except that the reconstructed WIMP mass has been used.

shifted velocity distribution function given in Eq. (44) could indeed offer an estimate of the Earth's orbital velocity $v_{\rm e} = v_0 + \Delta v$ with a much higher precision. Such a trick would be helpful to improve the estimation of the Earth's orbital velocity $v_{\rm e}$.

Input: shifted Maxwellian velocity distribution $f_{1,\rm sh}(v)$						
Reconstruction: variated shifted Maxwellian velocity distribution $f_{1,\rm sh,\Delta v}(v)$						
Parameter	WIMP mass	Prob. dist.	Max. $p_{\rm median}$	Median	1σ range	2σ range
v_0 [km/s]	Input	Gaussian	221.6	$221.6 \pm 8.4\,(\pm 15.4)$	[213.2, 230.0]	[206.2, 237.0]
	Reconst.	Gaussian	221.6	$221.6 \pm 14.0\,(\pm 29.4)$	[207.6, 235.6]	[192.2, 251.0]
Δv [km/s]	Input	Gaussian	11.1	$11.1 \pm 5.2\,(^{+10.4}_{-11.7})$	[5.9, 16.3]	[−0.6, 21.5]
	Reconst.	Gaussian	11.1	$11.1 \pm 7.8\,(^{+15.6}_{-14.3})$	[3.3, 18.9]	[−3.2, 26.7]

Table 7: The reconstructed results of v_0 and Δv with the variated shifted Maxwellian velocity distribution $f_{1,\rm sh,\Delta v}(v)$ as well as the $1\,(2)\,\sigma$ uncertainty ranges of the median values.

Input: modified Maxwellian velocity distribution $f_{1,\mathrm{Gau},k}(v)$					
Fitting model	Parameter	Input/theoretical value	Scanning range	Expected value	1σ uncertainty
Simple	v_0 [km/s]	~ 220	[160, 300]	230	20
1–para. shifted	v_0 [km/s]	~ 175	[100, 300]	200	40
Shifted	v_0 [km/s]	~ 175	[100, 300]	200	40
	v_e [km/s]	~ 185	[50, 300]	200	40
Variated shifted	v_0 [km/s]	~ 175	[100, 300]	200	40
	Δv [km/s]	~ 10	$[-120, 80]$	-20	40
Modified	v_0 [km/s]	220	[160, 300]	230	20
	k	2	[0.5, 3.5]	1	0.5

Table 8: The input setup for the modified Maxwellian velocity distribution $f_{1,\mathrm{Gau},k}(v)$ used for generating WIMP signals as well as the theoretical estimated values, the scanning ranges, the expected values and the 1σ uncertainties on the fitting parameters used for different fitting velocity distribution functions.

Note however that, as shown in Tables 6 and 7, by using the variated shifted Maxwellian velocity distribution, the $1\,(2)\,\sigma$ statistical uncertainties on the reconstructed v_0 would be $\sim 10\%$ larger. Meanwhile, from Eq. (45) the statistical uncertainty on v_e can be estimated by[10]

$$\begin{aligned}\sigma\left(v_e\right) &= \sqrt{\sigma^2\left(v_0\right) + \sigma^2\left(\Delta v\right) + 2\,\mathrm{cov}\left(v_0, \Delta v\right)\sigma\left(v_0\right)\sigma\left(\Delta v\right)} \\ &\leq \sqrt{\sigma^2\left(v_0\right) + \sigma^2\left(\Delta v\right)}\,. \end{aligned} \tag{46}$$

Then, according to the results given in Table 7, the $1\,(2)\,\sigma$ statistical uncertainties on v_e would be maximal $\lesssim 15\%$ enlarged, whereas the systematic deviation of v_e is much smaller.

In table 7, we list the reconstructed results of v_0 and Δv with the variated shifted Maxwellian velocity distribution $f_{1,\mathrm{sh},\Delta v}(v)$ as well as the $1\,(2)\,\sigma$ uncertainty ranges of the median values.

3.3 Modified Maxwellian velocity distribution

In this subsection, we consider another recently often used theoretical one–dimensional WIMP velocity distribution function. In Refs. [18, 10], a modification of the simple Maxwellian velocity distribution in Eq. (40) has been suggested:

$$f_{1,\mathrm{Gau},k}(v) = \begin{cases} \frac{v^2}{N_{f,k}}\left(e^{-v^2/kv_0^2} - e^{-v_{\mathrm{max}}^2/kv_0^2}\right)^k, & (\text{for } v \leq v_{\mathrm{max}}), \\ 0, & (\text{for } v > v_{\mathrm{max}}). \end{cases} \tag{47}$$

Here v_{max} is the maximal cut-off velocity of $f_{1,\mathrm{Gau},k}(v)$ and $N_{f,k}$ is the normalization constant depending on the value of the power index k.

[10]Since, according to Eq. (45), for a fixed value of v_e two fitting parameters v_0 and Δv should be "anti–correlated".

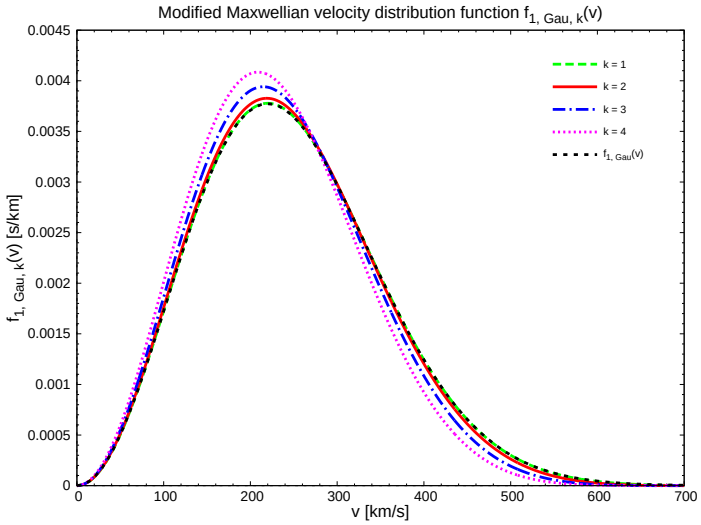

Figure 13: The normalized modified Maxwellian velocity distribution function $f_{1,\mathrm{Gau},k}(v)$ given in Eq. (47) with a common value of the Solar orbital velocity $v_0 = 220$ km/s and different power indices k: $k = 1$ (dashed light–green), $k = 2$ (solid red), $k = 3$ (dash–dotted blue) and $k = 4$ (dotted magenta). As a comparison, the simple Maxwellian velocity distribution $f_{1,\mathrm{Gau}}(v)$ with $v_0 = 220$ km/s is also given as the short–dashed black curve.

In Fig. 13, we give the *normalized* modified Maxwellian velocity distribution function $f_{1,\mathrm{Gau},k}(v)$ with a common value of the Solar orbital velocity $v_0 = 220$ km/s and different power indices k: $k = 1$ (dashed light–green), $k = 2$ (solid red), $k = 3$ (dash–dotted blue) and $k = 4$ (dotted magenta). As a comparison, the simple Maxwellian velocity distribution $f_{1,\mathrm{Gau}}(v)$ with $v_0 = 220$ km/s is also given as the short–dashed black curve.

In Table 8, we list the input setup for the modified Maxwellian velocity distribution $f_{1,\mathrm{Gau},k}(v)$ used for generating WIMP signals as well as the theoretical estimated values, the scanning ranges, the expected values and the 1σ uncertainties on the fitting parameters used for different fitting velocity distribution functions.

3.3.1 Simple Maxwellian velocity distribution

As in Sec. 3.2, we start to fit to the reconstructed data points given by Eqs. (14) and (25) with the simple Maxwellian velocity distribution function $f_{1,\mathrm{Gau}}(v)$.

In Figs. 14, we use first the flat probability distribution for the fitting parameter v_0 with either the precisely known (input) (upper) or the reconstructed (lower) WIMP mass, respectively. As shown in Figs. 1 and 3, although prior knowledge about the Solar orbital velocity is *absent*, one could in principle pin down the fitting parameter v_0 very precisely with systematic deviations of *only a few* km/s and $1\,(2)\,\sigma$ statistical uncertainties of only $^{+11.2}_{-12.6}\,(^{+36.4}_{-22.4})$ km/s and $^{+21.0}_{-18.2}\,(^{+53.2}_{-32.2})$ km/s.

In Figs. 15, we use the Gaussian probability distribution for v_0 with an expected value of $v_0 = 230$ km/s and a 1σ uncertainty of 20 km/s. As summarized in Table 9, the statistical uncertainties on the reconstructed v_0 could now in principle be reduced by $\sim 10\%$ to $\sim 30\%$. In addition, even with the reconstructed WIMP mass and thus a larger statistical fluctuation, the 1σ statistical uncertainties shown in Figs. 15 are (much) smaller than the given uncertainty on the expected value of v_0 (20 km/s). Moreover, although an expected value of $v_0 = 230$ km/s, which differs (slightly) from the true (input) one, is used, the value of the fitting parameter v_0 could still be pin down precisely with a negligible systematic deviation.

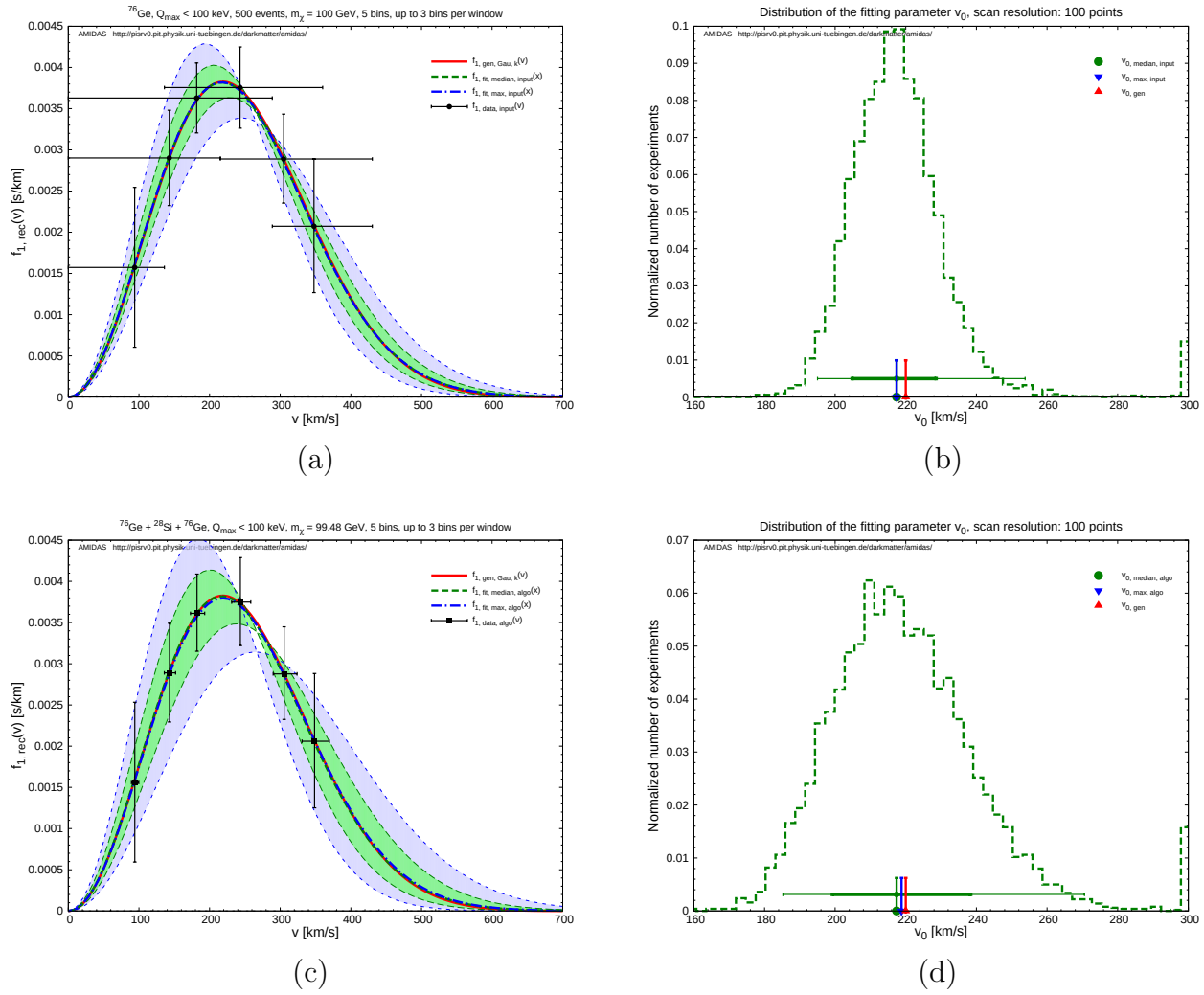

Figure 14: As in Figs. 5, except that the modified Maxwellian velocity distribution function given in Eq. (47) has been used for generating WIMP signals.

Furthermore, remind here that, either, as shown in Figs. 14, two reconstructed (dashed green and dash-dotted blue) velocity distribution functions match the true (input) (solid red)

Input: modified Maxwellian velocity distribution $f_{1,\mathrm{Gau},k}(v)$						
Reconstruction: simple Maxwellian velocity distribution $f_{1,\mathrm{Gau}}(v)$						
Parameter	WIMP mass	Prob. dist.	Max. p_{median}	Median	1σ range	2σ range
v_0 [km/s]	Input	Flat	217.4	$217.4\,^{+11.2}_{-12.6}\,(^{+36.4}_{-22.4})$	[204.8, 228.6]	[195.0, 253.8]
		Gaussian	218.8	$220.2 \pm 9.8\,(^{+26.6}_{-18.2})$	[210.4, 230.0]	[202.0, 246.8]
	Reconst.	Flat	218.8	$217.4\,^{+21.0}_{-18.2}\,(^{+53.2}_{-32.2})$	[199.2, 238.4]	[185.2, 270.6]
		Gaussian	220.2	$220.2\,^{+15.4}_{-14.0}\,(^{+36.4}_{-26.6})$	[206.2, 235.6]	[193.6, 256.6]

Table 9: The reconstructed results of v_0 for all four considered cases with the simple Maxwellian velocity distribution $f_{1,\mathrm{Gau}}(v)$ as well as the $1\,(2)\,\sigma$ uncertainty ranges of the median values.

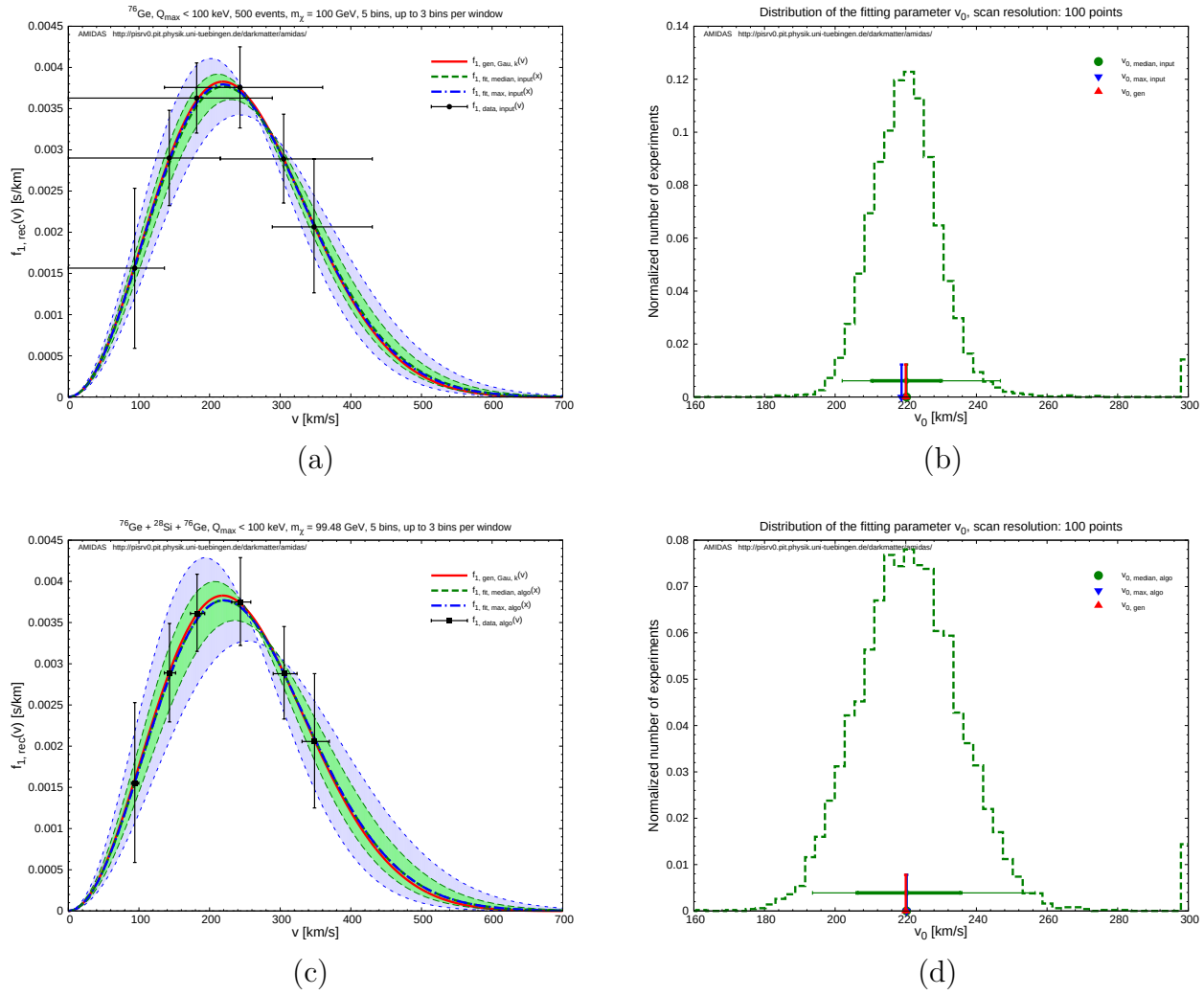

Figure 15: As in Figs. 14, except that the Gaussian probability distribution for v_0 with an expected value of $v_0 = 230$ km/s and a 1σ uncertainty of 20 km/s has been used.

one very well, but the reconstructed Solar orbital velocity v_0 would shift slightly away from the true (input) value, or, as shown in Figs. 15, v_0 could be determined very precisely, but the reconstructed velocity distribution functions would differ slightly from the true (input) one. This is because of the fact that we have *artificially* used an input value of $k = 2$ and, as shown in Fig. 13, the modified Maxwellian velocity distribution function with $k = 2$ is slightly different from the simple Maxwellian distribution.

In table 9, we list the reconstructed results of v_0 for all four considered cases with the simple Maxwellian velocity distribution $f_{1,\mathrm{Gau}}(v)$ as well as the $1\,(2)\,\sigma$ uncertainty ranges of the median values of v_0.

3.3.2 One–parameter shifted Maxwellian velocity distribution

Now, as a comparison of Sec. 3.2.1, we consider as the next trail the reconstruction with the one–parameter shifted Maxwellian velocity distribution function to fit the modified simple Maxwellian velocity distribution.

As usual, in Figs. 16 we use first the flat probability distribution for the fitting parameter v_0 with either the precisely known (input) (upper) or the reconstructed (lower) WIMP mass, respectively. It can be seen that, firstly, although the $1\,(2)\,\sigma$ statistical uncertainty bands could

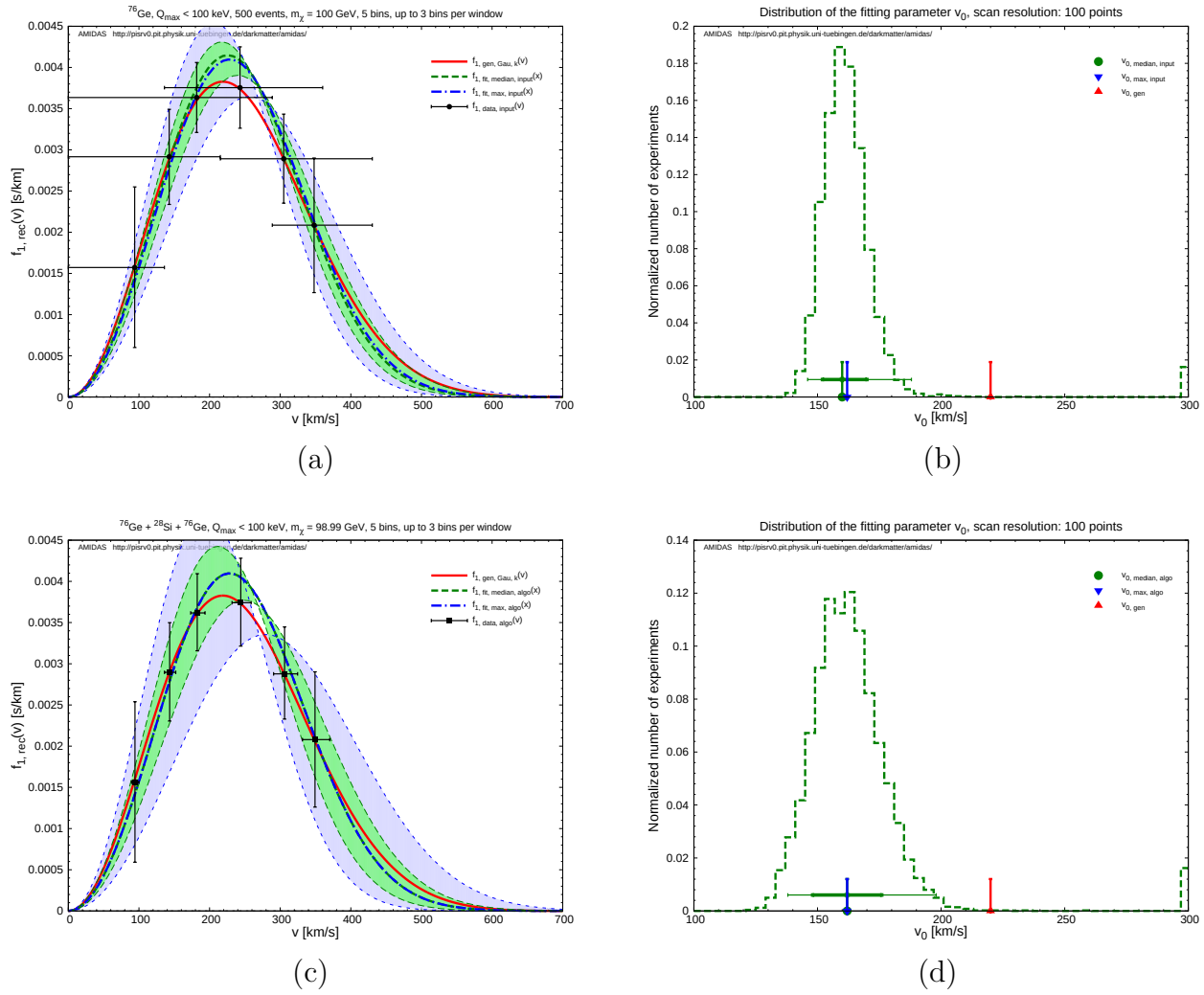

Figure 16: As in Figs. 14, except that the one–parameter shifted Maxwellian velocity distribution function $f_{1,\mathrm{sh},v_0}(v)$ with the unique fitting parameter v_0 has been used as the fitting velocity distribution.

still cover the true (input) velocity distribution (well), the systematic deviations of the peaks of the reconstructed velocity distributions from that of the true (input) one would be ~ 15 km/s. The comparisons between reconstructed results shown in Figs. 16(a) and (c) to Figs. 14(a) and (c) could indicate a high probability of the improper assumption of the fitting (one–parameter) shifted Maxwellian velocity distribution.

Moreover, Figs. 16(b) and (d) (see also Table 10) show clearly 4σ to even 6σ deviations of the reconstructed v_0 from the true (input) value of $v_0 = 220$ km/s. As discussed in Sec. 3.2.1, this observation implies also an improper use of the (one–parameter) shifted Maxwellian velocity distribution as our fitting function.

In Figs. 17, we use the Gaussian probability distribution for v_0 with a *slightly smaller* expected value of $v_0 = \mathit{200}$ km/s and a 1σ uncertainty of $\mathit{40}$ km/s. In contrast to our observations presented before, for this case the use of the Gaussian probability distribution would *not* reduce the 1 (2) σ statistical uncertainties for both cases with the true (input) and the reconstructed WIMP masses (see Table 10). This would be caused by the large difference between the given expected value and the most suitable one of the parameter v_0 (175 km/s, see Table 8). This would indicate that, in practical use of our Bayesian reconstruction method, some trial–and–error tests for determining a more suitable expected value of v_0 (and the other fitting parameters) would

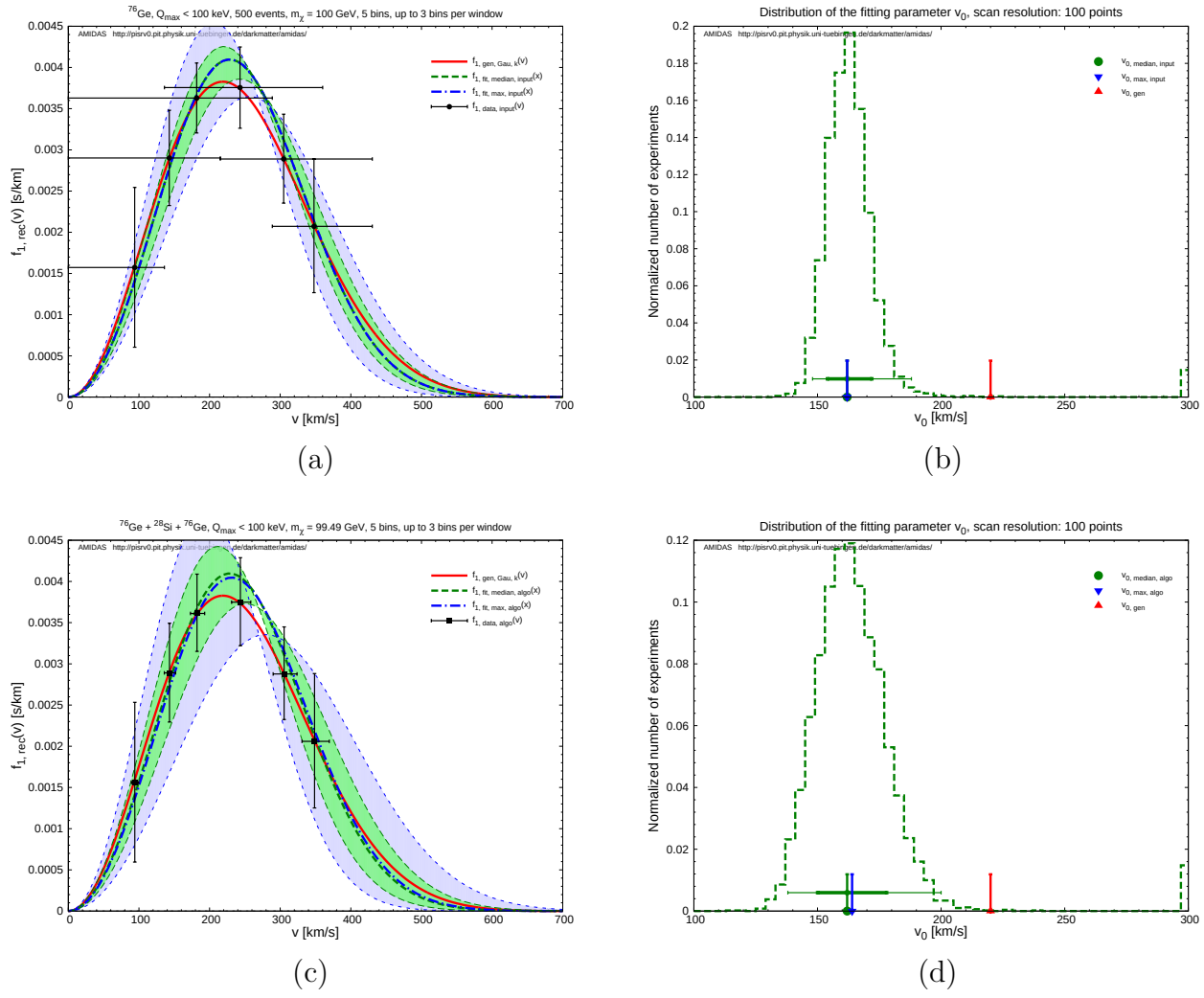
^{76}Ge, Q_{max} < 100 keV, 500 events, m_χ = 100 GeV, 5 bins, up to 3 bins per window
AMIDAS http://pisrv0.pit.physik.uni-tuebingen.de/darkmatter/amidas/
$f_{1,rec}(v)$ [s/km]
v [km/s]
(a)
Distribution of the fitting parameter v_0, scan resolution: 100 points
AMIDAS http://pisrv0.pit.physik.uni-tuebingen.de/darkmatter/amidas/
Normalized number of experiments
v_0 [km/s]
(b)
^{76}Ge + ^{28}Si + ^{76}Ge, Q_{max} < 100 keV, m_χ = 99.49 GeV, 5 bins, up to 3 bins per window
AMIDAS http://pisrv0.pit.physik.uni-tuebingen.de/darkmatter/amidas/
$f_{1,rec}(v)$ [s/km]
v [km/s]
(c)
Distribution of the fitting parameter v_0, scan resolution: 100 points
AMIDAS http://pisrv0.pit.physik.uni-tuebingen.de/darkmatter/amidas/
Normalized number of experiments
v_0 [km/s]
(d)

Figure 17: As in Figs. 16, except that the Gaussian probability distribution for v_0 with an expected value of $v_0 = 200$ km/s and a 1σ uncertainty of 40 km/s has been used.

Input: modified Maxwellian velocity distribution $f_{1,\mathrm{Gau},k}(v)$						
Reconstruction: one–parameter shifted Maxwellian velocity distribution $f_{1,\mathrm{sh},v_0}(v)$						
Parameter	WIMP mass	Prob. dist.	Max. p_{median}	Median	1σ range	2σ range
v_0 [km/s]	Input	Flat	162.0	$160.0\,^{+10.0}_{-8.0}\,(^{+28.0}_{-14.0})$	[152.0, 170.0]	[146.0, 188.0]
		Gaussian	162.0	$162.0\,^{+10.0}_{-8.0}\,(^{+26.0}_{-14.0})$	[154.0, 172.0]	[148.0, 188.0]
	Reconst.	Flat	162.0	$162.0 \pm 14.0\,(^{+36.0}_{-24.0})$	[148.0, 176.0]	[138.0, 198.0]
		Gaussian	164.0	$162.0\,^{+16.0}_{-12.0}\,(^{+38.0}_{-24.0})$	[150.0, 178.0]	[138.0, 200.0]

Table 10: The reconstructed results of v_0 for all four considered cases with the one–parameter shifted Maxwellian velocity distribution $f_{1,\mathrm{sh},v_0}(v)$ as well as the $1\,(2)\,\sigma$ uncertainty ranges of the median values.

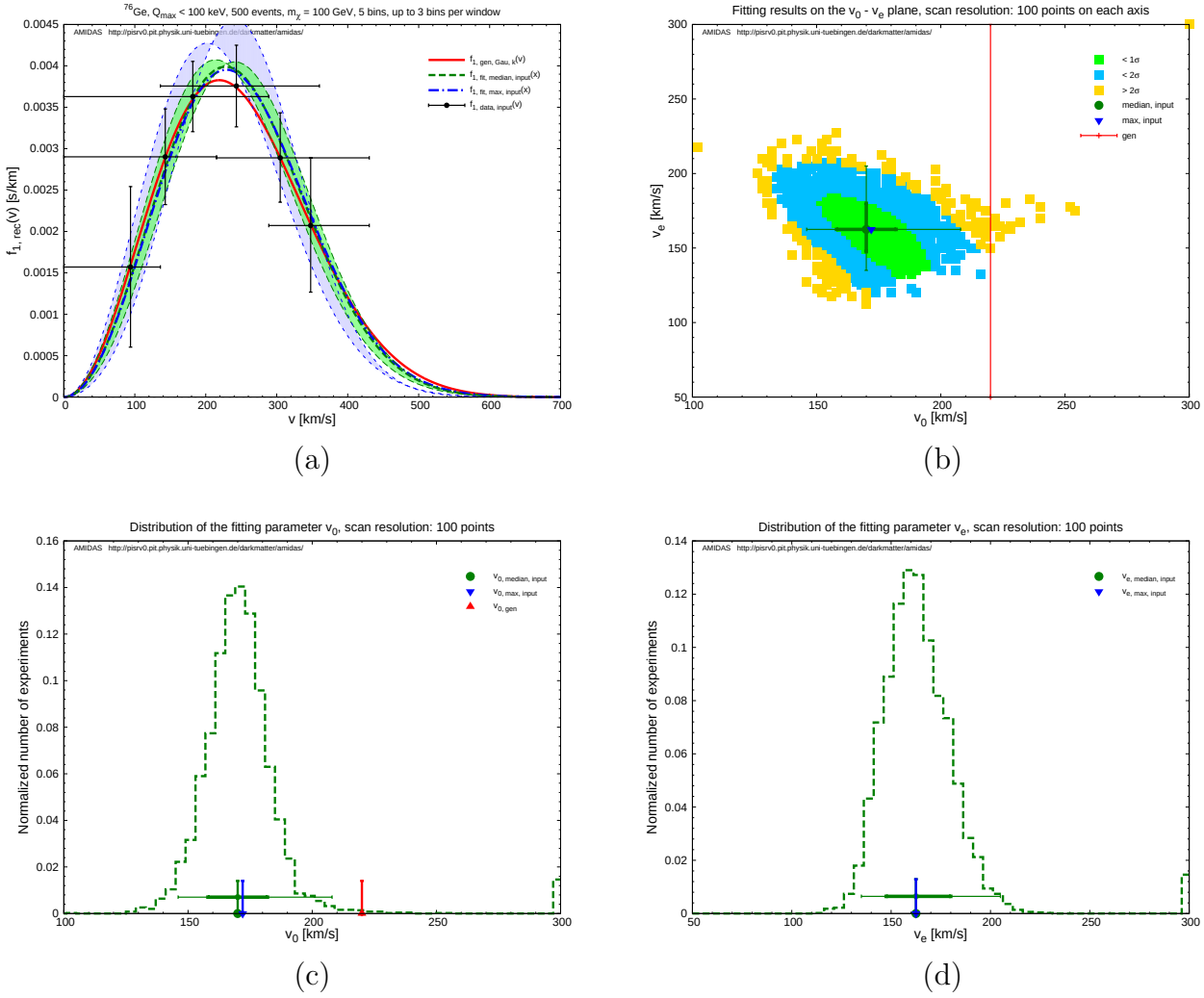

Figure 18: As in Figs. 9, except that the modified Maxwellian velocity distribution function given in Eq. (47) has been used for generating WIMP signals. Note that the solid red vertical line shown in (b) indicates the input value of the parameter v_0 (since no input value for v_e). The Gaussian probability distribution for both of two fitting parameters with a common expected value of $v_0 = v_e = 200$ km/s and a common 1σ uncertainty of 40 km/s has been used.

be necessary and could then improve the fitting results.

In table 10, we list the reconstructed results of v_0 for all four considered cases with the one–parameter shifted Maxwellian velocity distribution $f_{1,\mathrm{sh},v_0}(v)$ as well as the $1\,(2)\,\sigma$ uncertainty ranges of the median values of v_0.

3.3.3 Shifted Maxwellian velocity distribution

As in Sec. 3.2.3, we release now the fixed relation between v_0 and v_e given in Eq. (43) and consider the reconstruction of these two parameters simultaneously and independently. In addition, we also assume here that, from the (naive) trials with the simple and one–parameter shifted Maxwellian velocity distributions done previously, one could already obtain a rough idea about the shape of the velocity distribution of halo WIMPs as well as expected values of the Solar and Earth's orbital velocities v_0 and v_e. Hence, we consider here only the Gaussian probability distribution for both of two fitting parameters with a common expected value of $v_0 = v_e = 200$ km/s and a common 1σ uncertainty of 40 km/s (see Table 8). Note also that,

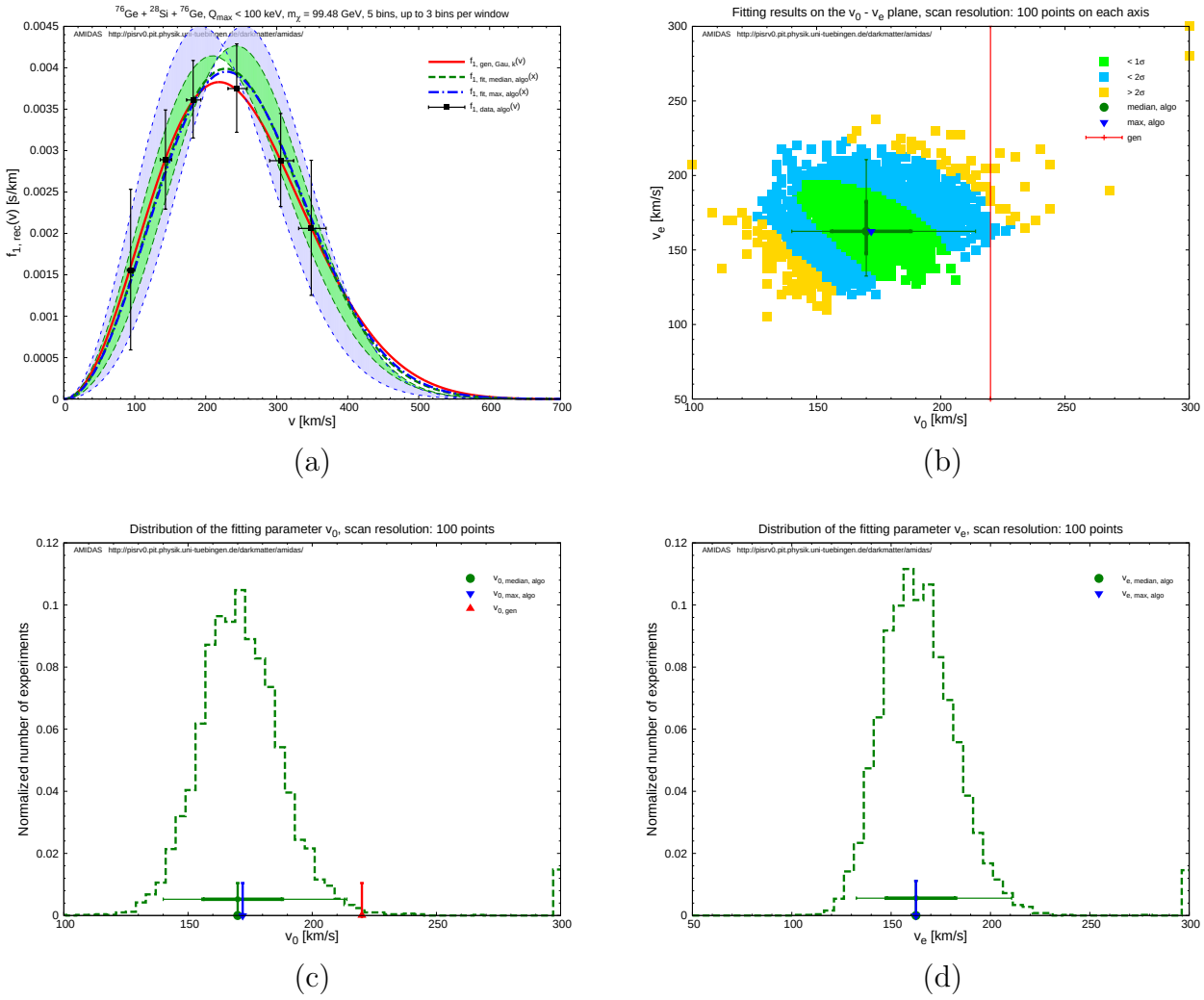

Figure 19: As in Figs. 18, except that the reconstructed WIMP mass has been used.

after some trial–and–error tests, we set the scanning ranges of v_0 and v_e as $v_0 \in [100, 300]$ km/s and $v_e \in [50, 300]$ km/s.

In Figs. 18, we consider first the case with the true (input) WIMP mass. As observed in Sec. 3.3.2, although the (low–velocity parts of the) $1\,(2)\,\sigma$ statistical uncertainty bands could cover the true (input) velocity distribution, the systematic deviations of the peaks of the reconstructed velocity distributions from that of the true (input) one would be ~ 10 km/s (a little bit better then results shown in Figs. 16(a) and (c)). Moreover, Figs. 18(c) and (d) show $\gtrsim 4\sigma$ deviations of the reconstructed values of v_0 and v_e from the true (input, estimated) values of $v_0 = 220$ km/s and $v_e = 231$ km/s. Additionally, the best–fit value of v_e is now even (~ 10 km/s) *smaller* than the best–fit value of v_0. Hence, as discussed in Sec. 3.3.2, this observation (combined with the results given in Sec. 3.3.2) would indicate evidently a high probability of the improper assumption of the fitting shifted Maxwellian velocity distribution. Moreover, in Figs. 19 we show our simulations with the reconstructed WIMP mass. The $1\,(2)\,\sigma$ statistical uncertainties on v_0 and v_e would be $\sim 10\%$ to $\sim 50\%$ enlarged.

Figs. 18 and 19 as well as Table 11 show that one could fit an improper model to experimental data (somehow) well with combinations of special, probably unusual values of the fitting parameters. On one hand, the reconstructed results could offer us (rough) information about the (shape of the) velocity distribution of Galactic WIMPs. On the other hand, however, the

Input: modified Maxwellian velocity distribution $f_{1,\mathrm{Gau},k}(v)$						
Reconstruction: shifted Maxwellian velocity distribution $f_{1,\mathrm{sh}}(v)$						
Parameter	WIMP mass	Prob. dist.	Max. $\mathrm{p}_{\mathrm{median}}$	Median	1σ range	2σ range
v_0 [km/s]	Input	Gaussian	172.0	$170.0 \pm 12.0\,(^{+38.0}_{-24.0})$	[158.0, 182.0]	[146.0, 208.0]
	Reconst.	Gaussian	172.0	$170.0\,^{+18.0}_{-14.0}\,(^{+44.0}_{-30.0})$	[156.0, 188.0]	[140.0, 214.0]
v_{e} [km/s]	Input	Gaussian	162.5	$162.5\,^{+17.5}_{-15.0}\,(^{+42.5}_{-27.5})$	[147.5, 180.0]	[135.0, 205.0]
	Reconst.	Gaussian	162.5	$162.5\,^{+20.0}_{-15.0}\,(^{+48.1}_{-30.0})$	[147.5, 182.5]	[132.5, 210.6]

Table 11: The reconstructed results of v_0 and v_{e} with the shifted Maxwellian velocity distribution $f_{1,\mathrm{sh}}(v)$ as well as the $1\,(2)\,\sigma$ uncertainty ranges of the median values.

observation that the reconstructed values of v_0 and v_{e} are 2σ to even $> 4\sigma$ different from our (theoretically) expected values would indicate evidently the improper assumption about the fitting velocity distribution function.

In table 11, we list the reconstructed results of v_0 and v_{e} with the shifted Maxwellian velocity distribution $f_{1,\mathrm{sh}}(v)$ as well as the $1\,(2)\,\sigma$ uncertainty ranges of the median values.

3.3.4 Variated shifted Maxwellian velocity distribution

As in Sec. 3.2.4, in order to correct the results given with the shifted Maxwellian velocity distribution function in Eq. (41), we consider here the use of its variation given in Eq. (44). As previously, we consider here only the Gaussian probability distribution for both of two fitting parameters v_0 and Δv, with a common 1σ uncertainty of *40* km/s. Moreover, according to the fitting results given in Sec. 3.3.3 and some trial–and–error tests, we set $v_0 = 200$ km/s and $\Delta v = -20$ km/s as the expected values as well as $v_0 \in [100, 300]$ km/s and $\Delta v \in [-120, 80]$ km/s as the scanning ranges.

Comparing Figs. 20 to Figs. 18, it can be seen clearly that the use of the variated shifted Maxwellian velocity distribution could indeed offer a more reasonable and preciser reconstruction: not only that the ($1\,(2)\,\sigma$ statistical uncertainty bands of the) reconstructed velocity distribution function can match the true (input) one more closer, the $1\,(2)\,\sigma$ statistical uncertainties on v_0 is also only $\lesssim 70\%$ of the uncertainties shown in Figs. 18(c). Additionally, by using Eq. (46), the upper bound of the $1\,(2)\,\sigma$ statistical uncertainties on v_{e} can be (approximately) given as: $^{+16.12}_{-12.80}\,(^{+41.23}_{-24.41})$ km/s, which is also maximal (approximately) equal to or even smaller than the uncertainties given in Table 12. Hence, we would like to conclude that our introduction of the variated shifted Maxwellian velocity distribution (and/or probably some other variations) could indeed be a useful strategy for the practical use of our Bayesian reconstruction procedure.

On the other hand, in Figs. 21 we use the reconstructed WIMP mass. Comparing Figs. 21 to Figs. 20 (see also Table 12), although the width of the $1\,(2)\,\sigma$ statistical uncertainty bands of the reconstructed velocity distribution function as well as the $1\,(2)\,\sigma$ statistical uncertainties on v_0 would be clearly larger, the $1\,(2)\,\sigma$ statistical uncertainties on Δv are approximately equal to results with the true (input) WIMP mass. Meanwhile, even for this case with the reconstructed WIMP mass, the $1\,(2)\,\sigma$ statistical uncertainties on v_0 and Δv are (much) smaller than the given 1σ uncertainty of their Gaussian probability distributions (40 km/s).

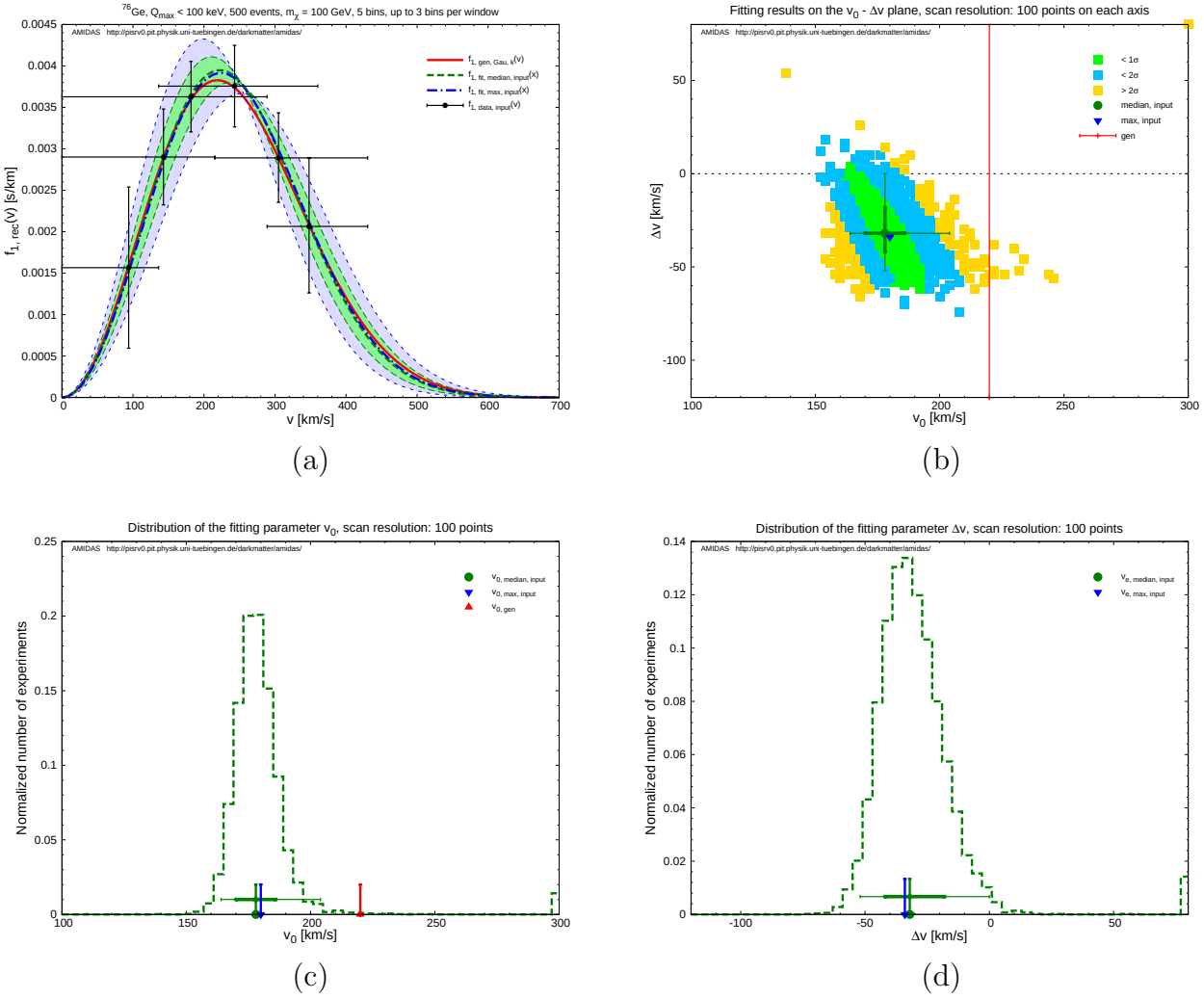

Figure 20: As in Figs. 18, except that the variated shifted Maxwellian velocity distribution function given in Eq. (44) with two fitting parameters v_0 and Δv is used. The Gaussian probability distribution for both of two fitting parameters with expected values of $v_0 = 200$ km/s and $\Delta v = -20$ km/s and a common 1σ uncertainty of 40 km/s has been used.

Input: modified Maxwellian velocity distribution $f_{1,\mathrm{Gau},k}(v)$						
Reconstruction: variated shifted Maxwellian velocity distribution $f_{1,\mathrm{sh},\Delta v}(v)$						
Parameter	WIMP mass	Prob. dist.	Max. p_{median}	Median	1σ range	2σ range
v_0 [km/s]	Input	Gaussian	180.0	$178.0 \pm 8.0\,(^{+26.0}_{-14.0})$	[170.0, 186.0]	[164.0, 204.0]
	Reconst.	Gaussian	180.0	$178.0\,^{+14.0}_{-12.0}\,(^{+34.5}_{-22.0})$	[166.0, 192.0]	[156.0, 212.5]
Δv [km/s]	Input	Gaussian	−34.0	$-32.0\,^{+14.0}_{-10.0}\,(^{+32.0}_{-20.0})$	[−42.0, −18.0]	[−52.0, 0.0]
	Reconst.	Gaussian	−32.0	$-32.0\,^{+14.0}_{-10.0}\,(^{+30.5}_{-20.0})$	[−42.0, −18.0]	[−52.0, −1.5]

Table 12: The reconstructed results of v_0 and Δv with the variated shifted Maxwellian velocity distribution $f_{1,\mathrm{sh},\Delta v}(v)$ as well as the $1\,(2)\,\sigma$ uncertainty ranges of the median values.

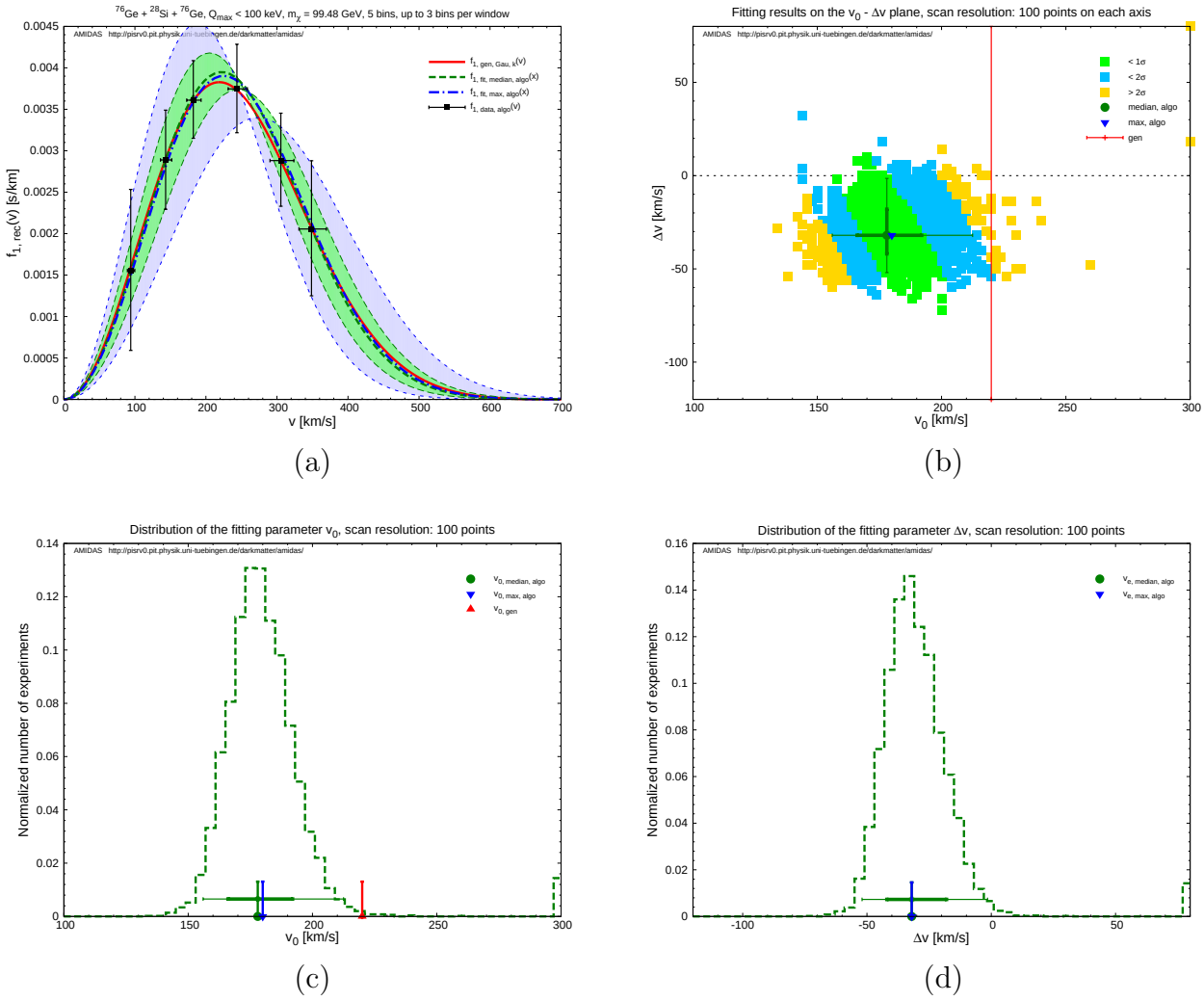

Figure 21: As in Figs. 20, except that the reconstructed WIMP mass has been used.

Remind that, our simulations of the use of the variated shifted Maxwellian velocity distribution function for fitting data generated by (modified) simple Maxwellian one shown here indicates again that, by using an "improper" assumption about the fitting velocity distribution function with prior knowledge about the fitting parameters (v_0, v_e or Δv), one would still reconstruct an approximate shape of the WIMP velocity distribution; the deviations of the peaks of the reconstructed velocity distributions from that of the true (input) one could even be $\lesssim$ *10* km/s, much smaller than the commonly used 1σ uncertainty on the Solar orbital velocity of ~ 20 km/s.

However, our simulations show also that, with an "improper" assumption about the fitting velocity distribution, one would obtain an "unexpected" result about each single fitting parameter. E.g. here we get 3σ to 5σ deviations of the reconstructed Solar orbital velocity from the theoretical estimate (see Table 12) and a large "negative" value for the difference between the Solar and Earth's orbital velocities. This observation indicates clearly that our initial assumption about the fitting velocity distribution function would be incorrect or at least need to be modified.

In table 12, we list the reconstructed results of v_0 and Δv with the variated shifted Maxwellian velocity distribution $f_{1,\mathrm{sh},\Delta v}(v)$ as well as the $1\,(2)\,\sigma$ uncertainty ranges of the median values.

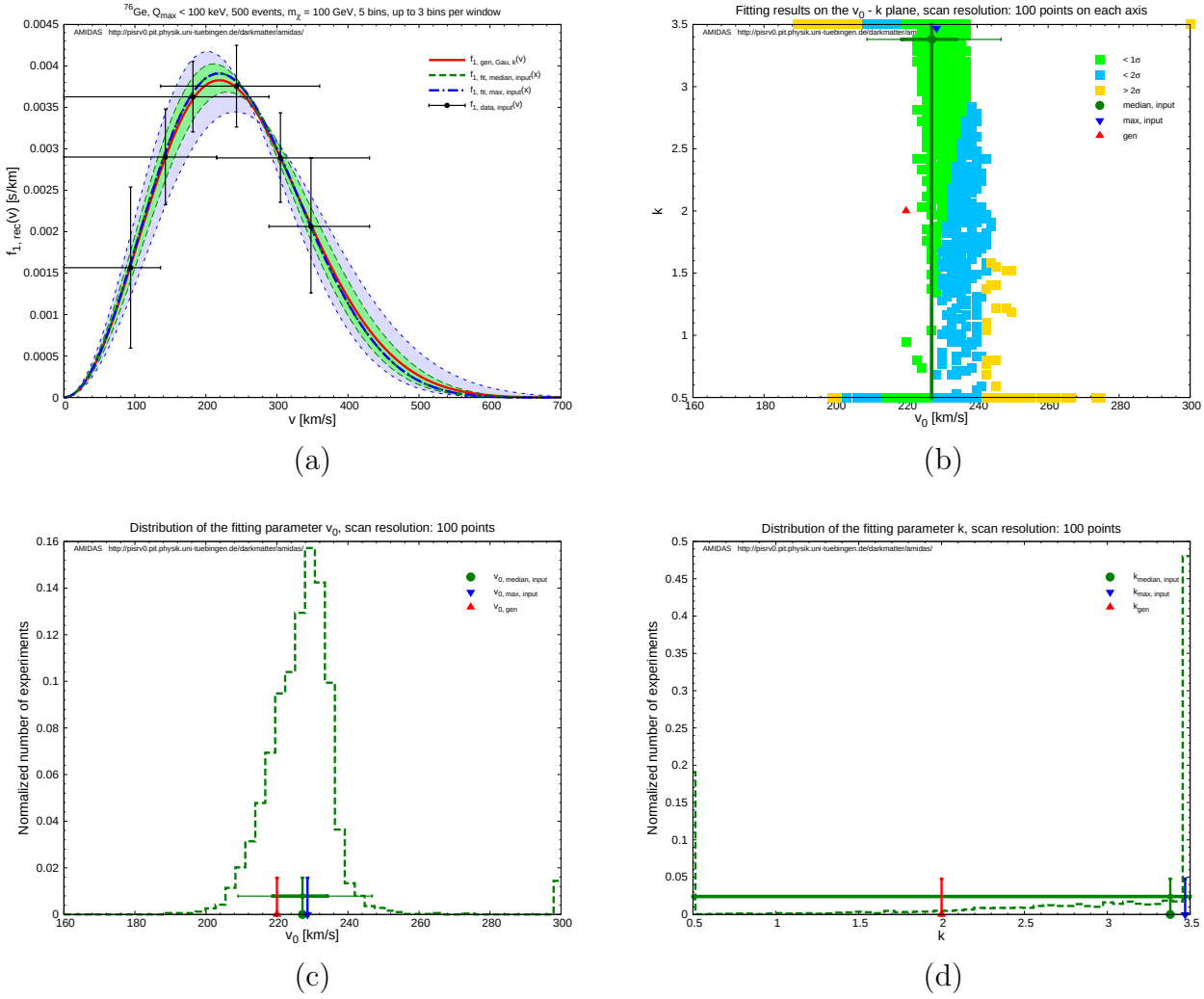

Figure 22: As in Figs. 18, except that the modified Maxwellian velocity distribution function given in Eq. (47) with two fitting parameters v_0 and k is used. The Gaussian probability distribution for v_0 with an expected value of $v_0 = 230$ km/s and a 1σ uncertainty of 20 km/s but the flat distribution for k have been used. Note that the bins at $k = 0.5$ and $k = 3.5$ are "overflow" bins, which contain also the experiments with the best–fit k value of either $k < 0.5$ or $k > 3.5$.

3.3.5 Modified Maxwellian velocity distribution

As the last tested fitting velocity distribution function with data generated by the modified Maxwellian velocity distribution given by Eq. (47), we consider now the reconstruction of the modified Maxwellian velocity distribution itself with two fitting parameters: the Solar orbital velocity v_0 and the power index k.

In Figs. 22 and 23, we use the Gaussian probability distribution for the fitting parameter v_0 with an expected value of $v_0 = 230$ km/s and a 1σ uncertainty of 20 km/s but the flat distribution for the parameter k, with either the precisely known (input) or the reconstructed WIMP mass, respectively. Note that in Figs. 22(d) and 23(d) the bins at $k = 0.5$ and $k = 3.5$ are "overflow" bins. This means that they contain also the experiments whose best–fit values of k would be either $k < 0.5$ or $k > 3.5$.

First, as shown in Sec. 3.3.1, the Solar orbital velocity v_0 could be pinned down very precisely: a small systematic deviation of < 10 km/s and 1σ statistical uncertainty of $\lesssim 10$ km/s could be

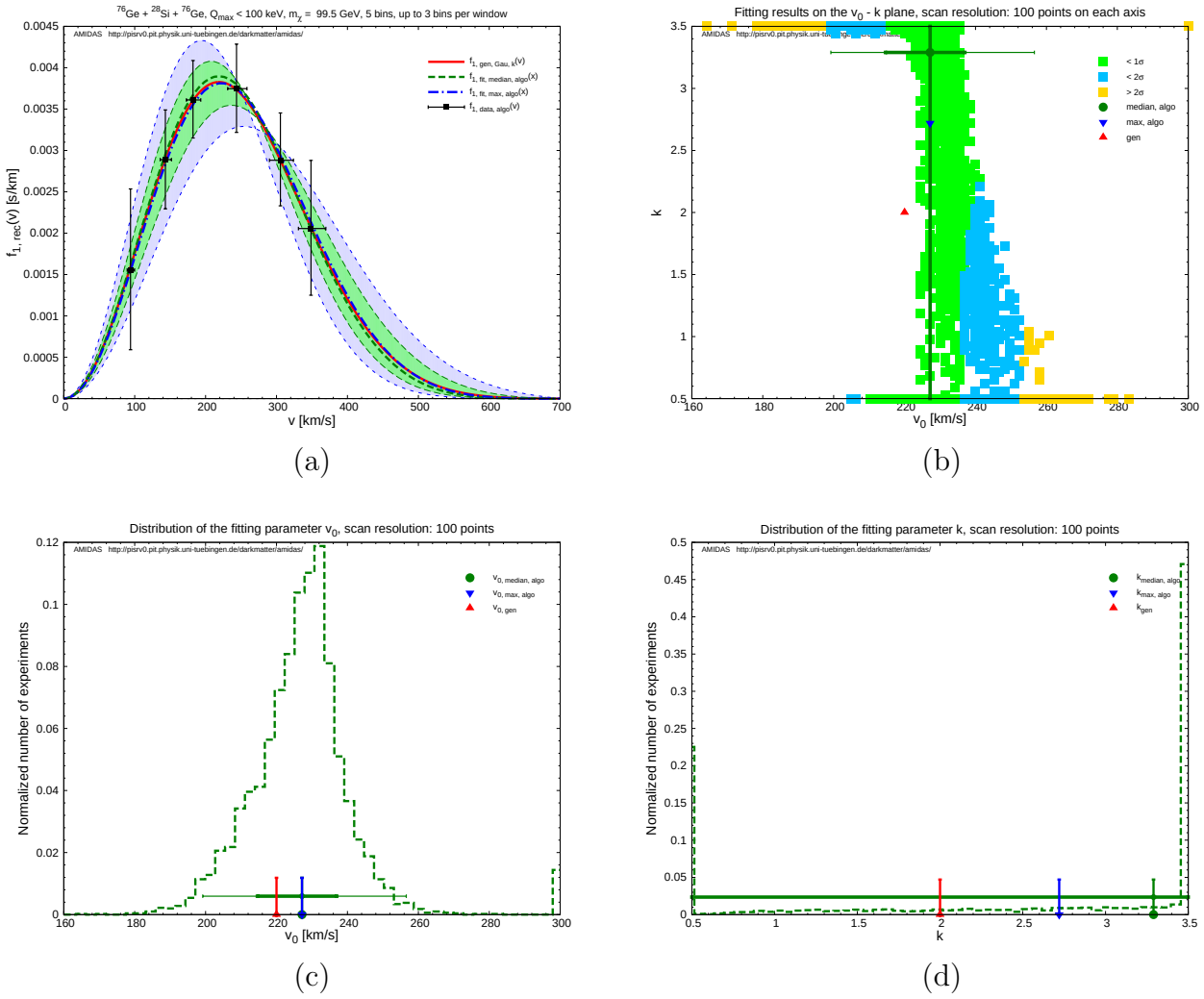

Figure 23: As in Figs. 22, except that the reconstructed WIMP mass has been used.

Input: modified Maxwellian velocity distribution $f_{1,\mathrm{Gau},k}(v)$						
Reconstruction: modified Maxwellian velocity distribution $f_{1,\mathrm{Gau},k}(v)$						
Parameter	WIMP mass	Prob. dist.	Max. p_{median}	Median	1σ range	2σ range
v_0 [km/s]	Input	Gaussian	228.6	$227.2\,^{+7.0}_{-8.4}\,(^{+19.6}_{-18.2})$	[218.8, 234.2]	[209.0, 246.8]
	Reconst.	Gaussian	227.2	$227.2\,^{+9.8}_{-12.6}\,(^{+29.4}_{-28.0})$	[214.6, 237.0]	[199.2, 256.6]
k	Input	Flat	3.47	3.38	[0.5, 3.5]	$\times$
	Reconst.	Flat	2.72	3.29	[0.5, 3.5]	$\times$

Table 13: The reconstructed results of v_0 and k with the modified Maxwellian velocity distribution $f_{1,\mathrm{Gau},k}(v)$ as well as the $1\,(2)\,\sigma$ uncertainty ranges of the median values. Note that, firstly, we use here the Gaussian probability distribution for v_0 but the flat one for k, respectively. Secondly, since the 1σ lower and upper bounds of the median values of k are already beyond our scanning range, the 2σ bounds are meanless to give here.

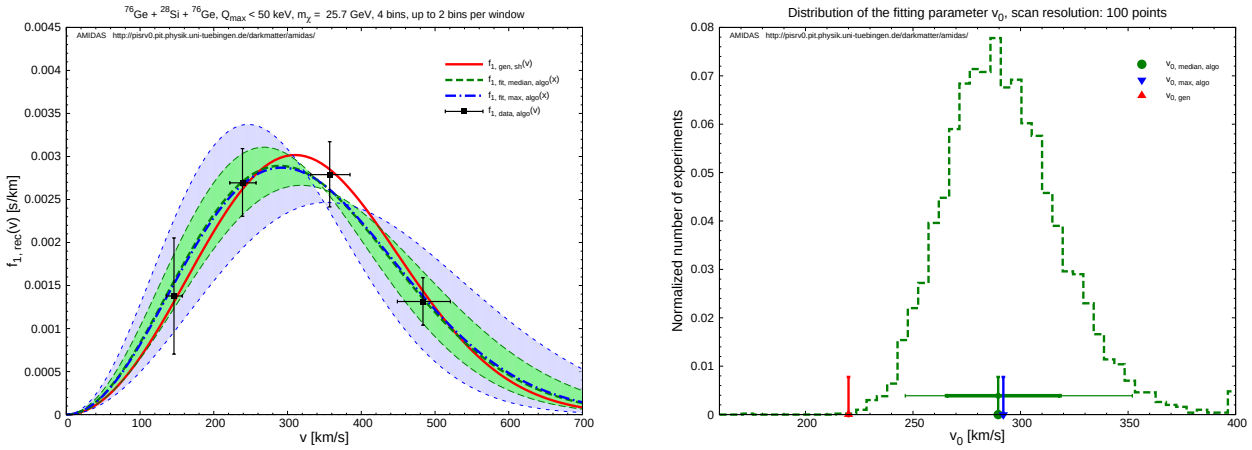

Figure 24: As in Figs. 5(c) and (d): shifted and simple Maxwellian velocity distributions have been used for generating WIMP events and as the fitting function, respectively; the flat probability distribution for v_0 and the reconstructed WIMP mass has been used, except that the input WIMP mass has been set as $m_\chi = 25$ GeV. See the text for further details about the simulation setup.

achieved. However, Figs. 22(b) and (d) as well as Figs. 23(b) and (d) show that, due to the small difference between the modified Maxwellian velocity distribution with different power indices k (see Fig. 13) and the large statistical fluctuation and 1σ reconstruction uncertainty with only 500 WIMP events (on average), our Bayesian reconstruction of the velocity distribution would be *totally non–sensitive* on the second fitting parameter (power index) k.

Nevertheless, the wild spread of the reconstructed power index k (in particular, the high cumulative numbers in the (overflow) bin $k = 3.5$) and, in contrast, the narrow widths of the $1(2)\sigma$ statistical uncertainty bands of the reconstructed velocity distribution function imply that, for reconstructing the rough information about the one–dimensional WIMP velocity distribution, a precise value of the power index k would *not be crucial*, and the *simple* Maxwellian velocity distribution $f_{1,\mathrm{Gau}}(v)$ given in Eq. (40) would already be a good approximation[11].

In Table 13 we give the reconstructed results of v_0 and k with the modified Maxwellian velocity distribution $f_{1,\mathrm{Gau},k}(v)$ as well as the $1\,(2)\,\sigma$ uncertainty ranges of the median values. Note that, since the 1σ lower and upper bounds of the median values of k are already beyond our scanning range, the 2σ bounds are meanless to give here.

3.4 For different WIMP masses

In the previous Secs. 3.1 to 3.3, we fixed the input WIMP mass as $m_\chi = 100$ GeV. As a further test of our Bayesian reconstruction method for the one–dimensional WIMP velocity distribution, in this subsection, we consider the cases for either a lighter WIMP mass of $m_\chi = 25$ GeV or a

[11] As described in Ref. [18], the modification of the simple Maxwellian velocity distribution function $f_{1,\mathrm{Gau},k}(v)$ given in Eq. (47) has significant difference from the simple Maxwellian one given in Eq. (40) in the high–velocity tail. Moreover, in Refs. [19, 20], another empirical modification of the simple Maxwellian velocity distribution with also a significant difference in the high–velocity tail has been introduced. Unfortunately, our simulations presented here show that it would be *impossible* to distinguish these subtle modifications by our Bayesian reconstruction method (with only a few hundreds of recorded WIMP events).

On the other hand, simulations with other (well–motivated) halo models and different fitting velocity distribution functions can be tested on the `AMIDAS` website [21, 22].

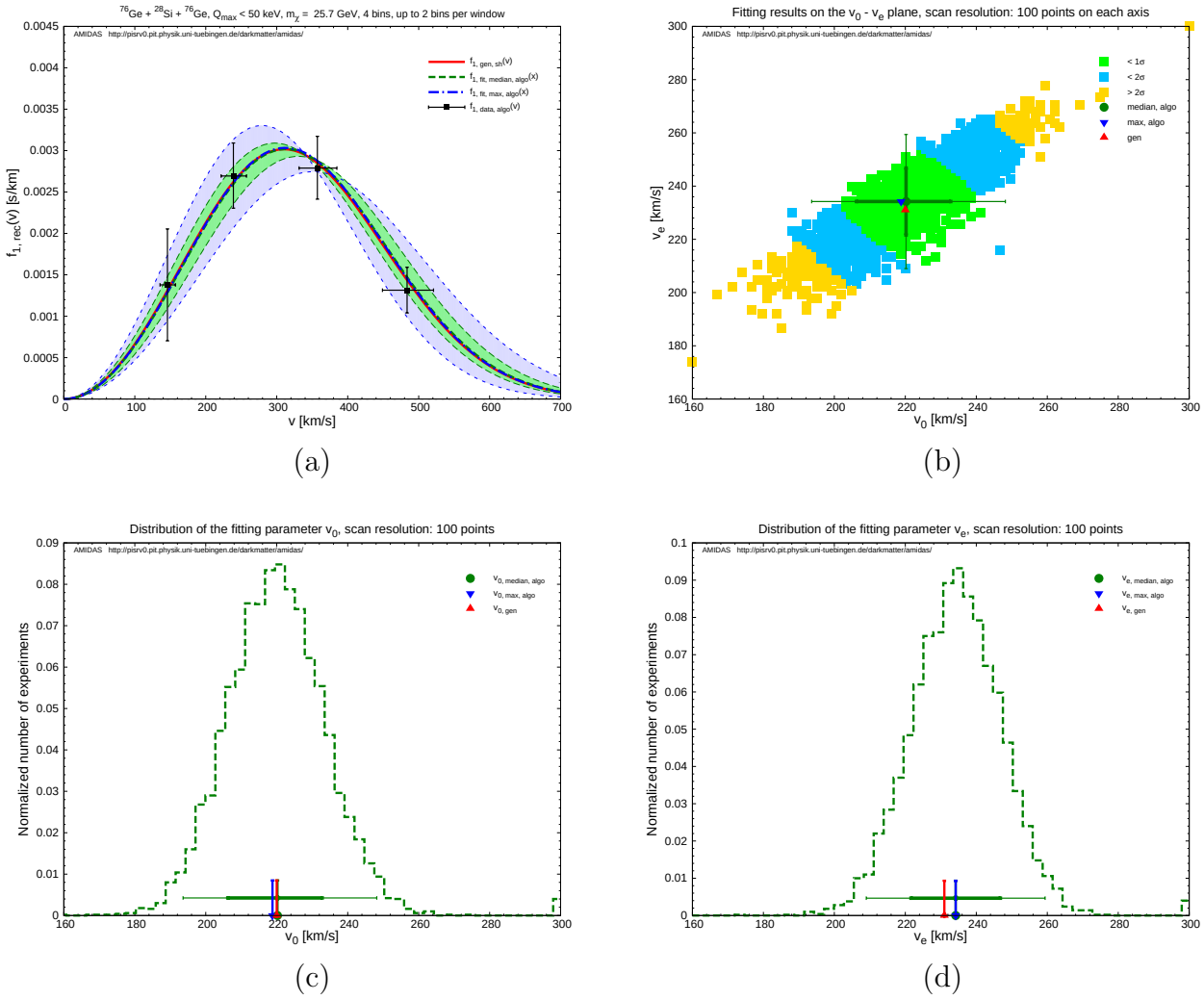

Figure 25: As in Figs. 10: the shifted Maxwellian velocity distribution function and the Gaussian probability distribution for both of two fitting parameters with expected values of $v_0 = 230$ km/s and $v_e = 245$ km/s and a common 1σ uncertainty of 20 km/s as well as the reconstructed WIMP mass have been used, except that the input WIMP mass has been set as $m_\chi = 25$ GeV.

heavier WIMP mass of $m_\chi = 250$ GeV.

Here we consider only the *shifted* Maxwellian velocity distribution given in Eq. (41) for generating WIMP events; three fitting functions: simple, shifted and variated shifted Maxwellian velocity distributions will be tested. All input setup and fitting parameters are the same as in Sec. 3.2 (see Table 3). Additionally, only the *reconstructed* WIMP mass is used.

3.4.1 For a light WIMP mass

We consider first a rather light WIMP mass of $m_\chi = 25$ GeV. Note that, firstly, since for our tested targets ^{28}Si and ^{76}Ge, the kinematic maximal cut–off energies given in Eq. (36) are only $Q_{\mathrm{max,kin,Si}} = 68.12$ keV and $Q_{\mathrm{max,kin,Ge}} = 52.65$ keV, respectively, the maximal experimental cut–off energy for both targets in our simulations demonstrated here has been reduced to only $Q_{\mathrm{max}} = 50$ keV. Secondly, since the lighter the WIMP mass, the shaper the expected recoil energy spectrum, the width of the first energy bin in Eq. (18) has been set as $b_1 = 5$ keV and the total number of bins has been reduced to only *four* bins between Q_{min} and Q_{max} ($B = 4$); up to *two* bins have been combined to a window and thus em four windows ($W = 4$) will be

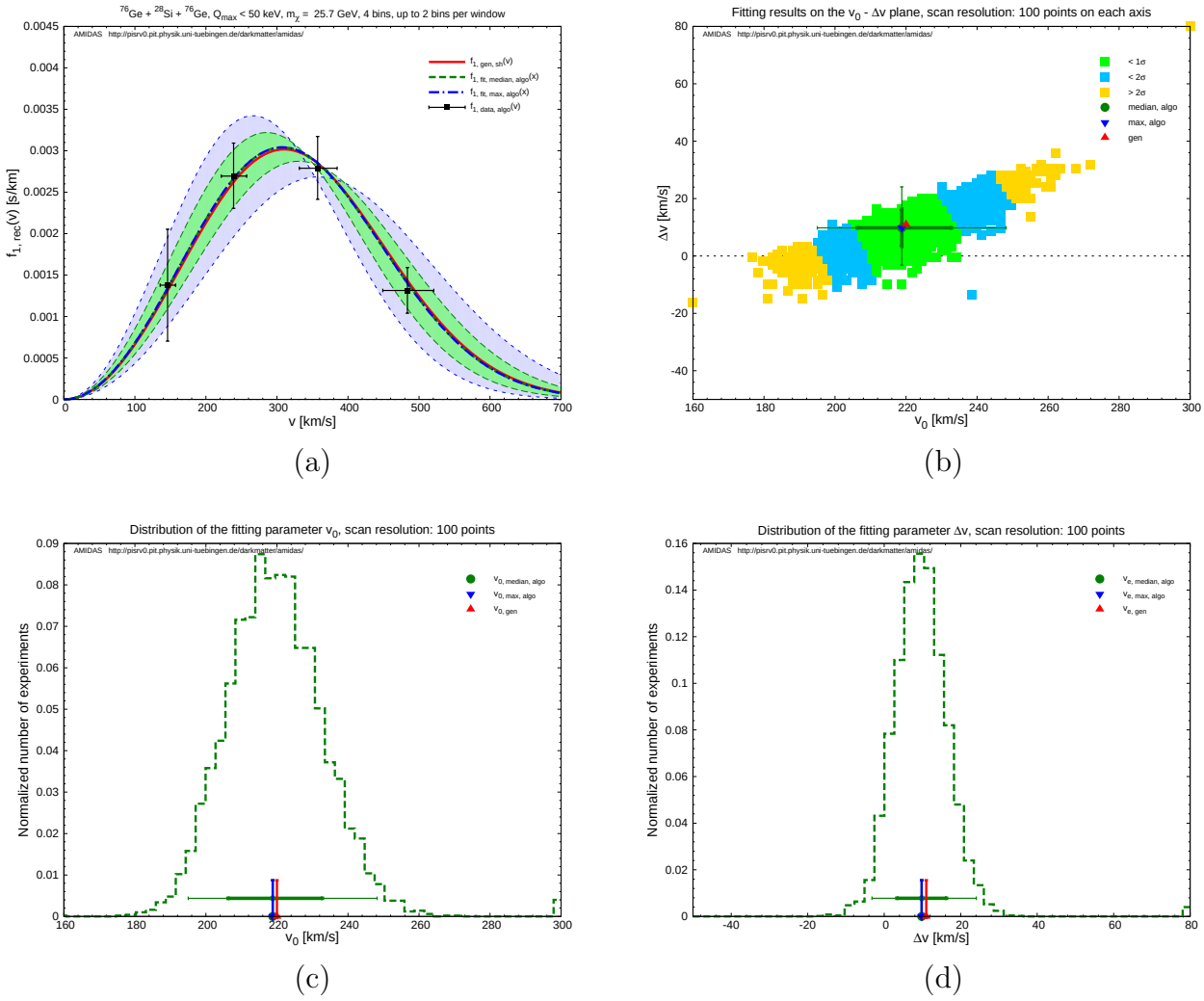

Figure 26: As in Figs. 25, except that the variated shifted Maxwellian velocity distribution function and the Gaussian probability distribution for both of two fitting parameters with expected values of $v_0 = 230$ km/s and $\Delta v = 15$ km/s and a common 1σ uncertainty of 20 km/s has been used (cf. also Figs. 12).

reconstructed[12, 13].

Simple Maxwellian velocity distribution

In Figs. 24 (cf. Figs. 5(c) and (d)), we use first the (improper) simple Maxwellian velocity distribution function with one parameter v_0 to fit the reconstructed–input data. As the first trial of the reconstruction of the one–dimensional WIMP velocity distribution *without* prior knowledge about the Solar orbital velocity, the flat probability distribution has been used here (results with the Gaussian probability distribution are given in Table 14).

Although we use the improper assumption about the fitting velocity distribution and only *four* available data points (solid black vertical bars), the 1 (2) σ statistical uncertainty bands could still cover the true (input) velocity distribution with a systematic deviation of the peak of

[12]The last window is neglected automatically in the `AMIDAS` code, due to a very few expected event number in the last bin (window).

[13]It has been found that, by reducing the total number of the energy bins (and in turn that of the windows) and thus collecting more events in one bin (window), the Bayesian reconstructed velocity distribution could be improved significantly.

Input: shifted Maxwellian velocity distribution $f_{1,\rm sh}(v)$						
Reconstruction: simple Maxwellian velocity distribution $f_{1,\rm Gau}(v)$						
Parameter	WIMP mass	Prob. dist.	Max. $p_{\rm median}$	Median	1σ range	2σ range
v_0 [km/s]	Input	Flat	296.8	$294.4\,^{+14.4}_{-12.0}\,(^{+31.2}_{-21.6})$	[282.4, 308.8]	[272.8, 325.6]
		Gaussian	294.4	$294.4\,^{+9.6}_{-12.0}\,(^{+24.0}_{-21.6})$	[282.4, 304.0]	[272.8, 318.4]
	Reconst.	Flat	292.0	$289.6\,^{+28.8}_{-24.0}\,(^{+62.4}_{-43.2})$	[265.6, 318.4]	[246.4, 352.0]
		Gaussian	292.0	$289.6 \pm 21.6\,(^{+48.0}_{-40.8})$	[268.0, 311.2]	[248.8, 337.6]
Reconstruction: one–parameter shifted Maxwellian velocity distribution $f_{1,{\rm sh},v_0}(v)$						
v_0 [km/s]	Input	Flat	220.2	$218.8\,^{+9.8}_{-7.0}\,(^{+19.6}_{-14.0})$	[211.8, 228.6]	[204.8, 238.4]
		Gaussian	221.6	$221.6 \pm 7.0\,(^{+15.4}_{-14.0})$	[214.6, 228.6]	[207.6, 237.0]
	Reconst.	Flat	217.4	$214.6\,^{+21.0}_{-16.8}\,(^{+44.8}_{-30.8})$	[197.8, 235.6]	[183.8, 259.4]
		Gaussian	218.8	$218.8 \pm 15.4\,(^{+32.2}_{-29.4})$	[203.4, 234.2]	[189.4, 251.0]
Reconstruction: shifted Maxwellian velocity distribution $f_{1,\rm sh}(v)$						
v_0 [km/s]	Input	Gaussian	221.6	$221.6 \pm 7.0\,(^{+15.4}_{-12.9})$	[214.6, 228.6]	[208.7, 237.0]
	Reconst.	Gaussian	218.8	$220.2\,^{+12.6}_{-14.0}\,(^{+28.0}_{-26.6})$	[206.2, 232.8]	[193.6, 248.2]
$v_{\rm e}$ [km/s]	Input	Gaussian	237.0	$237.0\,^{+7.0}_{-8.4}\,(^{+14.0}_{-16.8})$	[228.6, 244.0]	[220.2, 251.0]
	Reconst.	Gaussian	234.2	$234.2 \pm 12.6(\pm 25.2)$	[221.6, 246.8]	[209.0, 259.4]
Reconstruction: variated shifted Maxwellian velocity distribution $f_{1,{\rm sh},\Delta v}(v)$						
v_0 [km/s]	Input	Gaussian	221.6	$221.6 \pm 5.6\,(^{+12.6}_{-11.2})$	[216.0, 227.2]	[210.4, 234.2]
	Reconst.	Gaussian	218.8	$218.8\,^{+14.0}_{-12.6}\,(^{+29.4}_{-23.8})$	[206.2, 232.8]	[195.0, 248.2]
Δv [km/s]	Input	Gaussian	9.8	$11.1\,^{+3.9}_{-5.2}\,(^{+9.1}_{-11.7})$	[5.9, 15.0]	$[-0.6, 20.2]$
	Reconst.	Gaussian	9.8	$9.8 \pm 6.5\,(^{+14.3}_{-13.0})$	[3.3, 16.3]	$[-3.2, 24.1]$

Table 14: The reconstructed results with four fitting velocity distribution functions for the input WIMP mass of $m_\chi = 25$ GeV.

the reconstructed velocity distribution of $\lesssim 15$ km/s. However, the best–fit values of the Solar orbital velocity are now $\simeq 294$ km/s and $\sim 3\sigma$ apart from the theoretically expected value.

Moreover, our further simulations with the Gaussian probability distribution for the fitting parameter v_0 with an expected value of $v_0 = 280$ km/s and a 1σ uncertainty of 40 km/s show that, the $1\,(2)\,\sigma$ statistical uncertainties for such a light WIMP mass could be $\sim 60\%$ to $\sim 80\%$ reduced (see Table 14 and Table 4).

Shifted Maxwellian velocity distribution

In Figs. 25 (cf. Figs. 10), the shifted Maxwellian velocity distribution with two fitting parameters v_0 and $v_{\rm e}$ has been tested to fit to the reconstructed–input data. Only the Gaussian

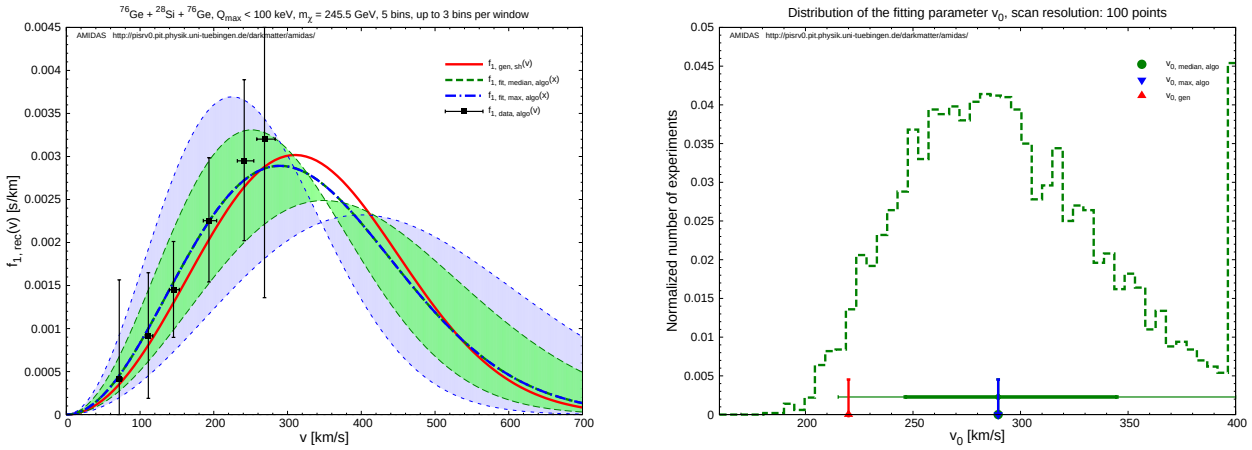

Figure 27: As in Figs. 24: the flat probability distribution for v_0 and the reconstructed WIMP mass have been used, except that the input WIMP mass has been set as $m_\chi = 250$ GeV.

probability distribution for both of two fitting parameters with expected values of $v_0 = 230$ km/s and $v_e = 245$ km/s and a common 1σ uncertainty of 20 km/s is considered here.

Astonishingly, with *only four* available data points the reconstructed velocity distribution functions could match the true (input) one very precisely: the systematic deviation of v_0 is negligible and that of v_e is *only a few* km/s, the $1\,(2)\,\sigma$ statistical uncertainties on two fitting parameters are also only $^{+12.6}_{-14.0}\,(^{+28.0}_{-26.6})$ and $\pm 12.6(\pm 25.2)$, respectively.

Variated shifted Maxwellian velocity distribution

In Figs. 26 (cf. Figs. 12), the variated shifted Maxwellian velocity distribution with two fitting parameters v_0 and Δv has been tested to fit to the reconstructed–input data. Only the Gaussian probability distribution for both of two fitting parameters with expected values of $v_0 = 230$ km/s and $\Delta v = 15$ km/s and a common 1σ uncertainty of 20 km/s is considered here.

It can be seen that, although the $1\,(2)\,\sigma$ statistical uncertainty bands are a bit wilder than those given with the shifted Maxwellian distribution, with only four available data points the reconstructed velocity distribution function could also match the true (input) one very well. Moreover, as shown in Secs. 3.2.4 and 3.3.4, the second fitting parameter Δv could also be pinned down very precisely with a negligible systematic deviation.

In Table 14, we give the reconstructed results with all four fitting velocity distribution functions for the input WIMP mass of $m_\chi = 25$ GeV. Both cases with the true (input) and the reconstructed WIMP masses have been simulated and summarized.

3.4.2 For a heavy WIMP mass

We consider now a rather heavy WIMP mass of $m_\chi = 250$ GeV. The maximal experimental cut–off energy for both targets in our simulations demonstrated here has been set again as $Q_{\rm max} = 100$ keV. And, as usual, the width of the first energy bin in Eq. (18) has been set as $b_1 = 10$ keV, *five* bins between $Q_{\rm min}$ and $Q_{\rm max}$ are used ($B = 5$) and up to *three* bins have been combined to a window ($W = 6$).

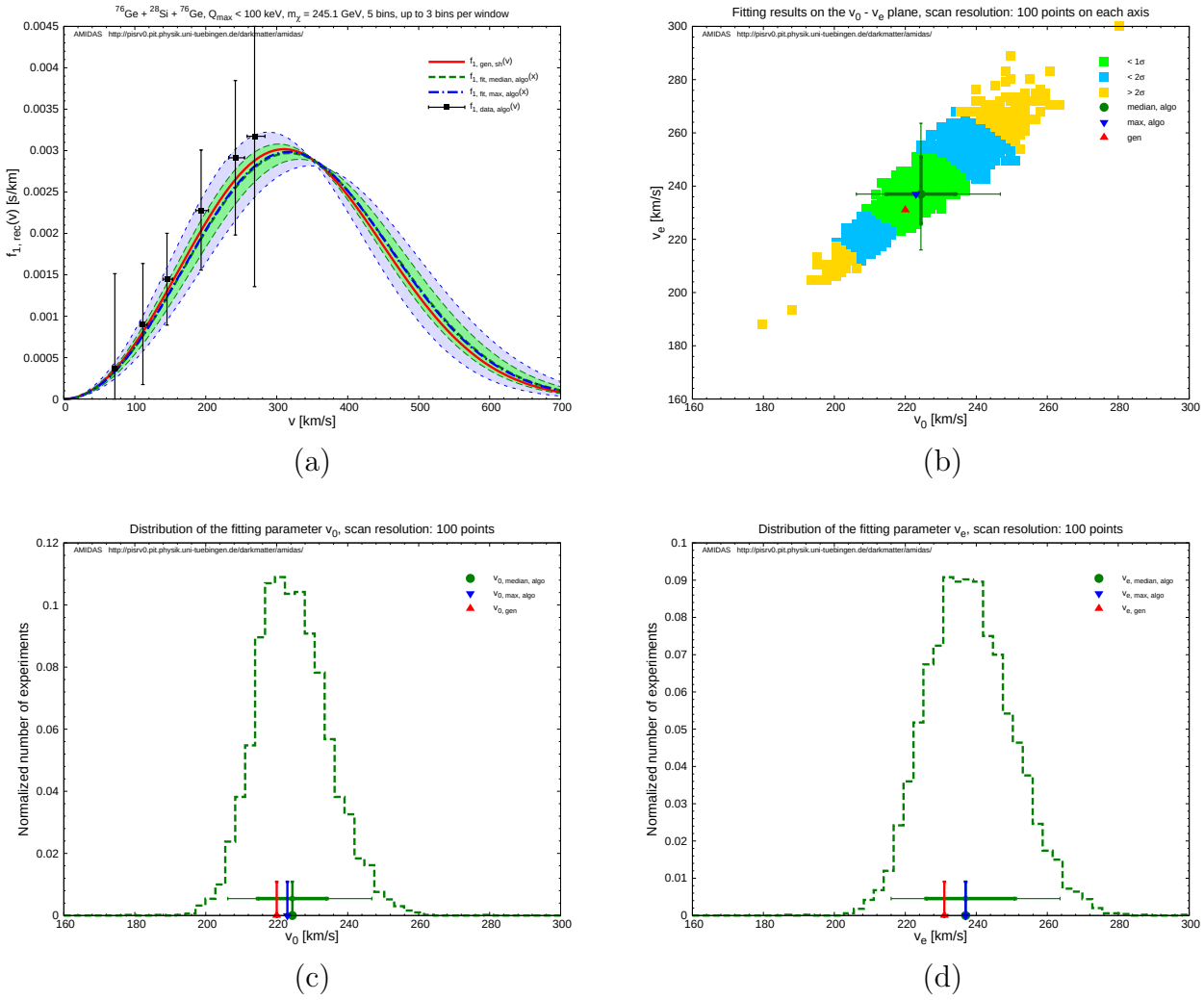

Figure 28: As in Figs. 25: the Gaussian probability distribution for both of two fitting parameters v_0 and v_e as well as the reconstructed WIMP mass have been used, except that the input WIMP mass has been set as $m_\chi = 250$ GeV.

Simple Maxwellian velocity distribution

For a heavy WIMP mass, due to the statistical fluctuation discussed in Ref. [6], our reconstructed velocity distribution functions given in Figs. 27(a) (cf. Figs. 5(c) and 24(a)) have clearly a (much) wilder $1\,(2)\,\sigma$ statistical uncertainty bands; the $1\,(2)\,\sigma$ statistical uncertainties on the reconstructed Solar orbital velocity are also (much) wilder as $^{+33.6}_{-31.2}$ ($^{+64.8}_{-60.0}$) km/s. And, as shown in Figs. 27(b), a considerable fraction of the reconstructed v_0 would excess our scanning upper bound of 400 km/s.

Nevertheless, comparing to the much larger 1σ statistical uncertainty on the reconstructed–input data (solid black vertical bars), our Bayesian reconstruction with an in fact improper fitting velocity distribution could still offer an approximation with only $\lesssim 15$ km/s systematic deviation of the peak of the reconstructed velocity distribution.

Shifted Maxwellian velocity distribution

In Figs. 28 (cf. Figs. 10 and 25), the shifted Maxwellian velocity distribution with two fitting parameters v_0 and v_e has been tested to fit to the reconstructed–input data. Only the Gaussian probability distribution for both of two fitting parameters with expected values of $v_0 = 230$ km/s

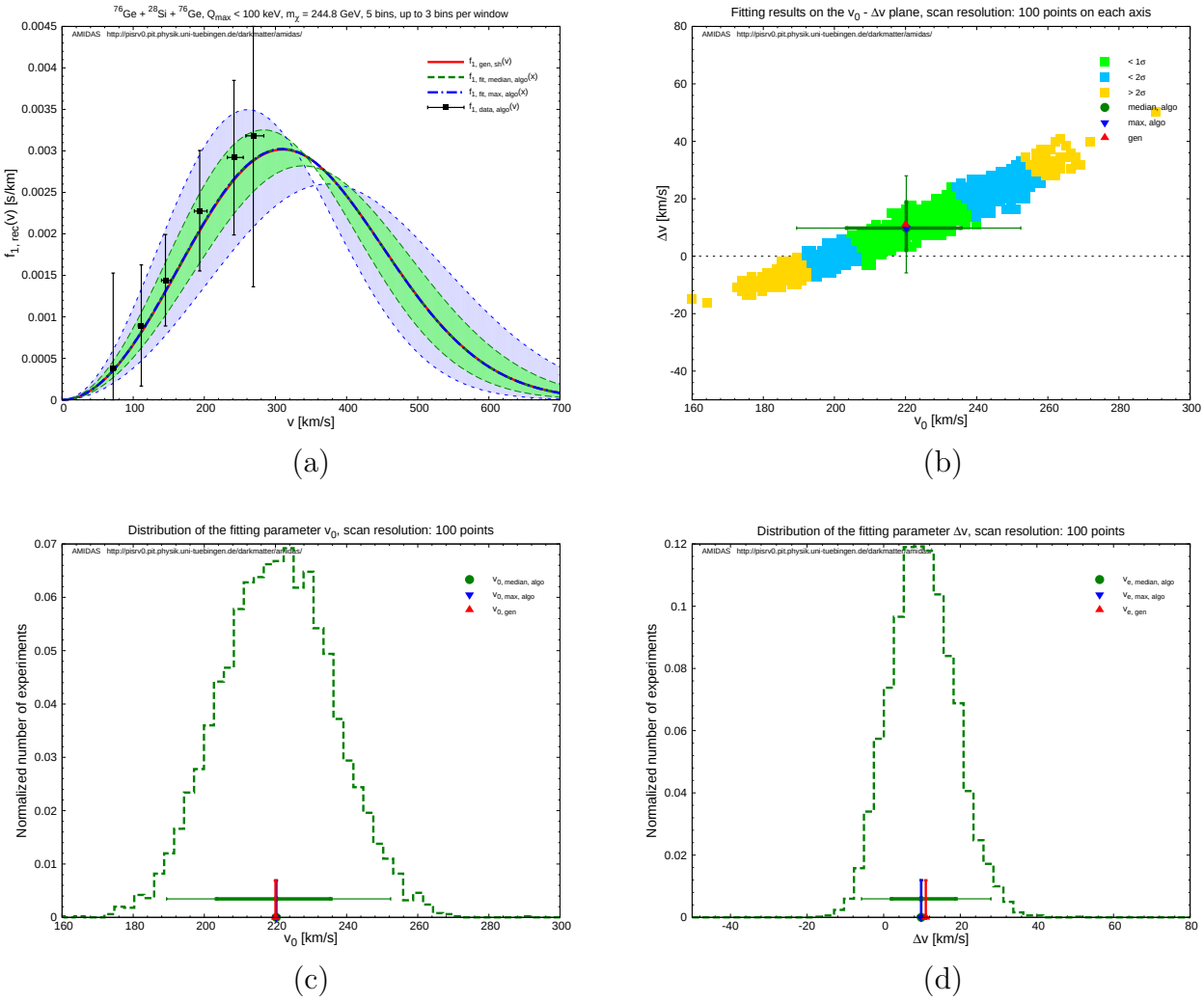

Figure 29: As in Figs. 26, the Gaussian probability distribution for both of two fitting parameters v_0 and Δv as well as the reconstructed WIMP mass have been used, except that the input WIMP mass has been set as $m_\chi = 250$ GeV.

and $v_e = 245$ km/s and a common 1σ uncertainty of 20 km/s is considered here.

With a proper fitting velocity distribution and *one more* fitting parameter, the reconstructed velocity distribution could now match the true (input) one very precisely with much narrower $1\,(2)\,\sigma$ statistical uncertainty bands. Additionally, the $1\,(2)\,\sigma$ statistical uncertainties on the fitting parameters v_0 and v_e can be significantly reduced to only $\pm 9.8\,(^{+22.4}_{-18.2})$ and $^{+14.0}_{-11.2}\,(^{+26.6}_{-21.0})$, respectively. Note that, as shown in Table 15, the use of the *one–parameter* shifted Maxwellian velocity distribution with *only one* fitting parameter v_0 and the fixed relation between v_0 and v_e would give a (much) wilder $1\,(2)\,\sigma$ statistical uncertainty bands of the reconstructed velocity distribution as well as a (much) larger $1\,(2)\,\sigma$ statistical uncertainties on the reconstructed Solar orbital velocity: $\sim 50\%$ to a factor of ~ 2 larger.

Variated shifted Maxwellian velocity distribution

Finally, in Figs. 29 (cf. Figs. 12 and 26), we test the possible improvement of the reconstruction precision by the use of the variated shifted Maxwellian velocity distribution with two fitting parameters v_0 and Δv. Only the Gaussian probability distribution for both of two fitting parameters with expected values of $v_0 = 230$ km/s and $\Delta v = 15$ km/s and a common 1σ uncertainty

Input: shifted Maxwellian velocity distribution $f_{1,\rm sh}(v)$						
Reconstruction: simple Maxwellian velocity distribution $f_{\mathbf{1,Gau}}(v)$						
Parameter	WIMP mass	Prob. dist.	Max. $p_{\rm median}$	Median	1σ range	2σ range
v_0 [km/s]	Input	Flat	287.2	$287.2\,^{+28.8}_{-21.6}\,(^{+69.6}_{-40.8})$	[265.6, 316.0]	[246.4, 356.8]
		Gaussian	284.8	$284.8\,^{+19.2}_{-16.8}\,(^{+36.0}_{-31.2})$	[268.0, 304.0]	[253.6, 320.8]
	Reconst.	Flat	289.6	$289.6\,^{+55.2}_{-43.2}\,(^{+110.4}_{-74.4})$	[246.4, 344.8]	[215.2, 400.0]
		Gaussian	289.6	$287.2\,^{+33.6}_{-31.2}\,(^{+64.8}_{-60.0})$	[256.0, 320.8]	[227.2, 352.0]
Reconstruction: one–parameter shifted Maxwellian velocity distribution $f_{\mathbf{1,sh},v_0}(v)$						
v_0 [km/s]	Input	Flat	209.0	$209.0\,^{+18.2}_{-15.4}\,(^{+43.4}_{-26.6})$	[193.6, 227.2]	[182.4, 252.4]
		Gaussian	218.8	$218.8 \pm 9.8\,(\pm 19.6)$	[209.0, 228.6]	[199.2, 238.4]
	Reconst.	Flat	211.8	$210.4\,^{+37.8}_{-29.4}\,(^{+89.6}_{-50.4})$	[181.0, 248.2]	[160.0, 300.0]
		Gaussian	218.8	$220.2 \pm 18.2\,(^{+36.4}_{-35.0})$	[202.0, 238.4]	[185.2, 256.6]
Reconstruction: shifted Maxwellian velocity distribution $f_{\mathbf{1,sh}}(v)$						
v_0 [km/s]	Input	Gaussian	223.0	$223.0\,^{+5.6}_{-7.0}\,(^{+12.6}_{-14.0})$	[216.0, 228.6]	[209.0, 235.6]
	Reconst.	Gaussian	223.0	$224.4 \pm 9.8\,(^{+22.4}_{-18.2})$	[214.6, 234.2]	[206.2, 246.8]
$v_{\rm e}$ [km/s]	Input	Gaussian	237.0	$237.0 \pm 7.0\,(^{+14.0}_{-15.4})$	[230.0, 244.0]	[221.6, 251.0]
	Reconst.	Gaussian	237.0	$237.0\,^{+14.0}_{-11.2}\,(^{+26.6}_{-21.0})$	[225.8, 251.0]	[216.0, 263.6]
Reconstruction: variated shifted Maxwellian velocity distribution $f_{\mathbf{1,sh},\Delta v}(v)$						
v_0 [km/s]	Input	Gaussian	218.8	$218.8\,^{+9.8}_{-8.4}\,(\pm 18.2)$	[210.4, 228.6]	[200.6, 237.0]
	Reconst.	Gaussian	220.2	$220.2\,^{+15.4}_{-16.8}\,(^{+32.2}_{-30.8})$	[203.4, 235.6]	[189.4, 252.4]
Δv [km/s]	Input	Gaussian	9.8	$9.8 \pm 5.2\,(^{+9.1}_{-10.4})$	[4.6, 15.0]	[−0.6, 18.9]
	Reconst.	Gaussian	9.8	$9.8\,^{+9.1}_{-7.8}\,(^{+18.2}_{-15.6})$	[2.0, 18.9]	[−5.8, 28.0]

Table 15: The reconstructed results with four fitting velocity distribution functions for the input WIMP mass of $m_\chi = 250$ GeV.

of 20 km/s is considered here.

While the reconstructed velocity distribution function could still match the true (input) one very precisely with however wilder 1 (2) σ statistical uncertainty bands, the "best–fit" values of both parameters v_0 and Δv (and in turn $v_{\rm e}$) could again be very precisely determined with negligible systematic deviations.

Remind that, since the heavier the WIMP mass, the smaller the transformation constant α defined in Eq. (5), for an experimental maximal cut–off energy $Q_{\rm max} \approx 100$ GeV, the reconstructible velocity range of our model–independent data analysis method would be much smaller than our maximal cut–off velocity $v_{\rm max}$ (e.g. ~ 285 km/s for $m_\chi = 250$ GeV and the ^{76}Ge tar-

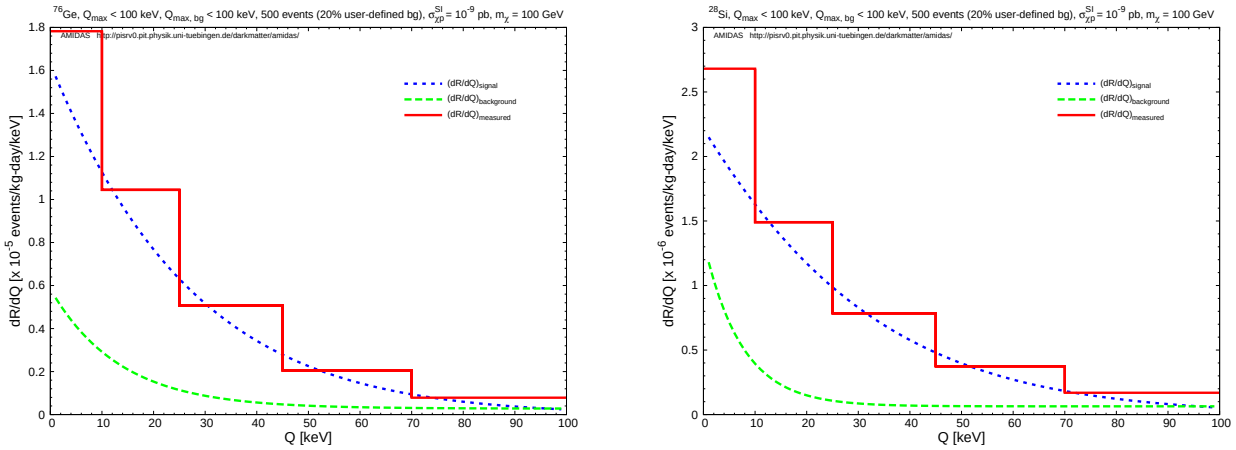
^{76}Ge, Q_{max} < 100 keV, $Q_{max, bg}$ < 100 keV, 500 events (20% user-defined bg), σ^{SI}_{xp} = 10^{-9} pb, m_χ = 100 GeV
AMIDAS http://pisrv0.pit.physik.uni-tuebingen.de/darkmatter/amidas/
$(dR/dQ)_{signal}$
$(dR/dQ)_{background}$
$(dR/dQ)_{measured}$
dR/dQ [x 10^{-5} events/kg-day/keV]
Q [keV]
^{28}Si, Q_{max} < 100 keV, $Q_{max, bg}$ < 100 keV, 500 events (20% user-defined bg), σ^{SI}_{xp} = 10^{-9} pb, m_χ = 100 GeV
AMIDAS http://pisrv0.pit.physik.uni-tuebingen.de/darkmatter/amidas/
$(dR/dQ)_{signal}$
$(dR/dQ)_{background}$
$(dR/dQ)_{measured}$
dR/dQ [x 10^{-6} events/kg-day/keV]
Q [keV]

(a) (b)

Figure 30: Measured recoil energy spectrum (solid red histogram) for a ^{76}Ge (a) and a ^{28}Si (b) targets with an input WIMP mass of $m_\chi = 100$ GeV. The dotted blue curve is the elastic WIMP–nucleus scattering spectrum for generating signal events, whereas the dashed green curve shows the artificial background spectrum, normalized to fit to the background ratio of 20%.

get). Therefore, our simulations shown in this subsection demonstrate meaningfully that, our Bayesian reconstruction of the one–dimensional WIMP velocity distribution function would be an important improvement, which could offer more and preciser information about the Galactic halo, e.g. the position of the peak of the WIMP velocity distribution, for the WIMP mass between $\mathcal{O}(20)$ GeV and even $\mathcal{O}(500)$ GeV.

In Table 15, we give the reconstructed results with all four fitting velocity distribution functions for the input WIMP mass of $m_\chi = 250$ GeV. Both of the true (input) and the reconstructed WIMP masses have been simulated and summarized.

3.5 Background effects

In this last part of the presentation of the numerical simulations of our Bayesian reconstruction of the WIMP velocity distribution function, we consider the effects of *unrejected* background events. Similar to our earlier works in Refs. [16, 15], we take into account a small fraction of *artificially* generated background events in the *pseudo* experimental data sets and want to study how well the WIMP velocity distribution as well as the fitting parameters could be reconstructed.

In all simulations demonstrated in this subsection, a combination of the *target–dependent exponential* form of the residue background spectrum introduced in Ref. [16] with a small *constant* component has been used:

$$\left(\frac{dR}{dQ}\right)_{\rm bg} = \left(\frac{dR}{dQ}\right)_{\rm bg,ex} + r_{\rm const}\left(\frac{dR}{dQ}\right)_{\rm bg,const}\,, \tag{48}$$

where

$$\left(\frac{dR}{dQ}\right)_{\rm bg,ex} = \exp\left(-\frac{Q/{\rm keV}}{A^{0.6}}\right)\,, \tag{49}$$

and

$$\left(\frac{dR}{dQ}\right)_{\rm bg,const} = 1\,. \tag{50}$$

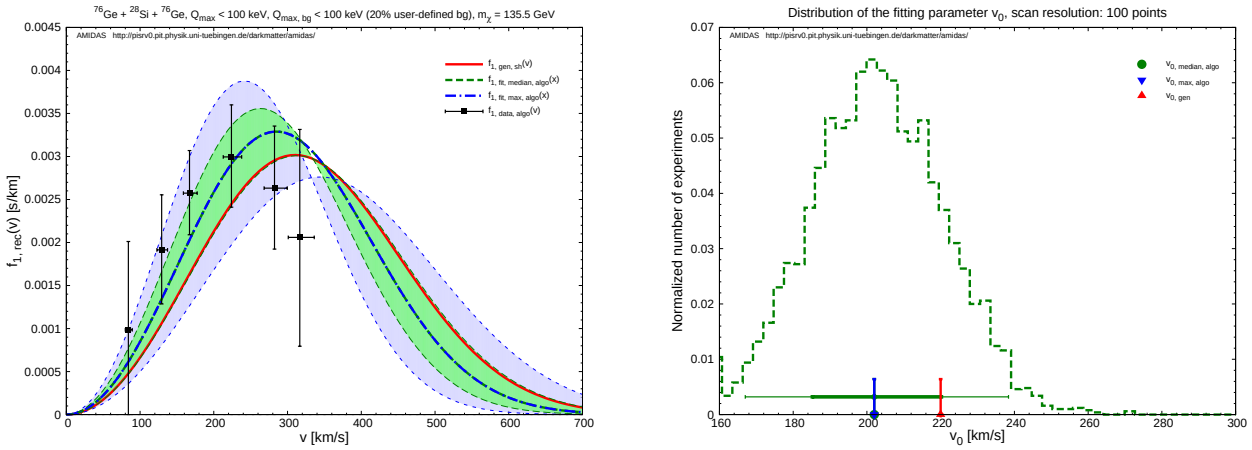
AMIDAS http://pisrv0.pit.physik.uni-tuebingen.de/darkmatter/amidas/
v [km/s]
Distribution of the fitting parameter v0, scan resolution: 100 points
Normalized number of experiments
v0 [km/s]

(a) (b)

Figure 31: As in Figs. 8(c) and (d): the one–parameter shifted Maxwellian velocity distribution and the Gaussian probability distribution for the unique fitting parameter v_0 as well as the reconstructed WIMP mass have been used, except that a fraction of 20% background events generated by the spectrum given in Eq. (48) has been taken into account.

Here Q is the recoil energy, A is the atomic mass number of the target nucleus. The power index of A, 0.6, is an empirical constant, which has been chosen so that the exponential background spectrum is somehow similar to, but still different from the expected recoil spectrum of the target nuclei; otherwise, there is in practice no difference between the WIMP scattering and background spectra[14]. Additionally, $r_{\rm const}$ is the ratio between the exponential and constant components in the total *background* spectrum, which has been fixed as $r_{\rm const} = 0.05$ for all simulations.

Note that, firstly, as argued in Ref. [16], the exponential form of background spectrum is rather naive; but, since we consider here only *a few tens residue* background events induced by *several different* sources, pass all discrimination criteria, and then mix with other WIMP–induced events in our data sets of a few hundreds *total* events, an exact form of background spectrum for each target nucleus would not be crucial and the exponential + constant form of background spectrum in Eq. (48) should practically not be unrealistic. Secondly, as demonstrated in Refs. [5, 6] and in the previous subsections, our Bayesian reconstruction of the one–dimensional WIMP velocity distribution requires only measured recoil energies and occasionally prior knowledge about the Solar and Earth's orbital velocities. Hence, for applying this method to future real experimental data, prior knowledge about (different) background source(s) is *not required at all*.

In Figs. 30, we show the measured recoil energy spectrum (solid red histogram) for a ^{76}Ge (a) and a ^{28}Si (b) targets with an input WIMP mass of $m_\chi = 100$ GeV. The dotted blue curve is the elastic WIMP–nucleus scattering spectrum for *generating* signal events, whereas the dashed green curve shows the *artificial* background spectrum: the exponential background spectrum given in Eq. (49) accompanied with an extra constant component, normalized to fit to the background ratio of 20%.

[14]Note that, among different possible choices, we use in our simulations the atomic mass number A as the simplest, unique characteristic parameter in the general analytic form (49) for defining the residue background spectrum for different target nuclei. However, it does not mean that the (superposition of the real) background spectra would depend simply/primarily on A or on the mass of the target nucleus, $m_{\rm N}$. In other words, it is practically equivalent to use the expression (49) or $(dR/dQ)_{\rm bg,ex} = e^{-Q/13.5\ {\rm keV}}$ directly for a ^{76}Ge target (cf. [23]).

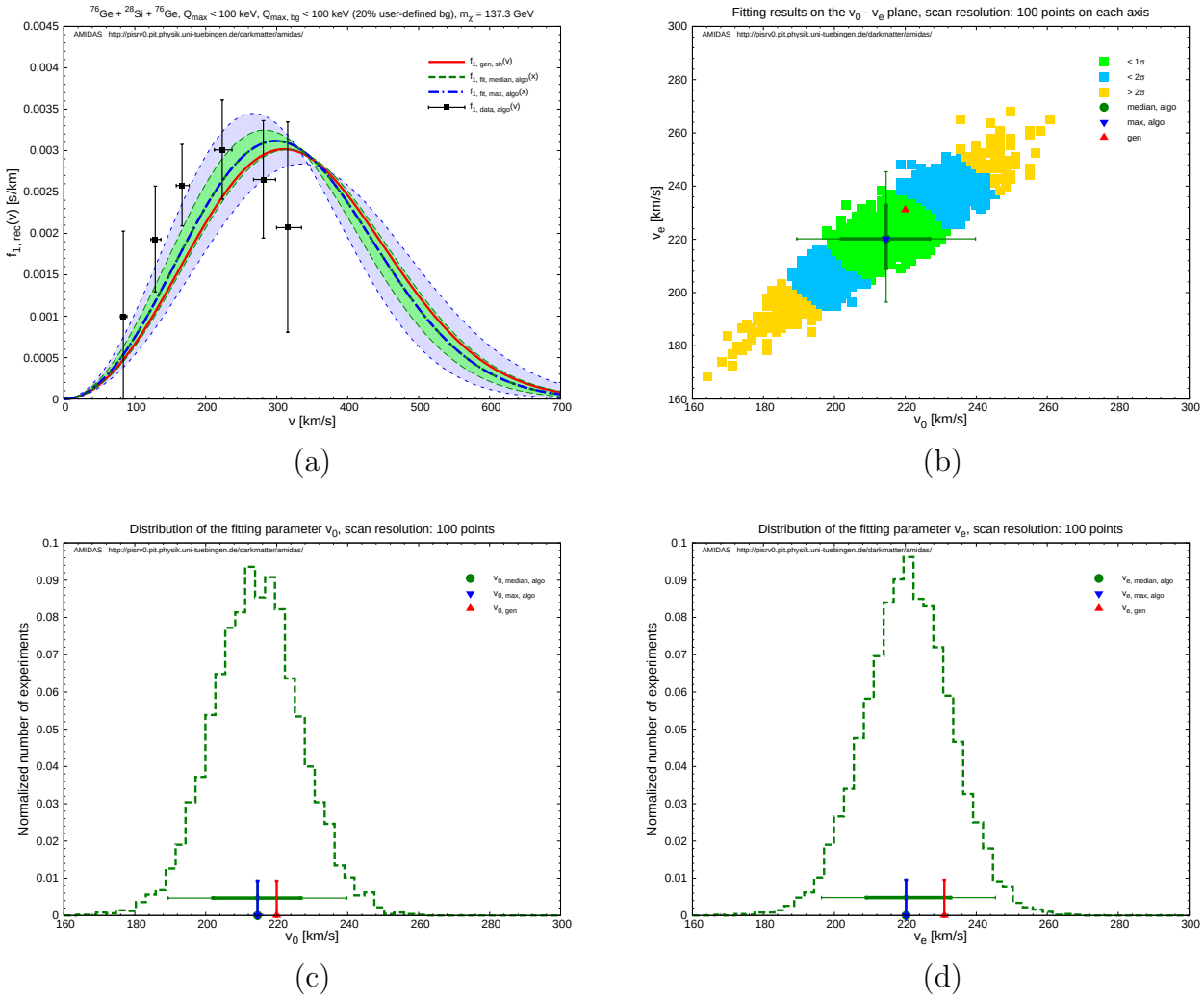

Figure 32: As in Figs. 10: the shifted Maxwellian velocity distribution function and the Gaussian probability distribution for both of two fitting parameters v_0 and v_e as well as the reconstructed WIMP mass have been used, except that a fraction of 20% background events has been taken into account.

3.5.1 For a moderate WIMP mass

We consider first the moderate input WIMP mass of $m_\chi = 100$ GeV. The *shifted* Maxwellian velocity distribution given in Eq. (41) is used for generating WIMP signals. All input setup and fitting parameters are the same as in Sec. 3.2 (see Table 3) and a fraction of 20% background events has been taken into account. Additionally, as in Sec. 3.4, we consider only the use of the Gaussian probability distribution for the fitting parameter(s): v_0 and v_e or Δv as well as the use of the reconstructed WIMP mass.

One–parameter shifted Maxwellian velocity distribution

In Fig. 31(a), it can be seen first that, due to the extra background events in both of the low and high energy ranges (see Figs. 30), the reconstructed–input data (solid black vertical bars) would be shifted (strongly) to the low–velocity range[15]: the peak of the solid black crosses is now at ~ 220 km/s, i.e. ~ 90 km/s smaller then the position of the true (input) velocity distribution. However, our simulation shown in Fig. 31(a) indicates clearly and importantly that, by assuming

[15]Note that, as shown in the plot, the reconstructed WIMP mass is now *overestimated*: $m_{\chi,\mathrm{rec}} \approx 136$ GeV.

Input: shifted Maxwellian velocity distribution $f_{1,\rm sh}(v)$						
Reconstruction: simple Maxwellian velocity distribution $f_{1,\rm Gau}(v)$						
Parameter	WIMP mass	Prob. dist.	Max. $p_{\rm median}$	Median	1σ range	2σ range
v_0 [km/s]	Input	Flat	284.8	$284.8\,^{+24.0}_{-19.2}\,(^{+52.8}_{-40.8})$	[265.6, 308.8]	[244.0, 337.6]
		Gaussian	284.8	$284.8 \pm 16.8\,(^{+36.0}_{-33.6})$	[268.0, 301.6]	[251.2, 320.8]
	Reconst.	Flat	253.6	$253.6\,^{+36.0}_{-31.2}\,(^{+79.2}_{-60.0})$	[222.4, 289.6]	[193.6, 332.8]
		Gaussian	258.4	$258.4\,^{+28.8}_{-26.4}\,(^{+57.6}_{-55.2})$	[232.0, 287.2]	[203.2, 316.0]
Reconstruction: one–parameter shifted Maxwellian velocity distribution $f_{1,{\rm sh},v_0}(v)$						
v_0 [km/s]	Input	Flat	211.8	$211.8\,^{+16.8}_{-15.4}\,(^{+36.4}_{-30.8})$	[196.4, 228.6]	[181.0, 248.2]
		Gaussian	217.4	$218.8\,^{+9.8}_{-11.2}\,(^{+21.0}_{-23.8})$	[207.6, 228.6]	[195.0, 239.8]
	Reconst.	Flat	188.0	$188.0\,^{+26.6}_{-22.4}\,(^{+56.0}_{-28.0})$	[165.6, 214.6]	[160.0, 244.0]
		Gaussian	202.0	$202.0\,^{+18.2}_{-16.8}\,(^{+36.4}_{-35.0})$	[185.2, 220.2]	[167.0, 238.4]
Reconstruction: shifted Maxwellian velocity distribution $f_{1,\rm sh}(v)$						
v_0 [km/s]	Input	Gaussian	225.8	$225.8\,^{+7.0}_{-8.4}\,(\pm 16.8)$	[217.4, 232.8]	[189.4, 239.8]
	Reconst.	Gaussian	214.6	$214.6\,^{+12.2}_{-12.6}\,(\pm 25.2)$	[202.0, 226.8]	[189.4, 239.8]
$v_{\rm e}$ [km/s]	Input	Gaussian	231.4	$231.4 \pm 8.4\,(^{+16.8}_{-18.2})$	[223.0, 239.8]	[213.2, 248.2]
	Reconst.	Gaussian	220.2	$220.2\,^{+12.6}_{-11.2}\,(^{+25.2}_{-23.8})$	[209.0, 232.8]	[196.4, 245.4]
Reconstruction: variated shifted Maxwellian velocity distribution $f_{1,{\rm sh},\Delta v}(v)$						
v_0 [km/s]	Input	Gaussian	220.2	$220.2\,^{+8.4}_{-9.8}\,(\pm 19.6)$	[210.4, 228.6]	[200.6, 239.8]
	Reconst.	Gaussian	204.8	$204.8\,^{+16.8}_{-15.4}\,(^{+32.2}_{-30.8})$	[189.4, 221.6]	[174.0, 237.0]
Δv [km/s]	Input	Gaussian	5.9	$5.9\,^{+5.2}_{-6.5}\,(^{+10.4}_{-13.0})$	$[-0.6, 11.1]$	$[-7.1, 16.3]$
	Reconst.	Gaussian	-0.6	$-0.6 \pm 7.8\,(\pm 15.6)$	$[-8.4, 7.2]$	$[-16.2, 15.0]$

Table 16: The reconstructed results with four fitting velocity distribution functions for data sets mixed with 20% background events and the input WIMP mass of $m_\chi = 100$ GeV.

the shifted Maxwellian WIMP velocity distribution and the *time–averaged* relation between the Solar and Earth's orbital velocities, the reconstructed WIMP velocity distributions could alleviate this systematic shift: the deviations of the peaks of the $(1\,(2)\,\sigma$ statistical uncertainty bands of the) reconstructed velocity distributions would only be $\sim 30\,^{+30}_{-20}\,(^{+60}_{-40})$ km/s.

In fact, it has also been found that, once an (approximately) precisely determined (true) WIMP mass could be used, the reconstructed WIMP velocity distribution could match the true (input) one very precisely: the deviation of the reconstructed v_0 would be $\lesssim 10$ km/s (flat) or even negligible (Gaussian) (see Table 16).

Note that, although a fraction of 20% unrejected background events has been mixed (artificially) into the analyzed (pseudo–)data sets, the (1σ statistical uncertainty of the) median

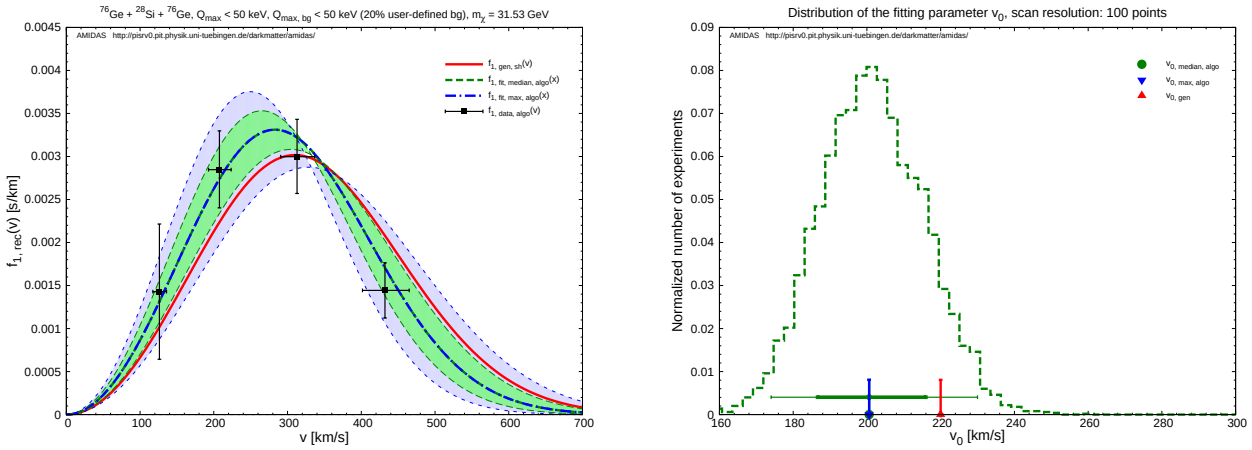
^{76}Ge + ^{28}Si + ^{76}Ge, Q_{max} < 50 keV, $Q_{max, bg}$ < 50 keV (20% user-defined bg), m_χ = 31.53 GeV
AMIDAS http://pisrv0.pit.physik.uni-tuebingen.de/darkmatter/amidas/
$f_{1, gen, sh}(v)$
$f_{1, fit, median, algo}(x)$
$f_{1, fit, max, algo}(x)$
$f_{1, data, algo}(v)$
$f_{1, rec}(v)$ [s/km]
v [km/s]
Distribution of the fitting parameter v_0, scan resolution: 100 points
AMIDAS http://pisrv0.pit.physik.uni-tuebingen.de/darkmatter/amidas/
$v_{0, median, algo}$
$v_{0, max, algo}$
$v_{0, gen}$
Normalized number of experiments
v_0 [km/s]

(a) (b)

Figure 33: As in Figs. 31, except that the input WIMP mass is set as $m_\chi = 25$ GeV (simulation setup as in Sec. 3.4.1).

value of the reconstructed v_0's ($202.0\,^{+18.2}_{-16.8}$ km/s) would still cover the true (input) Solar orbital velocity of $v_0 = 220$ km/s. Moreover, once we take into account the statistical fluctuation of the reconstructed–input data (the solid black vertical bars), the effect of residue background events on reconstructing information about the (shape of the) WIMP velocity distribution function would *not be significant*.

Shifted Maxwellian velocity distribution

In Figs. 32, we release the fixed relation between v_0 and v_e and determine these two parameters simultaneously and independently.

It can be seen that, firstly, the 1 (2) σ statistical uncertainty bands are obviously narrower than those shown in Fig. 31(a); the deviations of the peaks of the reconstructed velocity distributions from that of the true (input) one would be reduced to only $\lesssim 15$ km/s. In addition, the systematic deviations and the (1σ statistical uncertainties of the) median values of the reconstructed fitting paramaters v_0 and v_e shown in Figs. 32(c) and (d) are also (much) smaller than that shown in Fig. 31(b). (see Table 16). Note here that, as given in Table 16, once an (approximately) precisely determined (true) WIMP mass could be used, one could even reconstruct the WIMP velocity distribution function very precisely with very small or even negligible systematic deviations of both two fitting parameters. This means that, our Bayesian reconstruction method for the WIMP velocity distribution function would *not be affected* by a fraction of $\sim 20\%$ unrejected background events mixed in the analyzed data sets (for a WIMP mass of $\mathcal{O}(100)$ GeV).

In Table 16, we give the reconstructed results with all four fitting velocity distribution functions for data sets mixed with 20% background events and the input WIMP mass of $m_\chi = 100$ GeV. Both of the true (input) and the reconstructed WIMP masses have been simulated and summarized.

3.5.2 For a light WIMP mass

Now, we consider the case with a light input WIMP mass of $m_\chi = 25$ GeV. Simulation setup is the same as in Sec. 3.4.1 and a fraction of 20% background events has been taken into account.

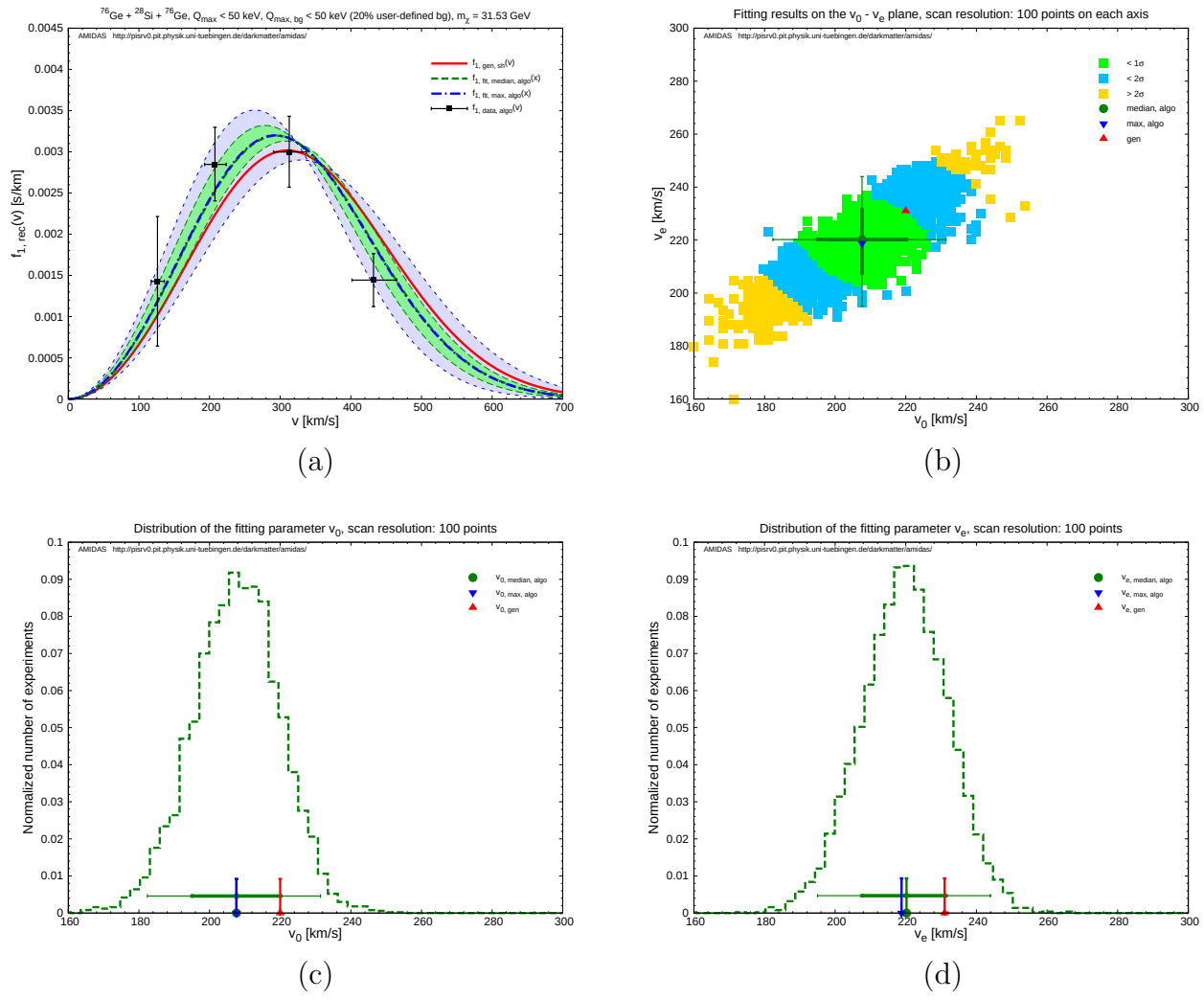

Figure 34: As in Figs. 32, except that the input WIMP mass is set as $m_\chi = 25$ GeV (simulation setup as in Sec. 3.4.1).

One–parameter shifted Maxwellian velocity distribution

Since the reconstructed WIMP mass would be $\sim 30\%$ *overestimated* ($m_{\chi,\mathrm{rec}} \approx 31.5$ GeV) due to the extra background events and *only four* reconstructed–input data points are available, Fig. 33(a) shows that the "best–fit" *one–parameter* shifted Maxwellian velocity distribution function would match not the true (input) velocity distribution (solid red curve), but the analyzed data points (solid black crosses) pretty well. Nevertheless, at least, the 2σ statistical uncertainty band of the reconstructed velocity distribution could still cover the true (input) one; the systematic deviations of the peaks of the reconstructed velocity distributions from that of the true (input) one would also only be ~ 30 km/s. Meanwhile, the (1σ statistical uncertainty of the) median value of the reconstructed v_0's ($200.6^{+15.4}_{-14.0}$ km/s) would still cover the true (input) Solar orbital velocity of $v_0 = 220$ km/s. This could be further improved by using an (approximately) precisely determined (true) WIMP mass to be $227.2\,^{+9.8}_{-8.4}$ km/s (flat) and 228.6 ± 7.0 km/s (Gaussian) (see Table 17).

Shifted Maxwellian velocity distribution

As the case of the 100 GeV WIMP mass shown in Figs. 31(a) and 32(a), the $1\,(2)\,\sigma$ statistical uncertainty bands reconstructed with the shifted Maxwellian velocity distribution with two

Input: shifted Maxwellian velocity distribution $f_{1,\rm sh}(v)$						
Reconstruction: simple Maxwellian velocity distribution $f_{\mathbf{1,Gau}}(v)$						
Parameter	WIMP mass	Prob. dist.	Max. $p_{\rm median}$	Median	1σ range	2σ range
v_0 [km/s]	Input	Flat	308.8	$306.4\,^{+16.8}_{-12.0}\,(^{+36.0}_{-24.0})$	[294.4, 323.2]	[282.4, 342.4]
		Gaussian	304.0	$304.0 \pm 12.0\,(\pm 24.0)$	[292.0, 316.0]	[280.0, 328.0]
	Reconst.	Flat	260.8	$260.8\,^{+24.0}_{-21.6}\,(^{+51.0}_{-40.8})$	[239.2, 284.8]	[220.0, 311.8]
		Gaussian	265.6	$263.2\,^{+21.6}_{-19.2}\,(^{+43.2}_{-38.4})$	[244.0, 284.8]	[224.8, 306.4]
Reconstruction: one–parameter shifted Maxwellian velocity distribution $f_{\mathbf{1,sh},v_0}(v)$						
v_0 [km/s]	Input	Flat	228.6	$227.2\,^{+9.8}_{-8.4}\,(^{+22.4}_{-15.4})$	[218.8, 237.0]	[211.8, 249.6]
		Gaussian	228.6	$228.6 \pm 7.0\,(^{+15.4}_{-14.0})$	[221.6, 235.6]	[214.6, 244.0]
	Reconst.	Flat	193.6	$193.6\,^{+16.8}_{-15.4}\,(^{+35.4}_{-29.4})$	[178.2, 210.4]	[164.2, 229.0]
		Gaussian	200.6	$200.6\,^{+15.4}_{-14.0}\,(^{+29.4}_{-26.6})$	[186.6, 216.0]	[174.0, 230.0]
Reconstruction: shifted Maxwellian velocity distribution $f_{\mathbf{1,sh}}(v)$						
v_0 [km/s]	Input	Gaussian	230.0	$230.0 \pm 7.0\,(\pm 14.0)$	[223.0, 237.0]	[216.0, 244.0]
	Reconst.	Gaussian	207.6	$207.6 \pm 12.6\,(^{+23.8}_{-25.2})$	[195.0, 220.2]	[182.4, 231.4]
$v_{\rm e}$ [km/s]	Input	Gaussian	239.8	$239.8\,^{+8.4}_{-7.0}\,(\pm 15.4)$	[232.8, 248.2]	[224.4, 255.2]
	Reconst.	Gaussian	218.8	$220.2\,^{+11.2}_{-12.6}\,(^{+23.8}_{-25.2})$	[207.6, 231.4]	[195.0, 244.0]
Reconstruction: variated shifted Maxwellian velocity distribution $f_{\mathbf{1,sh},\Delta v}(v)$						
v_0 [km/s]	Input	Gaussian	228.6	$228.6 \pm 7.0\,(^{+14.0}_{-12.6})$	[221.6, 235.6]	[216.0, 242.6]
	Reconst.	Gaussian	203.4	$204.8 \pm 12.6\,(\pm 23.8)$	[192.2, 217.4]	[181.0, 228.6]
Δv [km/s]	Input	Gaussian	12.4	$11.1 \pm 5.2\,(\pm 10.4)$	[5.9, 16.3]	[0.7, 21.5]
	Reconst.	Gaussian	2.0	$2.0 \pm 6.5\,(\pm 13.0)$	$[-4.5, 8.5]$	$[-11.0, 15.0]$

Table 17: The reconstructed results with four fitting velocity distribution functions for data sets mixed with 20% background events and the input WIMP mass of $m_\chi = 25$ GeV.

independent fitting parameters v_0 and $v_{\rm e}$ shown in Fig. 34(a) would clearly be much narrower than those reconstructed with only one parameter v_0. Meanwhile, in contrast to other (presented) cases, our simulations with the true (input) WIMP mass show that the reconstructed–input data as well as the $(1\,(2)\,\sigma$ statistical uncertainty bands of the) reconstructed velocity distribution function would slightly shift to the *high–velocity* range.

Furthermore, comparing results given in Table 17 to those in Table 16, it has been found interesting and probably importantly that, for an (input) WIMP mass of $\mathcal{O}(20)$ GeV, the use of our *variated* shifted Maxwellian velocity distribution given in Eq. (44) could offer preciser reconstruction results with (relatively) smaller statistical uncertainties, although fewer (four in

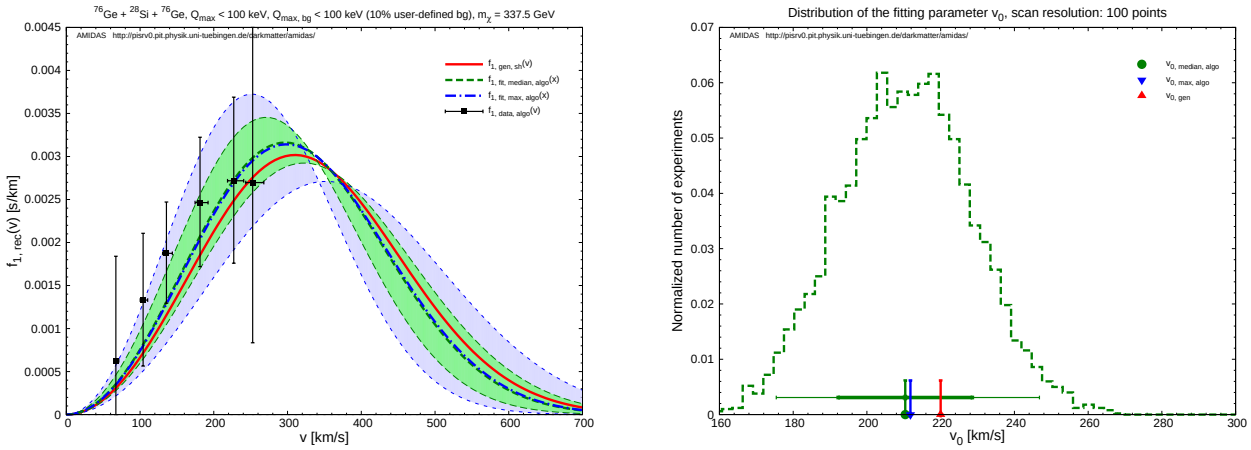
^{76}Ge + ^{28}Si + ^{76}Ge, Q_{max} < 100 keV, $Q_{max, bg}$ < 100 keV (10% user-defined bg), m_χ = 337.5 GeV
AMIDAS http://pisrv0.pit.physik.uni-tuebingen.de/darkmatter/amidas/
$f_{1, gen, sh}(v)$
$f_{1, fit, median, algo}(x)$
$f_{1, fit, max, algo}(x)$
$f_{1, data, algo}(v)$
$f_{1, rec}(v)$ [s/km]
v [km/s]
Distribution of the fitting parameter v_0, scan resolution: 100 points
AMIDAS http://pisrv0.pit.physik.uni-tuebingen.de/darkmatter/amidas/
$v_{0, median, algo}$
$v_{0, max, algo}$
$v_{0, gen}$
Normalized number of experiments
v_0 [km/s]

(a) (b)

Figure 35: As in Figs. 31, except that the input WIMP mass is set as $m_\chi = 250$ GeV (simulation setup as in Sec. 3.4.2) and a fraction of *10%* background events has been taken into account.

our simulations) data points are available.

In Table 17, we give the reconstructed results with all four fitting velocity distribution functions for data sets mixed with 20% background events and the input WIMP mass of $m_\chi = 25$ GeV. Both of the true (input) and the reconstructed WIMP masses have been simulated and summarized.

3.5.3 For a heavy WIMP mass

As the last case, we consider a heavy input WIMP mass of $m_\chi = 250$ GeV. Simulation setup is the same as in Sec. 3.4.2. Note however that, since the constant component of the background spectrum used in our simulations would cause a strongly *overestimated* WIMP mass, in particular, once WIMPs are heavy (e.g. the 250 GeV input WIMP mass would now be reconstructed as $\simeq 338$ GeV) [16], the ratio of the background events in the analyzed data sets has been set as *only 10%* [15].

One–parameter shifted Maxwellian velocity distribution

As usual, we use first the one–parameter shifted Maxwellian velocity distribution function to fit the reconstructed–input data points.

In Figs. 35, we can see unexpectedly that, although the input WIMP mass is pretty heavy, the systematic deviation would be only ~ 10 km/s (for 10% background ratio!). This might be due to that, as shown in Sec. 3.4.2, for our used experimental maximal cut–off energy $Q_{\rm max} = 100$ GeV and the ^{76}Ge target, the reconstructible velocity range would only be ~ 270 km/s (shifted slightly to the *low*–velocity range due to the *overestimated* WIMP mass) and thus this maximal reconstructible velocity is theoretically smaller than the position of the peak of the velocity distribution function (see e.g. Fig. 35(a)). This means that the approximately *monotonically increased* shape of the reconstructed–input data points (solid black vertical bars) with pretty large 1σ statistical uncertainties would alleviate the effects of the overestimations of the analyzed (reconstructed–input) data points and the reconstructed WIMP mass caused by the extra background events.

Shifted Maxwellian velocity distribution

Now we use the shifted Maxwellian velocity distribution function with two independent fitting

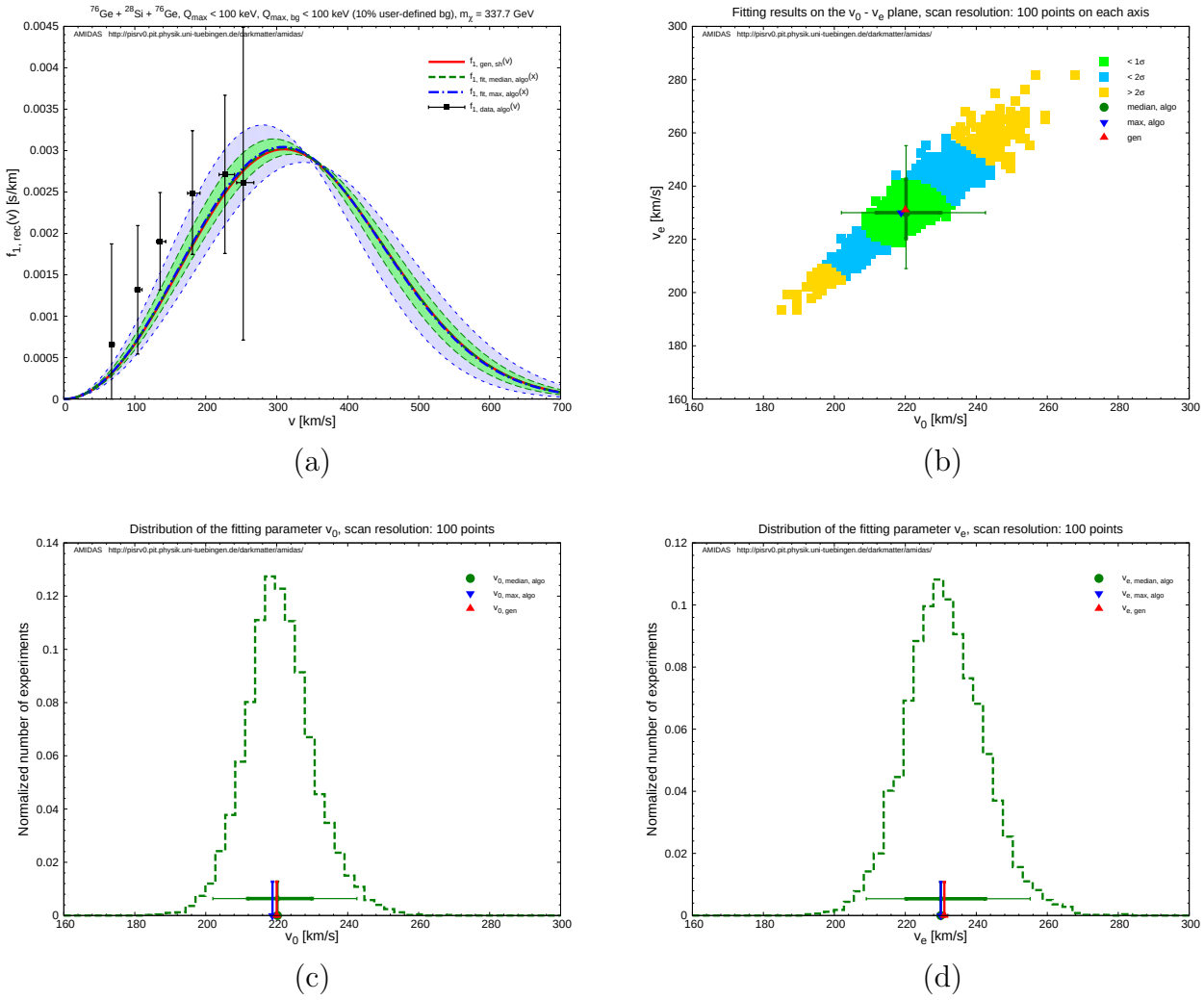

Figure 36: As in Figs. 32, except that the input WIMP mass is set as $m_\chi = 250$ GeV (simulation setup as in Sec. 3.4.2) and a fraction of *10%* background events has been taken into account.

parameters v_0 and v_e to fit the reconstructed–input data points. Astonishingly and unexpectedly (probably accidentally), Figs. 36 show that both of the "best–fit" results of the parameters v_0 and v_e are *almost exact* as the true (input) values and the 1σ statistical uncertainties on v_0 and v_e are only ~ 10 km/s.

Meanwhile, in contrast to our simulation results with the variated shifted Maxwellian velocity distribution function shown previously, for the case of the 250 GeV WIMP mass with 10% background ratio, the Bayesian reconstructed parameter Δv could have a (much) larger deviations from the true (estimated) value (see Table 18)!

In Table 18, we give the reconstructed results with all four fitting velocity distribution functions for data sets mixed with *10%* background events and the input WIMP mass of $m_\chi = 250$ GeV. Both of the true (input) and the reconstructed WIMP masses have been simulated and summarized.

Input: shifted Maxwellian velocity distribution $f_{1,\mathrm{sh}}(v)$						
Reconstruction: simple Maxwellian velocity distribution $f_{1,\mathrm{Gau}}(v)$						
Parameter	WIMP mass	Prob. dist.	Max. p_{median}	Median	1σ range	2σ range
v_0 [km/s]	Input	Flat	277.6	$277.6\,^{+26.4}_{-21.6}\,(^{+64.8}_{-38.4})$	[256.0, 304.0]	[239.2, 342.4]
		Gaussian	277.6	$278.8 \pm 18.0\,(^{+37.2}_{-32.4})$	[260.8, 296.8]	[246.4, 316.0]
	Reconst.	Flat	263.2	$263.2\,^{+48.0}_{-38.4}\,(^{+115.2}_{-62.4})$	[224.8, 311.2]	[200.8, 378.4]
		Gaussian	268.0	$268.0\,^{+33.6}_{-31.2}\,(^{+67.2}_{-55.2})$	[236.8, 301.6]	[212.8, 335.2]
Reconstruction: one–parameter shifted Maxwellian velocity distribution $f_{1,\mathrm{sh},v_0}(v)$						
v_0 [km/s]	Input	Flat	203.4	$203.4\,^{+19.2}_{-14.0}\,(^{+44.8}_{-28.0})$	[189.4, 222.6]	[175.4, 248.2]
		Gaussian	216.0	$216.0\,^{+9.8}_{-11.2}\,(^{+19.6}_{-21.0})$	[204.8, 225.8]	[195.0, 235.6]
	Reconst.	Flat	195.0	$193.6\,^{+33.6}_{-28.0}\,(^{+78.4}_{-33.6})$	[165.6, 227.2]	[160.0, 272.0]
		Gaussian	211.8	$210.4 \pm 18.2\,(^{+36.4}_{-35.0})$	[192.2, 228.6]	[175.4, 246.8]
Reconstruction: shifted Maxwellian velocity distribution $f_{1,\mathrm{sh}}(v)$						
v_0 [km/s]	Input	Gaussian	221.6	$223.0\,^{+5.6}_{-8.4}\,(^{+12.6}_{-15.4})$	[214.6, 228.6]	[207.6, 235.6]
	Reconst.	Gaussian	218.8	$220.2\,^{+9.8}_{-8.4}\,(^{+22.4}_{-18.2})$	[211.8, 230.0]	[202.0, 242.6]
v_{e} [km/s]	Input	Gaussian	232.8	$234.2\,^{+7.0}_{-8.4}\,(^{+14.0}_{-16.8})$	[225.8, 241.2]	[217.4, 248.2]
	Reconst.	Gaussian	230.0	$230.0\,^{+12.6}_{-9.8}\,(^{+25.2}_{-21.0})$	[220.2, 242.6]	[209.0, 255.2]
Reconstruction: variated shifted Maxwellian velocity distribution $f_{1,\mathrm{sh},\Delta v}(v)$						
v_0 [km/s]	Input	Gaussian	216.0	$217.4\,^{+8.4}_{-9.8}\,(^{+18.2}_{-19.6})$	[207.6, 225.8]	[197.8, 235.6]
	Reconst.	Gaussian	210.4	$211.8\,^{+16.8}_{-15.4}\,(^{+33.6}_{-30.8})$	[196.4, 228.6]	[181.0, 245.4]
Δv [km/s]	Input	Gaussian	7.2	$7.2\,^{+5.2}_{-5.2}\,(^{+10.4}_{-11.7})$	[2.0, 12.4]	[−4.5, 17.6]
	Reconst.	Gaussian	4.6	$4.6\,^{+7.8}_{-7.8}\,(^{+16.9}_{-14.3})$	[−3.2, 12.4]	[−9.7, 21.5]

Table 18: The reconstructed results with four fitting velocity distribution functions for data sets mixed with *10%* background events and the input WIMP mass of $m_\chi = 250$ GeV.

4 Summary and conclusions

In this paper, we extended our earlier work on the development of the model–independent data analysis method for the reconstruction of the (time–averaged) one–dimensional velocity distribution of Galactic WIMPs and introduced the Bayesian fitting procedure of the theoretical velocity distribution functions.

In this fitting procedure the (rough) velocity distribution reconstructed by using raw experimental data, i.e. measured recoil energies, with one or more different target nuclei has been used as reconstructed–input data (points). By assuming a fitting WIMP velocity distribution function and scanning the parameter space based on the Bayesian analysis, the (fitting) astro-

nomical characteristic parameters, e.g. the Solar and Earth's orbital velocities v_0 and v_e, would be pinned down as the output results and thus the functional form of the one–dimensional velocity distribution can be reconstructed (instead of only a few discrete points).

As the first test of our Bayesian reconstruction method for the one–dimensional WIMP velocity distribution function, we used the simplest isothermal spherical Galactic halo model for both generating WIMP–signal events and as the assumed velocity distribution with the unique fitting parameter: the Solar orbital velocity v_0. Our simulations show that, with (only) 500 recorded events (on average) and without prior knowledge about the Solar orbital velocity, v_0 could in principle be pinned down with a negligible deviation and a 1σ statistical uncertainty of only ~ 12 km/s (with a precisely known WIMP mass) or ~ 20 km/s (with a reconstructed WIMP mass), respectively. Moreover, once (rough) information about the Solar orbital velocity can be given, the statistical uncertainties on the reconstructed v_0 could even be reduced to $\sim 70\%$.

For more realistic consideration, we then took into account the orbital motion of the Solar system around our Galaxy as well as that of the Earth around the Sun and turned to use the shifted Maxwellian velocity distribution function for generating WIMP signals. As comparisons, four different fitting functions have been considered: the simple and the (one–parameter and variated) shifted Maxwellian velocity distributions. It has been found that, firstly, with an improper assumed fitting function (e.g. the simple Maxwellian velocity distribution here), the WIMP velocity distribution could still be reconstructed and offer some important information about Galactic WIMPs, e.g. the rough position of the peak of the one–dimensional velocity distribution function. The deviations of the peaks of the reconstructed velocity distributions from that of the true (input) one would be only ~ 10 km/s. However, the best–fit value(s) of the fitting parameter(s) would be unexpected. For instance, the reconstructed Solar orbital velocity v_0 would be 2σ (with the reconstructed WIMP mass) or even 4σ (with the input WIMP mass) apart from the theoretical estimate of v_0. Such an observation could in turn be an important criterion on the assumption of fitting velocity distribution function.

Moreover, our simulations with the (one–parameter and variated) shifted Maxwellian velocity distributions show that, although in all of these three cases the reconstructed velocity distributions could match the true (input) one pretty precisely, with two fitting parameters the 1 (2) σ statistical uncertainty bands of the reconstructed velocity distributions would be narrower then those with only one fitting parameter. In addition, the use of the variation of the shifted Maxwellian velocity distribution could (strongly) reduce the systematic deviations of the determinations of the characteristic Solar and Earth's orbital velocities v_0 and v_e, with however a bit larger statistical uncertainties.

Furthermore, we considered also a modification of the simple Maxwellian velocity distribution with an extra power index as the generating WIMP velocity distribution. First, we used the simple Maxwellian velocity distribution without the power index as the test fitting function. Since the difference between the modification and the original simple Maxwellian velocity distributions are very tiny, the reconstructed velocity distribution function could match the true (input) one very precisely and the characteristic Solar orbital velocity could also be reconstructed with negligible systematic deviation.

Meanwhile, our simulations with the (one–parameter and variated) shifted Maxwellian velocity distribution functions show that, although the positions of the peak of the reconstructed velocity distribution would be only $\lesssim 10$ km/s deviated from the true (input) one, a clear 2σ to even 6σ difference between the best–fit values of the Solar and/or the Earth's orbital velocities and the true (input) ones could be observed. Such results would in turn indicate evidently the improper assumption of the shifted Maxwellian velocity distribution function.

Moreover, from the simulations with the modified simple Maxwellian velocity distribution with the power index as the second fitting parameter, it has been found that our Bayesian reconstruction of the WIMP velocity distribution would be (totally) non–sensitive on the power index. This means that, unfortunately, with only a few hundreds of recorded WIMP events it would still be impossible to distinguish (evidently) different subtle variations of the (simple and shifted) WIMP velocity distribution functions.

As comparisons, we considered also a light and a heavy input WIMP masses. For the case of light WIMPs, due to the sharp shape of the recoil energy spectrum and the small kinetic maximal cut–off energy, the recorded WIMP events would need to be separated into fewer bins/windows. However, our simulations show that, with only four available reconstructed–input data points, the true (input) (shifted Maxwellian) velocity distribution function could astonishingly be reconstructed very precisely. On the other hand, once WIMPs are heavy, the statistical fluctuation on the reconstructed WIMP mass becomes pretty large and hence the Bayesian reconstructions of the velocity distribution as well as of the Solar and Earth's velocities would have large statistical uncertainties. Nevertheless, the reconstructed velocity distribution function with the best–fit characteristic Solar and Earth's velocities could still match the true (input) one very precisely.

Finally, the effects of residue (unrejected) background events mixed in data sets to analyze have also been considered. Three different WIMP masses with background ratios of 10% or 20% have been tested. Although, due to the choice of our artificial residue background spectrum, the reconstructed WIMP masses would be overestimated and the (rough shape of) the reconstructed–input data points would thus shift (significantly) to lower velocities, the functional forms of the chosen fitting velocity distributions would somehow alleviate these systematic shifts and the $1\,(2)\,\sigma$ statistical uncertainty bands could still cover the true (input) velocity distribution. In particular, for heavy WIMPs, since the reconstructed–input data points should be in the velocity range smaller than the position of the peak of the velocity distribution function, its approximately monotonically increased shape with pretty large 1σ statistical uncertainties would alleviate the effects of the overestimations of the analyzed (reconstructed–input) data points and the reconstructed WIMP mass caused by the extra background events. The reconstructed velocity distribution function could match the true (input) one pretty well.

It would be worth to emphasize that, first, comparing to the pretty large (1σ) statistical uncertainties on the input data points (offered by our model–independent method developed in Ref. [5] with raw experimental measured recoil energies), our Bayesian reconstruction of the WIMP velocity distribution function introduced here with only a few km/s deviation and $\mathcal{O}(10)$ km/s 1σ statistical uncertainties on the reconstructed Solar and Earth's velocities would be a remarkable improvement.

Second, all our simulations show importantly that, even initial values different slightly from the true (input) setup have been used as the expected values for the Gaussian probability distribution of the fitting parameters, these fitting parameters could still be pinned down (pretty) precisely. As long as a proper assumed fitting velocity distribution function is used, the best–fit values of the reconstructed parameters could always be less than 1σ apart from the true (input/theoretical) values. This observation indicates that rough, slightly incorrect prior knowledge about our fitting parameters would not affect significantly the reconstructed results in our Bayesian reconstruction procedure.

Moreover, by rewriting the functional form of the (basic) fitting velocity distribution function, one could not only pin down the fitting parameters more precisely, but also occasionally reduce the statistical uncertainties on the reconstructed parameters.

In summary, we developed in this paper the Bayesian reconstruction procedure for fitting

theoretical predicted models of the one–dimensional WIMP velocity distribution function to data (points), which can be reconstructed directly from experimental measured recoil energies. Hopefully, this extension of our earlier work could offer more useful information about the Dark Matter halo, which could be used further in e.g. indirect DM detection experiments.

Acknowledgments

The author appreciates Mei-Yu Wang for useful discussions about models of the velocity distribution of Galactic WIMPs. The author would also like to thank the Physikalisches Institut der Universität Tübingen for the technical support of the computational work presented in this paper as well as the friendly hospitality of the Graduate School of Science and Engineering for Research, University of Toyama, the Institute of Modern Physics, Chinese Academy of Sciences and the Center for High Energy Physics, Peking University, where part of this work was completed. This work was partially supported by the National Science Council of R.O.C. under contracts no. NSC-98-2811-M-006-044 and no. NSC-99-2811-M-006-031.

A Formulae needed in Sec. 2.1

Here we list all formulae needed for the model–independent method for the reconstruction of the one–dimensional WIMP velocity distribution function described in Sec. 2.1. Detailed derivations and discussions can be found in Ref. [5].

First, by using the standard Gaussian error propagation, the expression for the uncertainty on the logarithmic slope k_n can be given from Eq. (11) directly as

$$\sigma^2(k_n) = k_n^4 \left\{ 1 - \left[\frac{k_n b_n/2}{\sinh(k_n b_n/2)} \right]^2 \right\}^{-2} \sigma^2 \left(\overline{Q - Q_n}|_n \right) , \tag{A1}$$

with

$$\sigma^2 \left(\overline{Q - Q_n}|_n \right) = \frac{1}{N_n - 1} \left[\overline{(Q - Q_n)^2}|_n - \overline{Q - Q_n}|_n^2 \right] . \tag{A2}$$

For replacing the "bin" quantities by "window" quantities, one needs the covariance matrix for $\overline{Q - Q_\mu}|_\mu$, which follows directly from the definition (23):

$$\begin{aligned} &\mathrm{cov} \left(\overline{Q - Q_\mu}|_\mu, \overline{Q - Q_\nu}|_\nu \right) \\ &= \frac{1}{N_\mu N_\nu} \sum_{n=n_{\nu-}}^{n_{\mu+}} \left[N_n \left(\overline{Q}|_n - \overline{Q}|_\mu \right) \left(\overline{Q}|_n - \overline{Q}|_\nu \right) + N_n^2 \sigma^2 \left(\overline{Q - Q_n}|_n \right) \right] . \end{aligned} \tag{A3}$$

Note that, firstly, $\mu \leq \nu$ has been assumed here and the covariance matrix is, of course, symmetric. Secondly, the sum is understood to vanish if the two windows μ, ν do not overlap, i.e. if $n_{\mu+} < n_{\nu-}$. Moreover, from Eq. (24), we can get

$$\mathrm{cov}(r_\mu, r_\nu) = \frac{1}{w_\mu w_\nu} \sum_{n=n_{\nu-}}^{n_{\mu+}} N_n , \tag{A4}$$

where $\mu \leq \nu$ has again been taken. And the mixed covariance matrix can be given by

$$\mathrm{cov} \left(r_\mu, \overline{Q - Q_\nu}|_\nu \right) = \frac{1}{w_\mu N_\nu} \sum_{n=n_-}^{n_+} N_n \left(\overline{Q}|_n - \overline{Q}|_\nu \right) . \tag{A5}$$

Note here that this sub–matrix is *not* symmetric under the exchange of μ and ν. In the definition of n_- and n_+ we therefore have to distinguish two cases:

$$\begin{aligned} &n_- = n_{\nu-},\ n_+ = n_{\mu+}, && \text{if } \mu \leq \nu\,; \\ &n_- = n_{\mu-},\ n_+ = n_{\nu+}, && \text{if } \mu \geq \nu\,. \end{aligned} \tag{A6}$$

As before, the sum in Eq. (A5) is understood to vanish if $n_- > n_+$.

Furthermore, the covariance matrices involving the estimators of the logarithmic slopes k_μ, estimated by Eq. (11) with replacing $n \to \mu$, can be given from Eq. (A1) as

$$\begin{aligned} \mathrm{cov}\,(k_\mu, k_\nu) = k_\mu^2 k_\nu^2 &\left\{1 - \left[\frac{k_\mu b_\mu/2}{\sinh(k_\mu b_\mu/2)}\right]^2\right\}^{-1} \left\{1 - \left[\frac{k_\nu b_\nu/2}{\sinh(k_\nu b_\nu/2)}\right]^2\right\}^{-1} \\ &\times \mathrm{cov}\left(\overline{Q - Q_\mu}|_\mu, \overline{Q - Q_\nu}|_\nu\right)\,, \end{aligned} \tag{A7}$$

and

$$\mathrm{cov}\,(r_\mu, k_\nu) = k_\nu^2 \left\{1 - \left[\frac{k_\nu b_\nu/2}{\sinh(k_\nu b_\nu/2)}\right]^2\right\}^{-1} \mathrm{cov}\left(r_\mu, \overline{Q - Q_\nu}|_\nu\right)\,. \tag{A8}$$

References

[1] G. Jungman, M. Kamionkowski and K. Griest, *"Supersymmetric Dark Matter"*, *Phys. Rep.* **267**, 195–373 (1996), `arXiv:hep-ph/9506380`.

[2] M. Drees and G. Gerbier, *"Mini–Review of Dark Matter: 2012"*, updated minireview for *"The Review of Particle Physics 2012"*, `arXiv:1204.2373 [hep-ph]` (2012).

[3] T. Saab, *"An Introduction to Dark Matter Direct Detection Searches and Techniques"*, `arXiv:1203.2566 [physics.ins-det]` (2012).

[4] L. Baudis, *"Direct Dark Matter Detection: the Next Decade"*, Issue on *"The Next Decade in Dark Matter and Dark Energy"*, *Phys. Dark Univ.* **1**, 94–108 (2012), `arXiv:1211.7222 [astro-ph.IM]`.

[5] M. Drees and C.-L. Shan, *"Reconstructing the Velocity Distribution of Weakly Interacting Massive Particles from Direct Dark Matter Detection Data"*, *J. Cosmol. Astropart. Phys.* **0706**, 011 (2007), `arXiv:astro-ph/0703651`.

[6] M. Drees and C.-L. Shan, *"Model–Independent Determination of the WIMP Mass from Direct Dark Matter Detection Data"*, *J. Cosmol. Astropart. Phys.* **0806**, 012 (2008), `arXiv:0803.4477 [hep-ph]`.

[7] B. J. Barlow, *"Statistics: A Guide to the Use of Statistical Methods in the Physical Sciences"*, Wiley (1993).

[8] G. D'Agostini, *"Probability and Measurement Uncertainty in Physics: A Bayesian Primer"*, `arXiv:hep-ph/9512295` (1995).

[9] Y. Akrami, C. Savage, P. Scott, J. Conrad and J. Edsjö, *"Statistical Coverage for Supersymmetric Parameter Estimation: A Case Study with Direct Detection of Dark Matter"*, *J. Cosmol. Astropart. Phys.* **1107**, 002 (2011), arXiv:1011.4297 [hep-ph]; *"How Well Will Ton–Scale Dark Matter Direct Detection Experiments Constrain Minimal Supersymmetrh?"*, *J. Cosmol. Astropart. Phys.* **1104**, 012 (2011), arXiv:1011.4318 [astro-ph.CO].

[10] M. Pato, L. Baudis, G. Bertone, R. Ruiz de Austri, L. E. Strigari and R. Trotta, *"Complementarity of Dark Matter Direct Detection Targets"*, *Phys. Rev.* **D 83**, 083505 (2011), arXiv:1012.3458 [astro-ph.CO];
M. Pato, *"What Can(not) be Measured with Ton–Scale Dark Matter Direct Detection Experiments"*, *J. Cosmol. Astropart. Phys.* **1110**, 035 (2011), arXiv:1106.0743 [astro-ph.CO].

[11] C. Arina, J. Hamann and Y. Y. Y. Wong, *"A Bayesian View of the Current Status of Dark Matter Direct Searches"*, *J. Cosmol. Astropart. Phys.* **1109**, 022 (2011), arXiv:1105.5121 [hep-ph];
C. Arina, J. Hamann, R. Trotta and Y. Y. Y. Wong, *"Evidence for Dark Matter Modulation in CoGeNT"*, *J. Cosmol. Astropart. Phys.* **1203**, 008 (2011), arXiv:1111.3238 [hep-ph];
C. Arina, *"Chasing a Consistent Picture for Dark Matter Direct Searches"*, *Phys. Rev.* **D 86**, 123527 (2012), arXiv:1210.4011 [hep-ph]; *"Bayesian Analysis of Multiple Direct Detection Experiments"*, arXiv:1310.5718 [hep-ph] (2013).

[12] C. Strege, R. Trotta, G. Bertone, A. H. G. Peter and P. Scott, *"Fundamental Statistical Limitations of Future Dark Matter Direct Detection Experiments"*, *Phys. Rev.* **D 86**, 023507 (2012), arXiv:1201.3631 [hep-ph].

[13] D. G. Cerdeño *et al.*, *"Complementarity of Dark Matter Direct Detection: the Role of Bolometric Targets"*, *J. Cosmol. Astropart. Phys.* **1307**, 028 (2013), arXiv:1304.1758 [hep-ph].

[14] B. J. Kavanagh, *"Parametrizing the Local Dark Matter Speed Distribution: A Detailed Analysis"*, arXiv:1312.1852 [astro-ph.CO] (2013).

[15] C.-L. Shan, *"Effects of Residue Background Events in Direct Dark Matter Detection Experiments on the Reconstruction of the Velocity Distribution Function of Halo WIMPs"*, *J. Cosmol. Astropart. Phys.* **1006**, 029 (2010), arXiv:1003.5283 [astro-ph.HE].

[16] Y.-T. Chou and C.-L. Shan, *"Effects of Residue Background Events in Direct Dark Matter Detection Experiments on the Determination of the WIMP Mass"*, *J. Cosmol. Astropart. Phys.* **1008**, 014 (2010), arXiv:1003.5277 [hep-ph].

[17] K. Freese, J. Frieman and A. Gould, *"Signal Modulation in Cold-Dark-Matter Detection"*, *Phys. Rev.* **D 37**, 3388-3405 (1988);
K. Freese, M. Lisanti and C. Savage, *"Annual Modulation of Dark Matter: A Review"*, *Rev. Mod. Phys.* **85**, 1561–1581 (2013), arXiv:1209.3339 [astro-ph.CO].

[18] M. Lisanti, L. E. Strigari, J. G. Wacker and R. H. Wechsler, *"The Dark Matter at the End of the Galaxy"*, *Phys. Rev.* **D 83**, 023519 (2011), arXiv:1010.4300 [astro-ph.CO].

[19] Y.-Y. Mao, L. E. Strigari, R. H. Wechsler, H.-Y. Wu and O. Hahn, *"Halo–to–Halo Similarity and Scatter in the Velocity Distribution of Dark Matter" Astrophys. J.* **764**, 35 (2013), arXiv:1210.2721 [astro-ph.CO];

Y.-Y. Mao, L. E. Strigari and R. H. Wechsler, *"Connecting Direct Dark Matter Detection Experiments to Cosmologically Motivated Halo Models"*, *Phys. Rev.* **D 89**, 063513 (2014), arXiv:1304.6401 [astro-ph.CO].

[20] M. Kuhlen, A. Pillepich, J. Guedes and P. Madau, *"The Distribution of Dark Matter in the Milky Way's Disk"*, arXiv:1308.1703 [astro-ph.GA] (2013).

[21] C.-L. Shan, the AMIDAS (A Model–Independent Data Analysis System) package and website for direct Dark Matter detection experiments and phenomenology, http://pisrv0.pit.physik.uni-tuebingen.de/darkmatter/amidas/ (2009); the mirror website on TiResearch (Taiwan interactive Research), http://www.tir.tw/phys/hep/dm/amidas/.

[22] C.-L. Shan, *"AMIDAS-II: Upgrade of the AMIDAS Package and Website for Direct Dark Matter Detection Experiments and Phenomenology"*, arXiv:1403.xxxx [astro-ph.IM] (2014).

[23] A. M. Green, *"Determining the WIMP Mass from a Single Direct Detection Experiment, a More Detailed Study"*, *J. Cosmol. Astropart. Phys.* **0807**, 005 (2008), arXiv:0805.1704 [hep-ph].